

AN INTERNATIONAL FORUM FOR THE RAPID PUBLICATION OF
ORIGINAL SCIENTIFIC ARTICLES DEALING WITH SCIENCES AND
RELATED INTERDISCIPLINARY AREAS



SOUTHERN
JOURNAL OF SCIENCES

ESTABLISHED IN 1993

Formerly known as the Southern Brazilian Journal of Chemistry

VOLUME THIRTY-ONE, NUMBER THIRTY-SIX

ISSN: 2764-5967 - E-ISSN: 2764-5959

DECEMBER– 2023

Former Printed ISSN: 0104-5431 and E-ISSN: 2674-6891

SOUTHERN JOURNAL OF SCIENCES

ISSN: 2764-5967

E-ISSN: 2764-5959

Volume 31

Number 36

2023

Dados Internacionais de Catalogação na Publicação (CIP)

S727 Southern Journal of Sciences [recurso eletrônico] :
interdisciplinary path for scientific divulgation / Araucária
Associação Científica – (Fev. 2022). – Dados eletrônicos. –
Nova Prata. : Araucária Associação Científica, 2023-.

Semestral

Recurso on-line

Descrição baseada em: Vol. 30, n. 33 (JUN. 2022)

Formerly known as: Southern Brazilian Journal of
Chemistry

Modo de acesso: < <https://sjofsciences.com> >.

E-ISSN: 2764-5959

ISSN: 2764-5967

1. Química. 2. Física. 3. Biologia. 4. Ciências Naturais. 5.
Farmacologia. 6. Ciências exatas. 7. Ciências aplicadas. 8.
Ciências. I. Dr. D. Scientific Consulting.

UDC 001

Bibliotecário Responsável

Ednei de Freitas Silveira

CRB 10/1262

Journal E-mail: southbchem@gmail.com

Editorial Board

Editor-in-Chief

- Walter José Peláez, Ph.D., walter.pelaez@unc.edu.ar, Argentina, UNC.

Assistant Editors

- Ketevan Kupatadze, Ph.D., ketevan_kupatadze@iliauni.edu, Georgia, ISU.
- Shaima R. Banoon, MsC., shimarb@uomisan.edu.iq, Iraq, University of Misan.
- Cristián Andrés Quintero, Ph.D., cquintero@umaza.edu.ar, Argentina, Universidad Juan Agustín Maza.
- Aline Maria dos Santos, Ph.D., aline.santos@ifrj.edu.br Brazil, IFRJ.
- Cristiane de Souza Siqueira Pereira, Ph.D., cristiane.pereira@universidadevassouras.edu.br Brazil, Universidade de Vassouras.

General Secretary

- Luis Alcides Brandini De Boni, Ph.D., labdeboni@gmail.com, Brazil, TQG;

Scientific Council

- Teresa M. Roseiro Maria Estronca, Ph.D., troseiro@ci.uc.pt, UC, Portugal.
- Rafael Rodrigues de Oliveira, Ph.D., rafa_rdo@yahoo.com.br, Neoprospecta, Brazil.
- Eduardo Goldani, Ph.D., eduardogoldani@gmail.com, Brazil, TQG;
- Marcos Antônio Klunk, Ph.D., marcosak@edu.unisinos.br, UNISINOS, Brazil.
- Francisco José Santos Lima, Ph.D., limafjs@yahoo.com, UFRN, Brazil.
- Monica Regina da Costa Marques, Ph.D., mmarquesrj@gmail.com, UERJ, Brazil.
- Rodrigo Brambilla, Ph.D., kigobrambilla@gmail.com, UFRGS, Brazil.
- Gabriel Rubensam, Me., rubensam_quimico@hotmail.com, PUCRS, Brazil.
- Andrian Saputra, Ph.D., andriansaputra@fkip.unila.ac.id, University of Lampung, Indonesia.
- Zhanar Zhumadilova, Ph.D., zhanar_85@mail.ru, Satbayev University, Kazakhstan.
- Roberto Fernandez, Ph.D., rfernandezm@unicartagena.edu.co, Universidad de Cartagena, Colombia.

- Andrey Vladimirovich Sevbitov, Ph.D., avsevbitov@mail.ru, I. M. Sechenov First Moscow State Medical University, Russian Federation.
- Jorge Fernando Silva de Menezes, Ph.D., jorge_fernando@ufrb.edu.br, UFRB, Brazil.
- Paulo Sergio Souza, Ph.D., Brazil, paulosergio@fosorio.g12.br, Brazil, Fundação Osorio.
- Alessandra Deise Sebben, Ph.D., adsebben@gmail.com, Brazil
- Fredy Hernán Martínez Sarmiento, Ph.D., fhmartinezs@udistrital.edu.co, UD-FJC, Colombia.
- Fabiana de Carvalho Fim, Ph.D., fabianafim@ct.ufpb.br, UFPB, Brazil.
- Flavia Maria Pompeia Cavalcanti, MsC., flaviamaria@upf.br, Brazil, UPF.
- Gustavo Guthmann Pesenatto, MD., gustavoggp@gmail.com, Primary Health Care, Brazil.
- Fábio Herrmann, MD., fabioherrmannfh@gmail.com, Santa Casa de Misericórdia de Porto Alegre Hospital, Brazil.
- Marco Antonio Smiderle Gelain, MD., marco_gelain@hotmail.com, Dante Pazzanese Cardiology Institute, São Paulo - Brazil.
- Rene Francisco Boschi Gonçalves, Ph.D., renefbg@gmail.com, Technological Institute of Aeronautics - ITA, Brazil.
- Élcio J. de Oliveira, Ph.D., INNOSPACE, Korea/Brazil
- Ademir Oliveira da Silva, Ph.D., aosquimica@gmail.com, Federal University of Rio Grande do Norte - UFRN, Brazil.
- Francisco José Santos Lima, Ph.D., limafjs@yahoo.com, Federal University of Rio Grande do Norte - UFRN, Brazil.
- Anton Timoshin, Ph.D., anton-timoshin007@yandex.ru, I. M. Sechenov First Moscow State Medical University, Russian Federation.
- Intisar Razzaq Sharba, Ph.D., intisar.sharba@uokufa.edu.iq, University of Kufa, Iraq.
- Paulo Roberto Barros Gomes, Ph.D., prbgomes@yahoo.com.br, Federal Institute of Technical Education of Pará - IFPA, Brazil.
- Dra. Elizabeth Laura Moyano, Ph.D., e.laura.moyano@unc.edu.ar, INFIQC-CONICET-Universidad Nacional de Córdoba, Argentina.
- Dra. Ana Graciela Iriarte, Ph.D., airiarte@unc.edu.ar, INFIQC-CONICET-Universidad Nacional de Córdoba, Argentina.
- Ingrid Grazielle Sousa, M.sc., indi.sousa@gmail.com, Ph.D. candidate at Unicamp, Brazil.
- Nicholas Karasavvidis M. Sc., nick.kara014@gmail.com, University of Sydney, Australia.

SOUTHERN JOURNAL OF SCIENCES

ISSN: 2764-5959 (Online)

ISSN: 2764-5967 (Print)

DOI: 10.48141/2764-5959

Digital preservation: Portico

Former Southern Brazilian Journal of Chemistry

Former E-ISSN 2674-6891

Former ISSN 0104-5431

Available at

<https://sjofsciences.com>

Mission

The **SOUTHERN JOURNAL OF SCIENCES** is a double-blind peer review, open access, **multidisciplinary** Journal dedicated to publishing high-quality content and is intended to fill a gap in terms of scientific information for Southern Brazil. We have set high standards for the articles to be published by ensuring strong but fair refereeing by at least two reviewers. The Journal publishes original research articles in all the fields of Engineering, Mathematics, physics, Chemistry, Biology, Agriculture, Natural resource management, Pharmacy, Medicine, and others.

Occasionally the Journal will include review papers, interviews, and other types of communications. It will be published mainly in English, and at present, there are no page charges.

We hope this Journal will provide a forum for disseminating high-quality research in Science and are open to any questions and suggestions.

The responsibility for the articles is exclusive to the authors.

Subjects List

UDC 001

Correspondências

Av. Carlos Tarasconi, 281/202.

Bairro Sagrada Família. CEP: 95320-000

Nova Prata – RS. Brasil.

www.sjofsciences.com

southbchem@gmail.com

INDEX OF THE ISSUE NUMBER 36

ISSN: 2764-5967

E-ISSN: 2764-5959

Volume 31

2023

<p><u>1. Original research paper</u></p> <p>CEBALLOS, Noelia Marcela; BONEU, Gonzalo Daniel; RIMONDINO, Guido Noé; MALANCA, Fabio Ernesto; PELÁEZ, Walter José.</p> <p style="text-align: right;">Argentina</p> <p style="text-align: center;">PYROLYSIS OF SOYBEAN WASTE: A ROUTE TO BIOCARBON FOR PESTICIDES CAPTURE</p> <p>Pg. 01</p>	<p><u>2. Original research paper</u></p> <p>KUPATADZE, Ketevan.</p> <p style="text-align: right;">Georgia</p> <p style="text-align: center;">REVIEW OF AIR POLLUTION RESEARCH RESULTS ON THE EXAMPLE OF TBILISI</p> <p>Pg. 09</p>
<p><u>3. Original research paper</u></p> <p>MUSSI STOIZIK, Jessica Anabella; AVENA, Maria Virginia; ELIAS, María Lucia; HEREDIA, Lucia; BOARELLI, Vanina Paola.</p> <p style="text-align: right;">Argentina</p> <p style="text-align: center;">POTENTIAL EFFECTS OF KETOGENIC DIETS, A NARRATIVE REVIEW</p> <p>Pg. 20</p>	<p><u>4. Review paper</u></p> <p>TREIN, Felipe de Almeida; DE BONI, Luis Alcides Brandini.</p> <p style="text-align: right;">Brazil</p> <p style="text-align: center;">COMPARATIVE STUDY OF DPD REAGENTS FOR CHLORINE MEASUREMENT IN DRINKING WATER AND DEVELOPMENT OF A JAVASCRIPT INTERPOLATION TOOL</p> <p>Pg. 33</p>
<p><u>5. Original research paper</u></p> <p>BUONFIGLI, Julio; QUINTERO, Cristian; SÁNCHEZ, Diego; LEIVA Natalia; DAMIANI, Maria Teresa.</p> <p style="text-align: right;">Argentina</p> <p style="text-align: center;">STATISTICAL VALIDATION OF TRIPLE COLOCALIZATION ANALYSIS</p> <p>Pg. 46</p>	<p><u>6. Editorial</u></p> <p style="text-align: center;">DEAR READERS OF THE SOUTHERN JOURNAL OF SCIENCES</p> <p>Pg. 64</p>
<p><u>7. ATR 2023</u></p> <p style="text-align: center;">SOUTHERN JOURNAL OF SCIENCES ANNUAL TRANSPARENCY REPORT</p> <p>Pg. 66</p>	<p><u>8. Conference invitation</u></p> <p style="text-align: right;">Argentina/Brazil</p> <p style="text-align: center;">II Southern Science Conference - 2024</p> <p>Pg. 67</p>

For the most updated information, please visit the website of the Journal at <https://siofsciences.com/>

PYROLYSIS OF SOYBEAN WASTE: A ROUTE TO BIOCARBON FOR PESTICIDES CAPTURE

CEBALLOS, Noelia Marcela¹; BONEU, Gonzalo Daniel¹; RIMONDINO, Guido Noé¹; MALANCA, Fabio Ernesto.¹; PELÁEZ, Walter José^{1*}.

¹INFIQC – CONICET - Departamento de Físicoquímica, Facultad de Ciencias Químicas, Universidad Nacional de Córdoba. Argentina. X5000HUA.

* Corresponding author
e-mail: walter.pelaez@unc.edu.ar

Received 20 July 2023; received in revised form 30 August 2023; accepted 20 November 2023

ABSTRACT

Background: This study explores the potential use of biomass residues from soybean pressing via static pyrolysis to produce carbonaceous materials for pesticide adsorption. It emphasizes concerns regarding the environmental impact of agroindustrial waste and the persistent nature of pesticides in soil and water systems. **Aims:** To investigate the efficacy of biochar obtained from soybean waste in adsorbing pesticides. Specifically, to analyze the gas products generated during pyrolysis and characterize the obtained carbonaceous material for its adsorption capabilities. **Methods:** Soybean residue underwent static pyrolysis at various temperatures and durations. Gas analysis utilizing FTIR spectroscopy identified the gaseous products generated during the pyrolysis process. The obtained biochar underwent successive washes and characterization through FTIR spectra comparison with commercial activated carbon. Through absorption assays, using UV-VIS spectroscopy, investigations were conducted on the solid biocarbon fractions to evaluate their capacity for absorbing pesticides. **Results:** Gas Analysis: The study revealed the production of volatile organic compounds (VOCs) and highlighted the prevalence of mono-carbon compounds with increased temperature and pyrolysis time. The analysis demonstrated consistent carbon mass percentages across different reaction conditions. Characterization of Biochar: Comparison with activated carbon indicated structural similarities with heightened intensity in certain bands, suggesting the presence of incomplete cellulose cracking in the obtained biochar. Regarding the Chlorothalonil, Atrazine and Dicamba retention, notably, the concentration of Chlorothalonil in a 7:3 water: acetonitrile solution decreases by 77 % through adsorption on the carbons. **Discussion:** The investigation examined the adsorption efficiency of the biochar for Chlorothalonil, Atrazine, and Dicamba from aqueous solutions. Chlorothalonil exhibited substantial retention by the biochar, while Atrazine showed comparatively lower adsorption effectiveness. Remarkably, Dicamba did not demonstrate retention by either the biochar or activated carbon. **Conclusion:** The study underscores the potential of pyrolyzed soybean waste for pesticide adsorption, particularly highlighting Chlorothalonil's strong affinity with the carbonaceous structure. Further research is needed to optimize adsorption properties and explore potential enhancements of these materials through additional treatment methods, offering promising avenues for environmental remediation.

Keywords: Pyrolysis, mesoporous carbons, Chlorothalonil, Atrazine, Dicamba.

1. INTRODUCTION

Many agroindustrial processes yield side-products that constitute organic waste. Due to the high volumes of biomass produced this way, chemists have been intensively working to

revalorize these residues. The techniques applied to transform the biomass are biochemical or thermochemical. The latter allows processing of a great amount of feedstock in short periods. In particular, biomass pyrolysis meets the conditions to generate high-energy-density bio-oil or biochar (Wang *et al.*, 2021).

The open burning of biomass undoubtedly releases carbon dioxide and other volatile organic compounds into the atmosphere. Therefore, using pyrolysis techniques that allow careful control of the products leaving the process is key to minimizing the environmental impact. To this end, static pyrolysis under vacuum conditions is presented as an advantageous technique for the study of volatile and non-volatile fractions of the pyrolysate (Pepino *et al.*, 2014; Firpo *et al.*, 2019)

In addition to the production of bio-oils and biochar, the transformation of biomass also produces coals that have multiple uses in the agricultural environment itself. For example, activated carbons obtained from pyrolysis can be used for industrial pollution abatement as an adsorbent for toxic pollutants in wastewater. In structure, activated carbons are highly microporous carbons with high internal surface area and porosity. Commercially, they are the most common adsorbents used to remove organic compounds from air and water streams. They are also often prepared from coal (a non-renewable source) or specially dedicated biomass such as bamboo wood. However, any material with high carbon and low inorganic content can be used as a raw material for activated carbon production (Lewoyehu, 2021).

At present, the modern intensive agricultural practices aimed at providing food for the increasing global population raise ecological concerns. Along with this comes the massive use of pesticides, which are chemicals that serve the purpose of eradicating unwanted pests to safeguard agricultural production. Pesticides include insecticides (insects), herbicides (weeds), and fungicides (fungi), among others (Hassaan and El Nemr, 2020). The agricultural demand fuels the growth of the agrochemical industry, providing a range of chemicals distinguished by diverse structural characteristics and intended targets. Figure 1 shows the structures and uses for the pesticides essayed in this work. Each of these chemicals plays a significant role in agricultural practices but also raises concerns related to environmental impact, health effects, and management of their residues in soil and water systems.

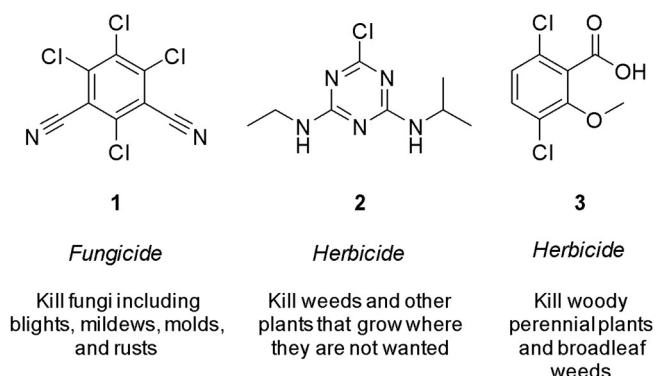


Figure 1. Chemical structures of Chlorothalonil (2,4,5,6-tetrachloroisophthalonitrile, **1**), Atrazine (1-chloro-3-ethylamino-5-isopropylamino-2,4,6-triazine, **2**), Dicamba (3,6-dichloro-2-methoxybenzoic acid, **3**)

The persistence of pesticides refers to their ability to remain in the environment after application. It involves how long they stay active, break down, or degrade. Factors like the type of pesticide, environmental conditions, and application methods influence their persistence. Some pesticides break down relatively quickly, especially when exposed to soil sunlight, air, water, or microbial activity. Others, however, might persist for longer periods, posing risks to the environment, including water sources, wildlife, and even human health through bioaccumulation in the food chain. For instance, the fungicide Chlorothalonil (CT) was banned in the United States and the European Union because of its permanence in humic acids and its transformation into potential toxic byproducts in groundwater (Kiefer *et al.*, 2020). However, besides this, it is still widely used in developing countries. In this way, primarily, solutions involve the photochemical transformation of the pesticide into more soluble byproducts with less toxicity. Moreover, the herbicide Atrazine (AT) is very persistent and does not degrade gradually (Chen *et al.*, 2019), so it emerged as the most frequently detected contaminant in aquifers across Latin America and mirrored similar occurrences in European and United States groundwater (Mohaupt *et al.*, 2020). Despite the herbicide ban in European countries in 2004 due to surpassing permitted drinking water limits ($0.1 \mu\text{g L}^{-1}$), its persistence in water and soil continues to result in its detection even years after prohibition.

Adsorption presents a viable method for extracting contaminants from water, holding significant promise, particularly when leveraging biomass or agricultural remnants for valorization, known as bio-based adsorption. This environmentally benign technique proves non-

invasive, ensuring elevated efficacy, straightforward operation, and convenient regeneration (Vievard *et al.*, 2023). Because of its simplicity and cost-effectiveness, adsorption was discovered to be the most preferred technique (Rani *et al.*, 2017).

As part of our study of gaseous products emitted to the atmosphere by burning industrial biomass residues from soybean pressing, it was reported here the obtention and utilization of carbons from soybean waste static pyrolysis to retain the fungicide Chlorothalonil from an aqueous matrix.

2. MATERIALS AND METHODS

The soybean residue used is the solid leftover obtained after pressing soybeans in the oil production process. This residue was ground to particle sizes of less than 1 mm. Subsequently, 500 mg of this material was placed in a Pyrex glass ampoule and evacuated for 2 minutes until a pressure of 10^{-2} mbar was reached. They were then sealed and subjected to static pyrolysis reactions at different times (10, 30, and 60 min) and temperatures (250 °C, 300 °C, and 350 °C) in an electrical furnace (ORL-T40400). Completed the pyrolysis step, the ampoule was connected to a glass vacuum line equipped with a capacitance pressure gauge (0-760 Torr, MKS Baratron). Once the ampoule opened, the total pressure of formed gases was measured and then transferred to a 210 mm-path gas cell placed inside the sample compartment of a Fourier transform infrared (FTIR) spectrometer (Bruker IFS-28). The composition of the gas mixture was performed for all the reactions. All spectra were recorded in the range $500\text{--}4000\text{ cm}^{-1}$ with a resolution of 2 cm^{-1} . For the identification and quantification of each component, reference spectra and the corresponding calibration curves of different gasses were obtained under the same experimental conditions. The remaining biochar was subjected to successive washes in a Soxhlet apparatus (3 x 120 mL ethanol, 98%) for 3 hours each time. Then, the same procedure was performed but with acetonitrile (ACN, HPLC 99.5%, Sintorgan). Finally, the recovered solid was dried at atmospheric pressure until a constant weight was achieved.

The selected solids were used to perform adsorption experiments with Chlorothalonil, Atrazine, and Dicamba. The process was monitored by UV-VIS spectroscopy on an Agilent

8354 spectrophotometer ($\lambda\text{L}=3.65\cdot 10^{-2}$ absorbance units) using a quartz cell with an optical path of 1 cm.

Chlorothalonil was purified from a commercial sample (compressed powder 82.5% w/w) by extraction with ethyl acetate, followed by chromatographic column purification using n-hexane and dichloromethane. Atrazine was obtained in a pure form by its isolation from a commercial sample of Atrazine TC 97%. Finally, Dicamba 96.4% (Riedel de Haën) was used without any further purification.

For each essay, 20.0 mg of the carbonaceous solid was placed in a disc extraction cartridge (3M Empore - Fischer Scientific, octadecyl, 10mm/6mL). Prior to the essay, the biocarbons were washed several times with water: acetonitrile solution (7:3) in 2 mL aliquots, following the process by UV-VIS spectroscopy. The washing process was concluded once the spectral curve of the aliquots showed no further changes. Subsequently, 2 mL of a freshly prepared solution of the pesticide in water: acetonitrile (7:3), was passed over the carbon under study. The solution flow was always performed in 2 mL aliquots using a flow rate of 0.4 mL/s.

3. RESULTS AND DISCUSSION:

3.1. Gas Analysis

A typical gas phase spectrum resulting from the FTIR analysis is presented in Figure 2.

A glance at the spectra allows the identification of signals corresponding to the generation of carbon dioxide (broad signal at around 2350 cm^{-1} and sharp peak at 667 cm^{-1}) and carbon monoxide (bands centered at 2140 cm^{-1}) as majority reaction products. Quantitative analysis revealed CO_2 values ranging between 17 and 81%, while CO ranged from 0.4 to 2.4%, depending the pyrolysis assay conducted. Furthermore, the observation of various volatile organic compounds (VOCs), whose presence and proportion are contingent upon the temperature and time of pyrolysis, was noted. Graphs 1 and 2 illustrate the general trends in the analysis of gaseous products for the 10 min reactions at 250 °C, 300 °C, and 350 °C.

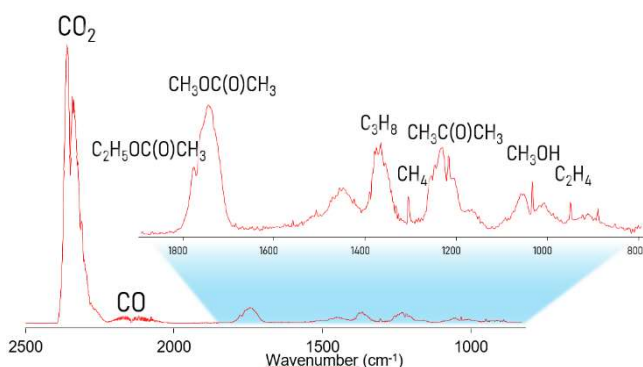
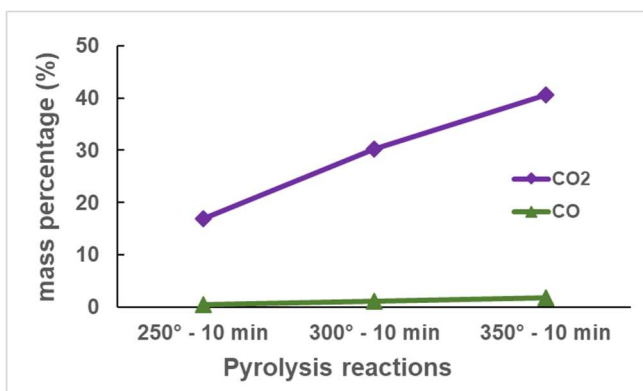
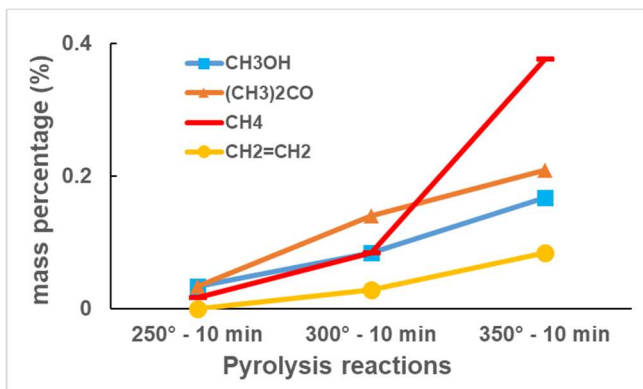


Figure 2. IR spectrum of the gas fraction obtained by pyrolysis of soybean residue at 350°C.



Graph 1. Mass percentage for the gases present in major proportion in 10 min reactions at different temperatures.



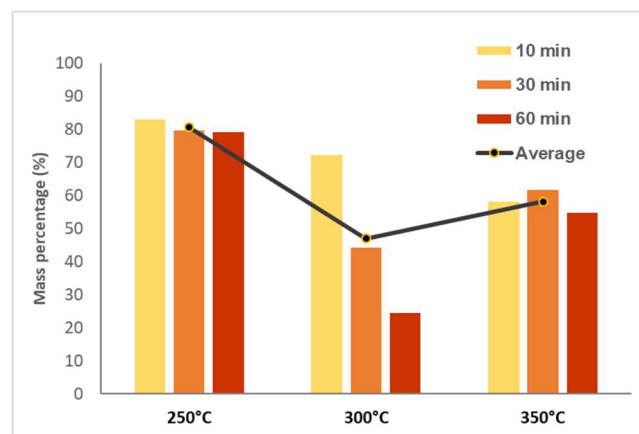
Graph 2. Mass percentage for the gases present in minor proportion in 10 min reactions at different temperatures.

Higher temperatures and prolonged pyrolysis times favored the formation of mono-carbon compounds. This phenomenon occurs due to a significant rise in cracking events with increasing temperatures, producing thermodynamically more stable compounds.

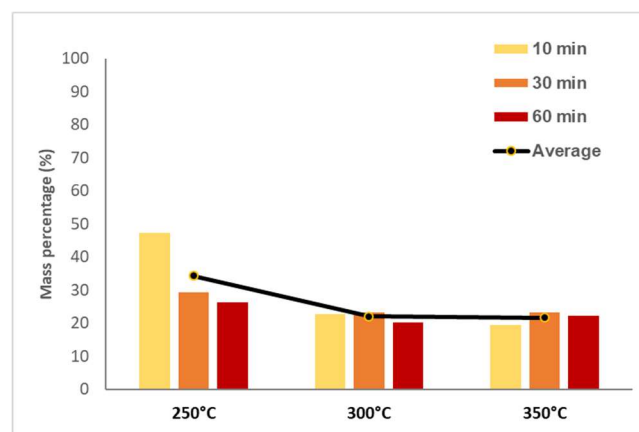
3.2. Carbon obtaining

Graph 3 illustrates the percentages of solid

crude oil recovery at each temperature and reaction time. Observably, the recovered mass in each pyrolysis reaction, representing coal and non-volatile compounds, tends to stabilize within a range of 47-58% as the temperature rises. This trend is more evident in Graph 4, which displays remarkably similar carbon mass percentages at 300°C and 350°C. Yet another noteworthy consideration is the consistent similarity in carbon mass percentages obtained at each temperature, regardless of the reaction times. In other words, the amount of carbon initially formed in the pyrolysis process remains unchanged throughout the experiment.



Graph 3. Mass percentage of non-volatile fraction obtained in the static pyrolysis of soybean waste at different times and temperatures.



Graph 4. Mass percentage of carbon fraction obtained in the static pyrolysis of soybean waste at different times and temperatures.

Soxlet equipment utilizing ethanol and acetonitrile as solvents was employed to wash the reaction crude and extract the solid carbons. An interesting observation was made: with increasing reaction temperature, the cleaning solution exhibited reduced coloration, indicating a lesser presence of organic residues adhering to the solid

material. This phenomenon can be attributed to the increased occurrence of biomass fragmentation at higher temperatures. This leads to a higher production of volatile compounds that are effectively eliminated during the reduced pressure drying of the solid carbons obtained.

The FTIR spectra of the biocarbons were compared with a commercial activated carbon sample (AC), analyzing the appearance, disappearance, or reduction of bands (Figure 3). In the activated carbon, distinct bands at approximately 1450 cm^{-1} correspond to C-C vibrations in aromatic rings, while bands around 1500 cm^{-1} indicate C=C stretching vibrations within the plane. Similarly, the biocarbons exhibit bands within the same range, validating the presence of C=C and C-C skeletal bonding. A distinguishing feature of these biocarbons was the heightened intensity of bands between $2900\text{--}3100\text{ cm}^{-1}$ associated with C-H stretching, indicating a higher degree of incomplete cellulose cracking.

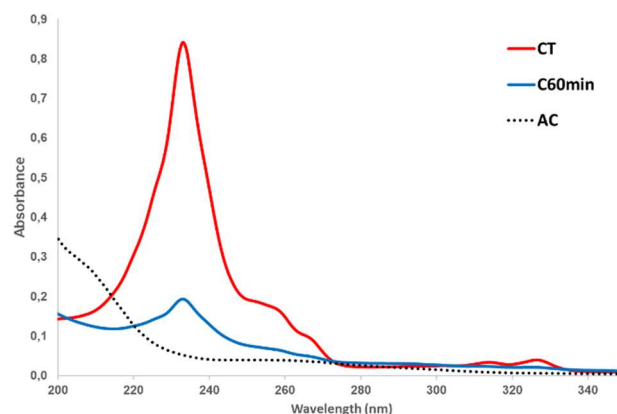
Consistent patterns emerge across all reaction durations and temperatures when comparing the biochars among themselves. Considering this, the carbons obtained at 350°C for 60 minutes (labeled as C60min) were chosen for the adsorption tests due to their easier washing properties.

3.3 Pesticide adsorption tests

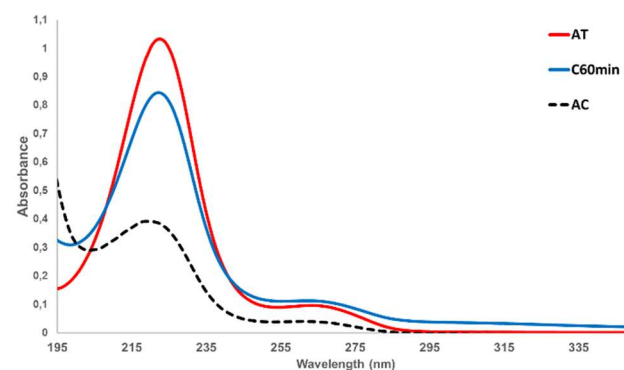
The molar absorption coefficient at the corresponding maximum absorption wavelengths obtained for three pesticides were Chlorothalonil: $\epsilon_{233\text{nm}} = 66400\text{ M}^{-1}\text{ cm}^{-1}$; Atrazine, $\epsilon_{222\text{nm}} = 34386\text{ M}^{-1}\text{ cm}^{-1}$ and Dicamba: $\epsilon_{205\text{nm}} = 35306\text{ M}^{-1}\text{ cm}^{-1}$.

After examining the spectral curves of the pesticide solution following its filtration through the C60min biocarbon, a significant decrease by 77% of its concentration was observed (Graph 3). AC also achieved good adsorption with 94% retention.

In the case of Atrazine, its adsorption was found to be not very effective, achieving only 18% retention by the C60min (Graph 4). Likewise, AC did not achieve near complete retention as it had with Chlorothalonil and showed a 62% decrease in Atrazine concentration.

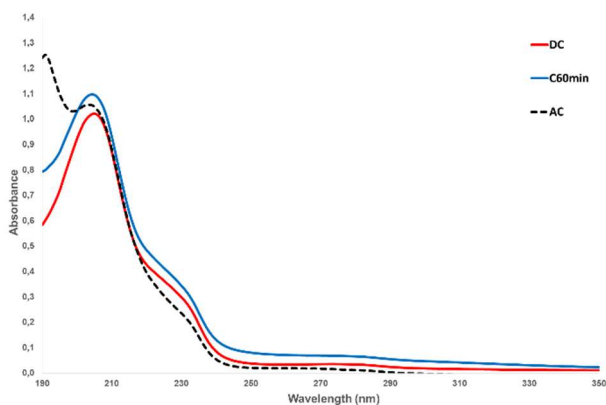


Graph 5. Spectral curves comparison for Chlorothalonil. Red line: CT $1.4\mu\text{M}$ solution. Blue line: CT $1.4\mu\text{M}$ solution after passage through the C60min. Dashed line: CT $1.4\mu\text{M}$ solution after passage through the commercial activated carbon.



Graph 6. Spectral curves comparison for Atrazine. Red line: $28\mu\text{M}$ AT solution. Blue line: $28\mu\text{M}$ AT solution after passage through the C60min. Dashed line: $28\mu\text{M}$ AT solution after passage through the AC.

The pesticide Dicamba exhibited distinct behavior, as it was not retained by either the C60min or the activated carbon. Upon a thorough analysis of spectral curves, it is evident that the transit of the Dicamba solution through the disc extraction cartridge housing C60min or activated carbon triggers an elevation in absorbance, presumably attributed to an augmented baseline. Essentially, it is conceivable that Dicamba facilitated the extraction or dissolution of carbon, potentially resulting in a cleansing effect.



Graph 7. Spectral curves comparison for Dicamba. Red line: 27 μ M DC solution. Blue line: 27 μ M DC solution after passage through the C60min. Dashed line: 27 μ M DC solution after passage through the AC.

Based on the findings, it is evident that CT demonstrates a stronger affinity towards the carbonaceous structure. This propensity could be attributed to its higher proportion of chloro substituents, which provide the molecule with an apolar character that facilitates an effective interaction between the solid material and the pesticide. Conversely, AT that also bears chloro groups shows a weaker interaction with the biocarbon. This can be explained by the more polar feature of the molecule due to the triazine ring and the secondary amine moieties, which reduce the AT engagement with the biocarbon. Lastly, DC, characterized by its acidity and being the most polar among the series, exhibits no retention, displaying a greater inclination towards the aqueous solvent system (water:acetonitrile, 7:3).

4. CONCLUSIONS:

The production of several VOCs of potential atmospheric impact from burning biomass soybean residues was evidenced. In addition, it was determined that the formation of mono-carbon compounds is favored by the increase in temperature and pyrolysis time because the cracking processes are promoted.

The carbonaceous solids obtained in this study displayed notable efficacy in retaining pesticides like Chlorothalonil and Atrazine within aqueous solutions. Considering that these carbons underwent no chemical activation, their demonstrated effectiveness is regarded as promising and suggests potential for

enhancement via supplementary treatment methods. The thermal or chemical activation of the carbonaceous solids studied is expected to further improve their compound adsorption properties. Exploring these carbons in aqueous matrices containing different pesticides or mixtures thereof would also be a valuable avenue for future research.

5. DECLARATIONS

5.1. Study Limitations

The study is limited to the sample size and the methods employed.

5.2. Acknowledgements

N. M. Ceballos thanks the CONICET for her Postdoctoral fellowship.

5.3. Funding source

The work at the Instituto de Investigaciones en Físicoquímica de Córdoba (INFIQC) was supported by Consejo Nacional de Investigaciones Científicas y Técnicas (CONICET grant number: PIP 11220170100423CO), Fondo para la Investigación Científica y Tecnológica (FONCyT grant number: PICT-2017-1555), Programa Institucional y Multidisciplinar (Primar) en Temas Prioritarios (Primar-PT 32520170100334CB) and Secretaría de Ciencia y Tecnología (SeCyT-UNC grant number: SeCyT N°411/18).

5.4. Competing Interests

The authors declare no conflict of interest.

5.5. Open Access

This article is licensed under a Creative Commons Attribution 4.0 (CC BY 4.0) International License, which permits use, sharing, adaptation, distribution, and reproduction in any medium or format, as long as you give appropriate credit to the original author(s) and the source, provide a link to the Creative Commons license,

and indicate if changes were made. The images or other third-party material in this article are included in the article's Creative Commons license unless indicated otherwise in a credit line to the material. Suppose material is not included in the article's Creative Commons license, and your intended use is not permitted by statutory regulation or exceeds the permitted use. In that case, you will need to obtain permission directly from the copyright holder. To view a copy of this license, visit <http://creativecommons.org/licenses/by/4.0/>.

ACKNOWLEDGMENTS:

6. REFERENCES:

1. Wang, G.; Dai, Y.; Yang, H.; Qingang, X.; Wang, K.; Zhou, J.; Li, Y. (2020). A Review of Recent Advances in Biomass Pyrolysis. *Energy Fuels*, 34(12), 15557–15578. <https://doi.org/10.1021/acs.energyfuels.0c03107>
2. Pepino, A. J.; Peláez, W. J.; Faillace, M.; Ceballos, N. M.; Moyano, E. L.; Arguello, G. A. (2014). (S)-5-Benzyl- and 5-benzylidene-imidazo-4-one derivatives synthesized and studied for an understanding of their thermal reactivity. *RSC Advances*, 4, 60092–60101. <https://doi.org/10.1039/C4RA11046C>
3. Firpo, G.; Cooke, M. V.; Peláez, W. J.; Chans, G. M.; Argüello, G. A.; Gómez, E.; Alvarez Toledano, C. (2017). Rearomatization of trifluoromethyl sulfonyl dihydropyridines: Thermolysis vs photolysis. *J Phys Org Chem*. e3789. <https://doi.org/10.1002/poc.3789>
4. Lewoyehu, M. (2021). Comprehensive review on synthesis and application of activated carbon from agricultural residues for the remediation of venomous pollutants in wastewater. *J. Anal. Appl. Pyrolysis*, 159, 105279-105296. <https://doi.org/10.1016/j.jaap.2021.105279>
5. Hassaan, M. A.; El Nemr, A. (2020). Pesticides pollution: Classifications, human health impact, extraction and treatment techniques. *Egypt. J. Aquat. Res.* 46(3), 207-220. <https://doi.org/10.1016/j.ejar.2020.08.007>
6. Kiefer, K.; Bader, T.; Minas, N.; Salhi, E.; Janssen, E. M.-L.; von Guten, U.; Hollender, (2020). Chlorothalonil transformation products in drinking water resources: Widespread and challenging to abate. *J. Water Research*, 183, 116066-116077. <https://doi.org/10.1016/j.watres.2020.116066>
7. Chen, X.; Zhou, Q.; Liu, F.; Peng, Q.; Teng, P. (2019) Removal of nine pesticide residues from water and soil by biosorption coupled with degradation on biosorbent immobilized laccase. *Chemosphere*, 233, 49-56. <https://doi.org/10.1016/j.chemosphere.2019.05.144>
8. Mohaupt, V.; Völker, J.; Altenburger, R.; Birk, S.; Kirst, I.; Kühnel, D.; Küster, E.; Semerádová, S.; Šubelj, G.; Whalley, C. (2020). Pesticides in European rivers, lakes and groundwaters - Data assessment. ETC/ICM Report 1/2020. *European Topic Centre on Inland, Coastal and Marine waters*. Retrieved from <https://www.eionet.europa.eu/etcs/etc-icm/products/etc-icm-reports/etc-icm-report-1-2020-pesticides-in-european-rivers-lakes-and-groundwaters-data-assessment>
9. Vievard, J.; Alem, A.; Pantet, A.; Ahfir, N.-R.; Arellano-Sánchez, M. G.; Devouge-Boyer, C.; Mignot, M. (2023). Bio-Based Adsorption as Ecofriendly Method for Wastewater Decontamination: A Review *Toxics*, 11(5), 404-437. <https://doi.org/10.3390/toxics11050404>
10. Rani, M.; Shanker, U.; Jassal, V. (2017). Recent strategies for removal and degradation of persistent & toxic organochlorine pesticides using nanoparticles: A review. *Journal of Environmental Management*, 190, 208-222. <https://doi.org/10.1016/j.jenvman.2016.12.068>

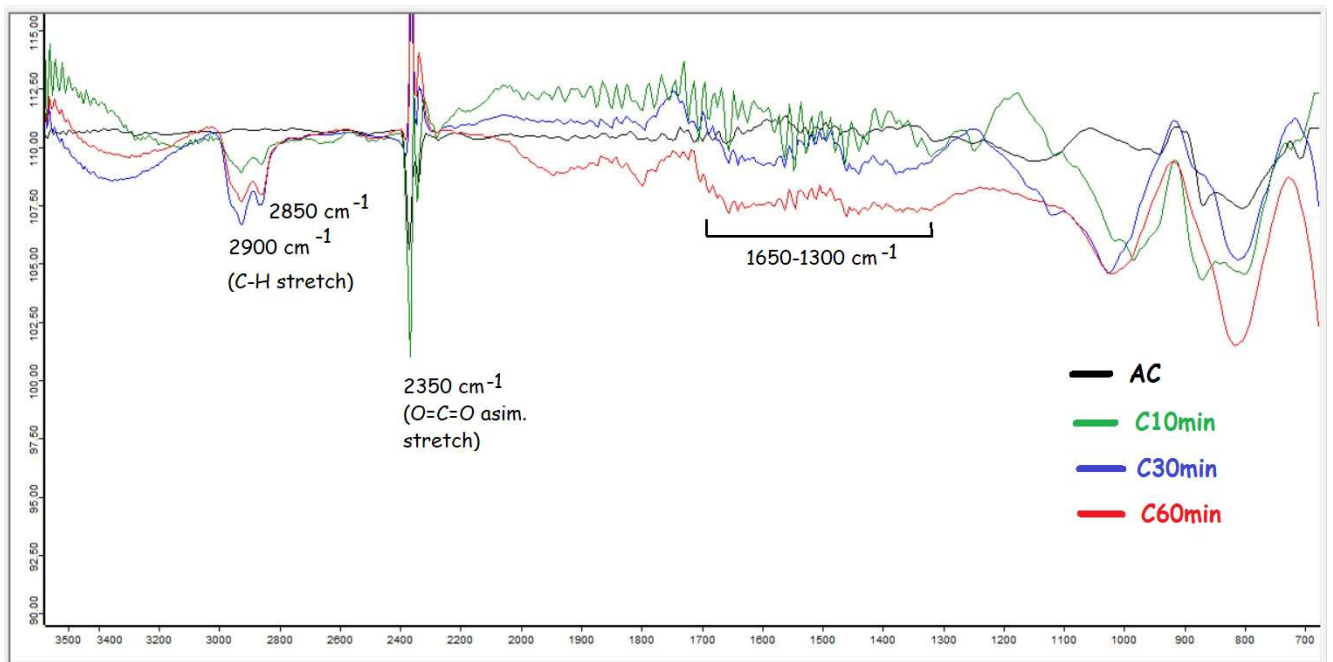


Figure 3. FTIR spectra comparison of commercial activated carbon (AC) and Biocarbons obtained at $350 \text{ }^{\circ}\text{C}$ at different reaction times.

REVIEW OF AIR POLLUTION RESEARCH RESULTS ON THE EXAMPLE OF TBILISI

KUPATADZE, Ketevan^{1*}

¹ Iliia State University, Faculty of Natural Science and Medicine

* Corresponding author

e-mail: ketevan_kupatadze@iliauni.edu.ge

Received 16 August 2023; received in revised form 18 September 2023; accepted 20 November 2023

ABSTRACT

Background: Air pollution is one of the significant environmental challenges facing modern humanity. Atmospheric air is polluted with harmful substances emitted from anthropogenic and natural sources. **Aim:** The presented paper provides an overview of monitoring results conducted in the Capital of Georgia for 2023. Results from air quality monitoring sensors show that particulate matter, sulfur, and nitrogen dioxide represent problematic pollutants in different city areas. **Methods:** The research was carried out through sensors installed in different districts of Tbilisi. The investigation was carried out within the NATO SPS program project REACT. **Results:** Atmospheric air pollution was monitored at four stationary sensor sets on K. Cholokashvili, Nutsubidze Street, Chavchavadze Avenues, and the Old Tbilisi area. The results are presented in the article in the form of tables. **Discussion:** Average indexes of sulfur dioxide and PM particles were observed in all areas. Nitrogen dioxide indices were both low and medium. **Conclusions:** Based on the data obtained, it can be assumed that the air in most districts of Tbilisi is moderately polluted, and in some cases, the data exceeds the maximum allowable norm. There may be several reasons for this.: 1. Unauthorized slashing of Green islands and massive construction of high-rise residential buildings on their place in Tbilisi. 2. Malfunctioning vehicles, the technical inspection of which has recently been made stringent. However, some vehicles still pollute the air. 3. Emissions produced by mini factories and enterprises.

Keywords: Air monitoring, Air Pollution, Pollutant agents, Air purity Recommendations.

1. INTRODUCTION

According to a study by the European Environment Agency (<https://www.eea.europa>), air pollution in European cities causes up to 400,000 premature deaths per year; Noise pollution - up to 12,000 premature deaths dramatically increases stress. All this, more and more painfully, affects the least affluent sections of the cities because they are the ones who live in the heavily polluted urban parts.

According to the report, due to ambient and indoor air pollution in Georgia, 140 people die per 100,000 inhabitants yearly, which is quite a high rate.

The 2018-2023 national action plan (<https://test.ncdc.ge/Handlers/GetFile.ashx?ID=951a795c-ab20-4bdd-8f32-57959e3e1728>) for the

environment and health of Georgia sets "the reduction of the harmful effects of atmospheric and indoor air pollution on the health of the population" as one of its strategic tasks. In 2018-2021, specific steps were taken in this direction; for example, the Parliament of Georgia investigated the causes of air pollution in Tbilisi, expanded the air pollution monitoring network, and approved new standards concerning primary air pollutants. From 2019, the information available at the automatic atmospheric air monitoring stations became available at www.air.gov.ge

In 2021, the Parliament of Georgia adopted the Law on Environmental Liability, the purpose of which is the legal regulation of environmental damage issues following the "polluter pays" principle. The law came into full force on July 1, 2023. However, air pollution remains a severe

problem in the country (<https://greenalt.org/en/blogs/7635/>).

Four sets of sensors were installed at different locations by the REACT research team of Ilia State University in Tbilisi. All four locations belong to Ilia State University. This ensures they function without damage/vandalism. Also, all four sites are of interest for research, and there are no sensors of the National Environment Agency located here. So, it is doubly essential to research the specified locations.

2. MATERIALS AND METHODS

2.1. Materials

The investigation was conducted within the NATO SPS project REACT with the following sensor sets.

- WMO-compliant MicroMET3 multichannel datalogger (8 channels)
- double power supply from 220V and solar panel 30W
- 12Ah buffer battery
- Local data storage 2GB SD card
- GPRS data transmission system
- IP65 box
- Cables, poles, and brackets

- Meteo sensors: temperature, relative humidity, atmospheric pressure, wind speed, wind direction
- Gas sensors: SO₂, NO₂
- Particulate matter sensor PM10-2.5-1
- Phonometer

Key data structure features

- S.D. local data storage (.txt) and frequency setting (5 min)
- Cumulative daily data file
- GSM transmission and frequency setting
- Desktop web access/download (.txt/.csv)
- Automatic access

2.2. Methods

2.2.1. Location M188

The Seismology Research Institute, which belongs to Ilia State University, has been selected as this location.

Next to the location of the M188 sensor, there is also construction (Fig. 1). This construction is illegal, and the research institute has filed a lawsuit in court. However, the decision was delayed, and the construction continued.



Figure 1. Sensor 188 and surrounding construction

2.2.2. Sensor M185

This set of sensors is located directly next to the main buildings of Ilia State University, on the side of the road, where G. Tsereteli Street is connected to Cholokashvili Avenue. There is always much traffic, and besides the fact that the sensors are protected, it is also a significant place for monitoring. Fig. 2.

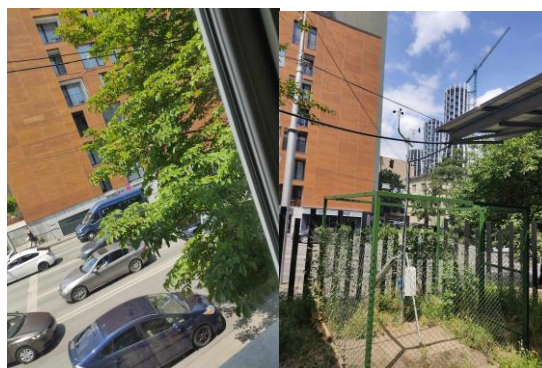


Figure 2. Sensor M185 and its surrounding area

2.2.3. Sensor 186

The sensors are located at Chavchavadze Avenue, #32. It is one of the central and busiest places in Tbilisi. Two large university buildings, cafes, restaurants, and shops are on the avenue. Therefore, it is very interesting for research, Fig. 3.



Figure 3. Sensor 186 and its surrounding area

2.2.4. Sensor 187

The sensors are located on the territory of the Scientific Research Institute of Botany (Fig. 4).

The institute is located on the upper side of the old sulfur baths. It is a very touristic place and therefore attractive for research.

Here, the sensor was installed first. Therefore, the investigation has been ongoing since March of 2023.

According to various sources (VanLoon, G.W. 2011; Cichowicz, 2017; Wetchakun, 2011), the permissible norm of NO_2 is up to 40 ppb (emission during one hour). 40-100 is good, 100-200 is average, 200-400 is bad, 400-1000 is alarming. fig. 1 See the action of nitrogen oxides to other air pollutants. Nitrogen dioxide is associated with the formation of PAN, VOC, PM, and nitric acid. In high temperature and humidity conditions, it appears as a precursor of smog (Castanas, 2016; Vallero, 2014). products.

3. RESULTS AND DISCUSSION

3.1. Results

The tables with results are presented in the appendix of the article (Tables 1-4).

3.2. Discussions

3.2.1. Location M187

The results obtained mean that the data is satisfactory. The maximum rate of NO_2 varies between 60-80 in March and April. Within 100-200, it is observed that max. The indicator is in the first half of May and June. fig. 5. According to the given NO_2 cycle, we can assume that the increased amount is due to the construction in the area. The construction was carried out in a small dose in March and April and resumed in May. Also, the traffic of construction vehicles increased. In general, this area has less traffic because it is a tourist and pedestrian area.



Figure 4. Sensor M187, Its surrounding area and construction

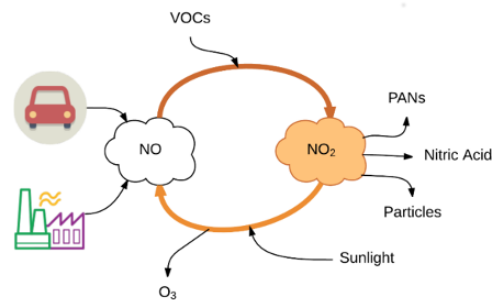


Figure 5. Simplified cycle of NO_2

Nitrogen dioxide and surface ozone are smog's primary and secondary triggering factors (Chapman, 2020; Tobiszewski, 2015; De Vito, 2009). Also, it is very harmful to the respiratory system. The amount of SO_2 in old Tbilisi is natural, as sulfur-enriched water comes in, releasing sulfur dioxide that reacts with hydrogen sulfide in the air to form water and sulfur. Excess dioxide reacts with the released water vapor, forming sulfuric acid. As a result, we get acid precipitation. The characteristic smell of rotten eggs (the smell of hydrogen sulfide) and sulfur can be felt in the area.

SO_2 levels up to 100 ppb pass very well. According to the data, the maximum here does not exceed 60-70.

The amount of PM1, PM2.5, and PM 10 particles is significant. Here, benzopyrene, dioxin, and heavy metal ions can be attracted to the central dust particles. PM1 -0-10 Good condition. According to our data, the number often reaches 15-20, which is undoubtedly due to construction dust.

PM2,5 0-20 is in good condition; 50-800 is very bad. According to our data, 205 indicators were recorded in the second half of March and 120 in the second half of June.

In other cases, it is 50-60 during the day; at night, it can be 0.11-8. In this case, the reason is again the construction and location. Here, we mean the vicinity of the botanical garden. The study period it coincided with the pollination period of various plants. Also, windiness is observed during this period, and we can assume these particles are mixed in the construction dust. Also, in May, there was a trend of increasing the number of PM particles throughout Georgia, especially noted on the National Environment Agency website. The agency cited the movement of large dust masses from the border regions.

PM10 is normal 0-20, 35-50 average, 50-above bad. In our study, two alarming increases are observed, with some days during the hot part

of the day in May with 219 and in June with 120 recorded during the day. The general trend is 10-12.

The maximum noise level is 70 decibels. According to data from various sources (Williams, J. 2012), this type of pollution is caused by construction and light vehicles (Fig.6).

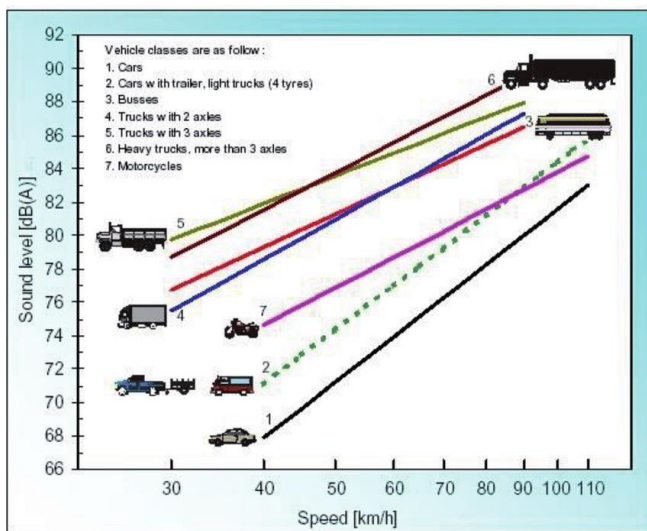


Figure 6. Noise indicators from vehicles.

As for July, Tbilisi always has a high temperature. Sulfur dioxide emissions are within normal limits this month. From average to bad, we can characterize the maximum nitrogen dioxide data. PM 1; The highs of 2.5 and 10 are high, but that's average this month. The increased number is also due to windy weather, adjacent construction, and the period of pollination of plants in the botanical garden (every plant has its characteristic period).

In August in Georgia, the so-called "thermal shock" manifested in very high temperatures and humidity. The sensor on location MM 187 shows a maximum temperature of 40 degrees. Humidity is also increased. Max. Nitrogen dioxide is 92.68, the minimum is 5.08, and the average is 43.7. However, even with the maximum indicator, it can still be considered a good indicator on average. The quantitative condition of sulfur dioxide is in the "good" indicator because max. 31.71 is fixed. There is an increase in PM particles, especially PM 2.5-10. Again, this could be due to construction. Also, the seasonal pollination of various plants and allergens has increased, spreading through the wind, and the sensor records this. For example, One of the most allergic

weed plants is ambrosia (Ambrosia) (Stefan, 2020; Spinelli, 2017), and its peak of flowering is in August. Various studies (Baldauf, 2008. Solomon, 2008; Kelly, 2017) have shown that high temperatures and air pollution contribute to weeds' long flowering and pollen spread.

The noise level varies within the norm.

3.2.2. Location M188

The study of NO₂ showed that the emission is fixed within the allowed norm. The minimum indicator is 15; the maximum is recorded in June at 85. In our opinion, the existence within the norm is since there is a forest around it. The minimum amount of SO₂ is eight, and the maximum is 43. This gas is also within the norm. The amount of PM1, PM2,5, and PM 10 are following:

PM1 min. 0.11, avereg. 7 and max. 69.

PM2,5 min. 0.12, avereg. 5 and max. In the first part of June, it was 167 ppm.

PM 10 min. 0.10, avereg. 7 and max. 195ppm.

At this location, construction dust affects the amount of PM particles. However, the maximum values are recorded in single days. The rest of the time, we see a relatively low value, which, we think, is also due to the proximity of the forest and many trees. The noise level ranges from 40-70 dB, which fully corresponds to the construction noise, although it does not exceed the norm.

In Georgia, particularly in Tbilisi, the months of July and August are characterized by exceptional heat and high humidity. So, for example, in July, the maximum temperature at this location is 34-36 C⁰. This is even though it is an elevated place with a forest park nearby. The maximum nitrogen dioxide is 73-80 ppb, so the situation is not bad. The maximum amount of Sulfur dioxide is 37-40 ppb. According to markers (Davide, A.2018), this condition can be considered very good. Fairly high maximum indicators are recorded for PM1, PM 2.5, and PM10 indicators, which can also be attributed to construction dust.

At this location in August, max. temperature is 42 degrees. The maximum nitrogen dioxide was recorded at 87.95, which is considered a good indicator. The amount of sulfur dioxide is within the range of good, max. 43.29ppb. PM particles are also increased in this area, and it can be said that sometimes max. The number reflects a deplorable situation. PM1 0,11/7.9/ 31.66; PM2.5 0.12/4.24/88.53; PM10 0.12/6.42/98.85. There is also illegal construction and forest cover near this location. Therefore, there may have been reasons

similar to the MM 187 location. However, in summer, the number of PM particles increases in Tbilisi. The noise is within the norm.

3.2.3. Sensor M185

Despite such traffic, nitrogen dioxide is within normal limits. In recent years, technical transport inspection and emission control rules have been tightened in Tbilisi. All constructions near this area have also been completed, affecting the amount of nitrogen dioxide. Also, the amount of sulfur dioxide is within the norm.

As for PM particles, their increased number is observed, especially in the second half of May and the beginning of June. The National Environment Agency also noted this fact and stated that a sharp increase in PM particles was observed in the entire Tbilisi territory during the specified period. The reason was transboundary pollution. Mainly since this period is characterized by windy weather. I think the rehabilitation works on the slightly higher side of University Street could also be the reason. Wind can spread Many PM particles from there (fig. 7).



Figure 7. Work at University Street

So, for example, In the second half of May and the beginning of June, the maximum number of PM 1 is 103, and the minimum is 0.23 avg. 35. The average of PM 2.5 and PM 10 The indicator ranges from 40-80, which is, of course, a very high number. The increase is mainly felt during the daytime hours.

The average noise level ranges from 43-70, which is considered a normal indicator.

According to the data for July, the amount of nitrogen dioxide can be considered a regular category and sulfur dioxide is fixed in a relatively small amount. It is holidays, most people are out of the city, and there is less traffic in this section. PM1; PM2.5; PM10 register quite high values only in some sections, but they are mostly within the normal range. The maximum values can be attributed to the dust brought by the wind. The noise level is within acceptable limits.

At this location in August, max. The temperature is 38 degrees. A maximum of 23.45 was recorded for nitrogen dioxide, considered a good indicator. The amount of sulfur dioxide is within the range of excellent, max. 3.52 shows. In this area, too, PM particles range from good to satisfactory. The fact that vehicle emission controls are being tightened reflects the results. The noise is within the norm.

3.2.4. Sensor 186

The amount of nitrogen dioxide is mostly within acceptable limits. Only in the second half of June is the maximum rate of 113.41 recorded, which is still not alarming data. Sulfur dioxide has a maximum value of 43, corresponding to the "very good" value of the air pollution index. The PM1 count is also very good at this stretch. PM2.5 recorded a maximum of 49.5, which qualifies as "poor," according to the index. This is fixed in May. In May, pollution was generally observed in the entire city, which the National Environment Agency noted. PM10 also shows a maximum value of 53 in May, which refers to "bad" conditions.

Special mention should be made of the noise sensor, which did not work at this location until we re-fixed it with a modified method. After that, the data variable was sent again, and the maximum value of 65-67 decibels was recorded.

High temperature is recorded in this location in July. Especially in the second half of the month, when, according to the National Environment Agency, heat waves began to enter Georgia. Increased humidity is recorded. The maximum amount of nitrogen dioxide is quite high. Sulfur dioxide is fixed within the norm. Also, time and time, the increased maximum amount of all PM particles is recorded. The noise level is within the norm.

At this location in August, max. The temperature is recorded at 40 degrees. A maximum of 100 was recorded for nitrogen dioxide, considered an average indicator. The amount of sulfur dioxide is within the excellent range. 82.08 shows. In this area, too, PM particles range from good to satisfactory. The fact that vehicle emission controls are being tightened reflects the results. The noise is within the norm. However, sometimes it is higher than other locations.

4. CONCLUSIONS

Based on the results obtained, it can be assumed that the air in most districts of Tbilisi is moderately polluted. However, in some cases, the data exceeds the maximum allowable norm. There may be several reasons for this.

Based on the research, the following recommendations can be made: Avoid parking the vehicle with the engine running; Replace the engine air filter on time; Maintain the recommended air pressure in the tires; Do not continue to refuel after the refueling device (pistol) automatically shuts off after filling up the tank; Use cruise control as much as possible, which itself regulates the speed of movement; Moving at low engine speeds reduces fuel consumption; The gearbox should be switched to high gear as early as possible and to low gear as late as possible; When moving the traffic light in red mode, move in approaching the traffic light using inertia; Plan the movement; Do not preheat the engine. Start the car and drive for a short time at low speeds until the engine warms up.

5. DECLARATIONS

5.1. Acknowledgements

Special acknowledgment to the REACT project team.

5.2. Funding source

The investigation is done in the scope of the NATO SPS program project "RACT".

5.3. Open Access

This article is licensed under a Creative Commons Attribution 4.0 (CC BY 4.0) International License, which permits use, sharing, adaptation, distribution, and reproduction in any medium or format, as long as you give appropriate credit to the original author(s) and the source, provide a link to the Creative Commons license, and indicate if changes were made. The images or other third-party material in this article are included in the article's Creative Commons license unless

indicated otherwise in a credit line to the material. Suppose material is not included in the article's Creative Commons license, and your intended use is not permitted by statutory regulation or exceeds the permitted use. In that case, you will need to obtain permission directly from the copyright holder. To view a copy of this license, visit <http://creativecommons.org/licenses/by/4.0/>.

6. REFERENCES:

1. <https://www.eea.europa>
2. <https://test.ncdc.gov/Handlers/GetFile.ashx?ID=951a795c-ab20-4bdd-8f32-57959e3e1728>
3. www.air.gov.ge
4. <https://greenalt.org/en/blogs/7635/>
5. Cichowicz, R., Wielgosiński, G. & Fetter, W. (2017) Dispersion of atmospheric air pollution in summer and winter season. *Environ Monit Assess*, 189, 605.
6. Wetchakun, K. Samerjai, T. (2011) Semiconducting metal oxides as sensors for environmentally hazardous gases. *Sensors and Actuators, B: Chemical*. vol. 160, no. 1, pp. 580–591.
7. Kampa, M., Castanas, E. (2016) Human Health effects of air pollution.
8. Vallero, D. (2014) Fundamentals of Air Pollution.
9. Stefan, C., Claudio, E. (2020) Air Quality Control through Bike Sharing Fleets. *IEEE Symposium on Computers and Communications (ISCC)*, pp.1-4.
10. Spinelle, L., Gerboles, M. (2017) Review of Portable and Low-Cost Sensors for the Ambient Air Monitoring of Benzene and Other Volatile Organic Compounds. *Sensors*. vol. 17, no. 7, p. 1520.
11. Chapman, J., Truong, V., Elbourne, A. (2020) "Combining Chemometrics and Sensors: Toward New Applications in Monitoring and Environmental Analysis," <https://dx.doi.org/10.1021/acs.chemrev.9b00616>.
12. Tobiszewski, M., Zabiegała, B. (2015) "Current air quality analytics and monitoring: A review," .
13. De Vito, S. (2009) C.O.
14. , NO₂ and NO_x urban pollution monitoring with on-field calibrated electronic nose by automatic bayesian regularization." *Sensors and Actuators, B: Chemical*. vol. 143, no. 1, pp. 182–191.
15. Desislava, I., Angel, E. (2019) Intelligent

- System for Air Quality Monitoring Assessment using the Raspberry Pi Platform. *International Conference on Information Technologies (InfoTech)*, pp.1-4.
16. Davide, A.(2018) Canarin II: Designing a smart e-bike eco-system. *15th IEEE Annual Consumer Communications & Networking Conference (CCNC)*, pp.1-6.
 17. Jerry, G. (2017) Crowd-Based Mobile Sensor Cloud Services — Issues, Challenges and Needs. *International Conference on Computational Science and Computational Intelligence (CSCI)*, pp.618-623.
 18. VanLoon, G.W. (2011) “Environmental Chemistry-a global perspective”. Oxford Group.
 19. Williams, J. (2012) “Environmental Chemistry”. J. Wiley & Sons, Canada.
 20. Baldauf, R., Thoma,E. (2008) Traffic and meteorological impacts on near-road air quality: Summary of methods and trends from the Raleigh near-road study. *Journal of the Air and Waste Management Association*. vol. 58, no. 7, pp. 865–878.
 21. Solomon, P. (2008) Key scientific findings and policy- and health-relevant insights from the U.S. Environmental Protection Agency’s particulate matter supersites program and related studies: An integration and synthesis of results.
 22. Kelly, K. (2017) Ambient and laboratory evaluation of a low-cost particulate matter sensor.” *Environmental Pollution*. vol. 221, pp. 491–500.

Table 1. Data from sensor 187

		Air temperature	Wind Direction	Wind Speed (m/s)	NO ₂ (ppb)	SO ₂ (ppb)	Humidity (%)	Air Pressure (hPa)	PM1 (mg/m ³)	PM2.5 (mg/m ³)	PM10 (mg/m ³)	Phonometer (db)
3-17 Mart	Min	-3.5 (7)	1	0.01	5.58	1.17	17.81	1012.68	0.11	1.12	0.12	41.8
	Max	17	358	3.97	61.56	43.06	99.8	1038.04	53.12	205.56	250.75	63.07
18-31 Mart	Min	1 (11)	1	0.03	9.38	1.18	15.13	989.45	0.12	0.12	0.12	41.79
	Max	24	378	4.28	68.29	34.01	99.6	1019.36	49.06	181.29	219.98	64.18
1-15 April	Min	4.2	1(148)	0.04	21.34	0.59	20.68	944.02	0.12	0.11	0.15	43.69
	Max	24.35	359	10.33	82.67	34.59	95.18	968.57	25.73	61.21	66.49	66.12
16-30 April	Min	8.36	1(153)	2.07	22.28	0.59	20.62	950.7	0.12	0.11 (10)	0.11(12)	43.96
	Max	26.27	359	8.79	81.5	34.15	95.7	972.24	24.15	52.36	62.3	64.98
1-15 May	Min	12.58	1(16)	0.04 (0.17)	5.28	6.71	23.7	1010.93	0.11 (7)	0.12 (8)	0.11 (10)	42.98
	Max	27.77	352	4.49	152.44	31.66	83.85	1022.09	23.8	56.75	62.97	69.59
16-31 May	Min	20.86	0	0	7.12	10.98	32.36	1009.44	0.12 (8)	0.12 (7)	0.12 (8)	45.26
	Max	29.13	0	0	262	32.06	77.92	1027.06	32.95	69.65	73.76	69.66
01-15 June	Min	15.57	1(146)	0.04 (2)	22.28	5.3	28.79	951.28	0.12 (6)	0.11 (3)	0.11 (4)	44.56
	Max	33.01	359	9.25	84.43	31.66	90.66	965.91	15.13	24.62	27.09	65.88
16-30 June	Min	15.12	1 (155.27)	0.04 (2)	24.04	2.93	26.68	949.37	0.12 (6)	3.41	4.24	44.2
	Max	33.61	359	10.02	90.85	32.83	95.35	965.39	20.17	120.54	159.47	66.72
1-15 July	Min	15	1(152)	2.59	21.95	0.61	18.39	949	0.12	2.68	3.49	44.12
	Max	34	359	14	84.15	32.83	93.26	966	15.24	28.41	32.44	67.64
16-31 July	Min	16	1(122)	2.95	15.83	0.59	22.12	952	0.11	4.7	5.99	43.68
	Max	36	359	11.63	85.01	57.93	92.04	963	15.36	27.55	29.37	65.55
1-31 August	Min	17	149	0.35	25.21	9.03	20.23	943	0.11/7.9	0.12/4.24	0.12/6.42	46.43
	Max	40	359	3.09	87.95	43.29	99.42	961	31.66	88.53	98.85	65.88
1-30 September	Min	11.50	1/174	0.31	26.99	15.71	22.78	948	9.43	5.42	6.68	55.37
	Max	35.44	324	6.4	113.16	83	97.39	970	45.12	166	205.61	83.12

Table 2. Data from sensor 188

		Air temperature	Wind Direction	Wind Speed (m/s)	NO ₂ (ppb)	SO ₂ (ppb)	Humidity (%)	Air Pressure (hPa)	PM1 (mg/m ³)	PM2.5 (mg/m ³)	PM10 (mg/m ³)	Phonometer (db)
4-18 Mart	Min	9	1(161)	1.24	15.24	9.3	15.36	1013.56	0.11 (15)	0.12(32)	1.02 (14)	40.81
	Max	18	359	4.43	43.83	71.77	99.53	1040.85	51.71	158	188	64.38
19-31 Mart	Min	11	1(185)	1.28	30.49	15.24	15.23	989.72	0.11(18)	0.11 (40)	0.12 (51)	41.34
	Max	22.53	350	4.62	76.29	45.73	99.9	1040.85	60.15	180	205	63.65
1-15 April	Min	11	1(190)	1.21	15.48	12.22	25.99	990.23	0.11(12)	0.11 (16)	0.10 (21)	40.92
	Max	23	360	9.26	76.22	45.73	99.55	1022.79	35.65	106.26	128.84	64.43
16-30 April	Min	4.7	1(190)	1.27	15.22	15.11	23.31	998.36	0.12 (8)	0.11 (5)	0.11 (7)	41.55
	Max	24.19	359	5.92	106.71	45.70	99.9	1028.45	24	49.57	58.38	70.53
1-15 May	Min	4.17 (15)	1(130)	0.67	18.56	8.79	24.1	950.26	0.11 (7)	0(2.85)	0(3.87)	45.55
	Max	26.29	359	3.51	69.18	43.39	97.51	963.88	24	69.65	74.23	66.19
16-31 May	Min	6 (20)	1(143)	0.22	19.35	7.04	22.43	949.4	0.11(8)	0.9 (5.13)	0.12 (7)	45.48
	Max	33	355	2.59	77.44	43.97	97.7	959.33	48.4	135	160	66.12
01-15 June	Min	14.33	1(140)	0.30	25.21	10.37	29.89	945.72	0.11 (7)	0.11 (2.36)	0.11 (3.94)	45.78
	Max	33.84	359	2.52	85.11	39.42	97.46	960.28	69.07	167.8	195.12	65.93
16-30 June	Min	14.24	1(132)	0.32	24.62	7.93	25.39	943.76	0.11 (7)	0 (2.35)	0(3.52)	45.87
	Max	33	359	2.76	73.29	39.63	99.15	959.44	37.05	120.54	132.74	66.38
1-15 July	Min	13	1 (142)	0.47	24	9.97	21	943	0.12 (7)	1.84	2.91	46.28
	Max	34	359	3.33	80.32	40	97	960	78	27.42	308.4	67.08
16-31 July	Min	14	1 (126)	0.55	29.9	10.43	25.32	946	7.89	2.37	3.85	45.99
	Max	36	359	3.55	73.87	37.52	95.34	957	29.2	63.19	71.53	65.19
1-31 August	Min	17.13	149	0.35	25.21	9.03	20.23	943	0.11/7.9	0.12/4.24	0.12/6.42	46.43
1-30 September	Max	11.73	1(133)	0.27	18.18	9.76	28.87	948	7.61	4.12	5.93	45.35
	Min	34.61	340	3.04	71.34	41.78	97.39	963	45.12	166	205.61	64.11

Table 3. Data from sensor 185

		Air temperature	Wind Direction	Wind Speed (m/s)	NO ₂ (ppb)	SO ₂ (ppb)	Humidity (%)	Air Pressure (hPa)	PM1 (mg/m ³)	PM2.5 (mg/m ³)	PM10 (mg/m ³)	Phonometer (db)
21.04-30.04.2023	Min	7.09		0.03	0(3.8)	0(0.07)	21.44	945.23	0.82	0.12	0.12	45.91
	Max	25.66		4.6	19.35	2.44	95.74	956.06	25.8	53.94	56.52	69.18
1.05-15.05.2023	Min	4.15		0.03	0.59	0(0.05)	21.45	950.23	0.49	0.12	0.11	46.73
	Max	25.63		6.5	22.28	3.66	95.39	964.09	28.54	47.93	49.02	68.78
16.05-31.05.2023	Min	7.37		0(0.68)	0.56	0(0.08)	20.15	949.11	0.59	0.12	0.12	43.94
	Max	33.67		4.27	25.21	4.1	93.45	959.1	34.01	91.82	100.14	69.02
1.06-15.06.2023	Min	14		0.03	0.59	0(0.08)	29.18	945.02	0.42	0.11	0.11	45.48
	Max	21.59		5.27	21.95	4.69	96.25	959.74	30.84	39.52	42.21	70.89
16.06-30.06.2023	Min	14.27		0.03	0.56	0(0.1)	24.2	943.64	0.35	0.11	0.11	45.39
	Max	33.29		7.86	26.22	3.05	95.32	959.22	25.56	29.08	30.14	70.04
1.-15 July	Min	14.3	1 (224)	0.03	0.59	0.07	19.22	943.25	0.12	0.11	0.11	44.85
	Max	33.97	359	5.4	24.04	3.39	93.63	960.39	25.09	37.52	40.92	68.1
16 -31 July	Min	15	1(248)	1.10	7.03	0.07	22.91	946	0.23	7.78	0.11	44.76
	Max	36	359	6.39	29.27	3.18	92.99	957	25.33	35.8	36.7	68.27
1-31 August	Min	17.18	1/216	0.03	0.59	0.072	20.06	942	1.99	0.12	0.15	44.31
	Max	38.36	359	7.77	23.45	3.52	97.67	960	25.8	31.95	32.8	69.61
1-30 September	Min	11.49	1/167	0.48	0.56/26	0.56	24.08	948	0.11/10	5.13	6.15	43.43
	Max	35.32	351	6.4	71.34	41.78	97.39	963	45.12	166.1	205.61	69.03

Table 4. Data from sensor 186

		Air temperature	Wind Direction	Wind Speed (m/s)	NO ₂ (ppb)	SO ₂ (ppb)	Humidity (%)	Air Pressure (hPa)	PM1 (mg/m ³)	PM2.5 (mg/m ³)	PM10 (mg/m ³)	Phonometer (db)
21.04-30.04.2023	Min	9.54		0.03	35.18	2.82	23.91	951.13	0.12	0.11	0.12	30
	Max	26.46		3.07	99.67	31.1	97.81	961.49	26.38	44.56	55.46	30
1.05-15.05.2023	Min	6.37		0.03	28.23	4.52	20.36	955.65	0.11	0.11	0.11	30
	Max	27.62		2.83	102.6	42.21	97.37	970.33	22.99	46.22	53.54	30
16.05-31.05.2023	Min	9.66		0.03	29.32	4.1	21.98	954.38	0.11	0.11	0.12	30
	Max	35.32		3.6	85.01	39.28	94.28	965.08	27.91	49.95	56.64	30
1.06-15.06.2023	Min	16.64		0.03	34.01	4.1	28.69	950.98	0.11	0.11	0.11	30
	Max	34.66		4.02	88.53	43.19	94.9	965.21	21.47	24.39	29.43	64.98
16.06-30.06.2023	Min	15.46		0.03	24.28	3.52	23.25	949.1	0.11	0.11	0.11	42.66
	Max	34.37		4.53	113.41	42.21	97.48	964.74	22.16	25.68	30.72	67.89
1.07-15.07.2023	Min	16.44	1(179)	0.03	18.29	6.35	20.13	949	0.11(11.3)	3.72	5	45.28
	Max	35.77	359	2.96	97.33	58.63	95.98	965	21.46	30.61	34	67.18
16.07-31.07.2023	Min	16	1(166)	0.56	29.32	6.45	23.42	951	0.11/11.3	5.36	7.1	45.26
	Max	41	359	3.26	97.11	41.63	94.4	962	29.08	38.23	45.97	65.68
1-31August	Min	19	1/205	0.36	18.18	4.69	19.53	948	0.11	0.20	0.17	42.36
	Max	40	359	4.02	100	82.08	99.2	965	28.96	38.66	46.22	73.66
1-30 September	Min	11.49	1/177	0.41	35.24	15.29	24.08	948	10.38	5.48	6.75	43.12
	Max	35.46	359	6.4	113.16	53.94	97.39	963	45.12	166.1	178.08	70.03

POTENTIAL EFFECTS OF KETOGENIC DIETS, A NARRATIVE REVIEW

MUSSI STOIZIK, Jessica Anabella^{1*}; AVENA, Maria Virginia²; ELIAS, María Lucia¹; HEREDIA, Lucia¹; BOARELLI, Vanina Paola¹.

¹ Universidad Juan Agustin Maza, Laboratorio de Doenças Metabólicas. Mendoza, Argentina.

² Instituto de Histología e Embriología de Mendoza, CONICET. Mendoza, Argentina.

* Corresponding author
e-mail: jsmussi@gmail.com

Received 17 August 2023; received in revised form 18 November 2023; accepted 01 December 2023

ABSTRACT

Background: Ketogenic diets have a long history of therapeutic use and have recently attracted significant attention due to their promising effects on a variety of disorders. However, no definitive links have been identified. This review aims to highlight the possible impacts of ketogenic diets as well as the mechanisms involved in metabolic processes and related non-communicable metabolic diseases. **Methods:** For our analysis, a bibliographic review of articles about ketogenic diets and their therapeutic effect on chronic pathologies was carried out, retrieved from the scientific literature. **Results and discussion:** These studies found both positive and negative outcomes for the effects and implications of ketogenic diets on metabolism. Significant differences in metabolic markers such as weight, glycemia, serum lipids and lipoproteins, anthropometric measures, and hormones such as insulin, leptin, and adiponectin have been reported. In addition to changes in the microbiome that have modest to moderate concurrent effects, changes in metabolism indicate the significance of dietary changes in treating and preventing chronic non-communicable diseases. **Conclusions:** In this review, we present the available scientific evidence on the effects of the ketogenic diet, and thus ketone bodies, on metabolism and related chronic diseases.

Keywords: *Ketogenic diet, ketone bodies, diet, metabolism, chronic non-communicable metabolic diseases.*

1. INTRODUCTION

Following a dietary plan or regimen, commonly known as a diet, is becoming increasingly popular, not only intending to maintain health but also as a non-pharmaceutical option to combat disease. Currently, there are several types of diets, hypocaloric, paleo, protein, alkaline, and regional, such as the Mediterranean diet, others designed explicitly with a dietary approach to hypertension, or those with a minimum percentage of carbohydrates, such as the ketogenic diet (KD), and protocols that diversify eating patterns, such as intermittent fasting, among others.

On the growing list, KD has a long history of clinical use and has recently gained considerable interest due to its promising potential effects on a wide group of pathologies. These diets

are high in fat and low in carbohydrates, with adequate protein and caloric content (Weber, 2019). Nutritional ketosis, the desired endpoint of KD, is achieved by restricting carbohydrate intake, moderating protein intake, and increasing the number of calories derived from lipids. Thus, a traditional KD consists of 90% of calories from fat, 8% from protein, and only 2% from carbohydrates, compared to the 45-65% of carbohydrates recommended in a standard diet (Wilder, 1921).

In the 1920s, KD was first used as a dietary adjunct in epilepsy to control seizures in patients who did not respond adequately to antiepileptic drugs (Wilder, 1921); (Ulamek-Kozioł, 2019); (Wheless, 2008); (Yuen, 2014). In 1921, Russell Wilder first proposed that a ketone-producing diet could be as effective as fasting for the treatment of epilepsy and coined the term 'ketogenic diet' (Wheless, 2008).

Four main types of KD have been described: classical or long-chain triglycerides (LCT), medium-chain triglycerides (MCT), modified Atkins (MAD), and low glycemic index (LIG) (Kossoff, 2018); (Huttenlocher, 1971). LCT is the most traditional type and is widely used in the clinical setting, with a 4:1 ratio corresponding to a fat/protein or carbohydrate ratio or their combination (Coppola, 2002); (Hassan, 1999). Thus, 90% of calories come from fat; however, when the ratio is 3:1, the caloric contribution from fat is 87%, and the remaining 13% from protein and carbohydrate (Kossoff, 2018); (Seo, 2007).

Due to the severe carbohydrate restriction in this type of KD, Long-chain triglycerides (LCTs) pose an issue due to their unpalatable nature and difficulty in preparation and maintenance. As an alternative, medium chain triglycerides (MCTs) containing octanoic and decanoic acids were devised in 1971, with 60% of the calories they provided. Compared to LCTs, MCTs are more acceptable, ketogenic, and effective, as confirmed by Huttenlocher (1971), Vaisleib (2004), Schwartz (1989), and Neal (2009). However, MCT often leads to gastrointestinal side effects like nausea, vomiting, and sometimes diarrhea (Huttenlocher, 1971); (Liu, 2013). On the other hand, the MAD is based on the Atkins diet, which was popularly used in weight loss. It does not have a strict ketogenic ratio and can usually vary between 1:1 and 1.5:1 and can sometimes reach 4:1. Furthermore, it does not include protein, fluid, or calorie restrictions, carbohydrate intake is restricted to 10-15g/day in the first month and can be increased later to 20g/day (Kossoff, 2003); (Kossoff, 2006); (Foster, 2003); (Kossoff, 2007); (Kang, 2007). Finally, the LIG is also low in carbohydrates, which are restricted to an intake of 40-60g/day, and includes the selection of foods with a low glycemic index and, like the MAD, is easy to implement (Huttenlocher, 1971).

In the initial period of the KD), glucose is primarily produced through gluconeogenesis from amino acids. However, as amino acid consumption decreases, the quantity of glucose acquired from triglyceride (TG) lysis increases due to glycerol liberation (Schutz, 2011); (Dienel, 2019); (Veldhorst, 2009). After a few days of limiting carbohydrate intake, the liver produces ketone bodies (KB) due to the increase in acetyl coenzyme A and fatty acid oxidation. KB is a metabolic state in which the body prefers fat as its primary source of fuel (Owen, 2005); (Bueno, 2013); (Westman, 2007); (McDonald, 2018). This theory emerged from the assessment that a low-carbohydrate, high-fat diet could generate

acetone, acetoacetate, and 3- β -hydroxybutyrate (β HB), the primary KB. These KBs have been associated with favorable impacts on the treatment of epilepsy and other disorders (Wilder, 1921); (Woodyatt, 1921); (Paoli, 2014); (Freeman, 2010). When KBs are introduced into the bloodstream, they are utilized by the brain, heart, and muscles to generate cellular energy within the mitochondria (Ulamek-Kozioł, 2019; Achanta, 2017; McCue, 2010). Elevated levels of circulating KB can result in the presence of KBs in the urine, known as ketonuria, which is often utilized as an indicator of dietary adherence (Paoli, 2014; Newman, 2017).

Thus, the KD can replicate the metabolic effects of fasting without requiring significant caloric deprivation. This dietary approach has generated considerable interest due to potential therapeutic effects on neurological disorders that are hard to treat using standard medications, as well as on specific metabolic parameters. Several studies have noted such potential benefits (Neal, 2008; Stafstrom, 2012; Rusek, 2019; Westman, 2018; Muscogiuri, 2019; Weber, 2020; Paoli, 2019). (Kong, 2021; Gangitano, 2021) It has been suggested that the KD may play a role in the metabolism of various diseases. Despite this, there is a lack of comprehensive reviews detailing such information. Therefore, this review aims to provide an overview of the potential effects of the KD and the mechanisms involved in metabolic processes and associated non-communicable metabolic diseases.

2. MATERIALS AND METHODS

For this study, it was thoroughly reviewed scientific literature on the KD. Our search included reputable databases such as Scielo, PubMed, Medline, Cochrane Library, and Researchgate. The inclusion criteria involved relevant keywords such as "diet", "ketogenic diet", "metabolic diseases", "obesity", "dyslipidemia", "microbiota", and "metabolic effects".

All authors evaluated the relevance of the retrieved records to the inclusion and exclusion criteria and their alignment with the consulted databases by assessing their titles, abstracts, and keywords.

Within the inclusion criteria, we included articles that were accessible in full text and published either in English or Spanish. Our selection incorporates both animal and human studies. For the human studies, we specifically

considered articles that featured adult male and female participants, with endpoints focusing on changes in body weight, lipid profile, or biomarkers of metabolic disease risk. Excluded from the analysis were studies conducted *in vitro*, studies conducted in animal models different from the established one, qualitative studies, and studies that examined the effect on acute diseases or in the absence of metabolic alterations. The search was conducted between March and September 2022. Additionally, while following the established criteria for study inclusion, we conducted manual searches of bibliographic references from the records to identify any pertinent documents that may have been overlooked in the bibliographic search strategies.

3. RESULTS AND DISCUSSION

3.1. Ketogenic diet and its metabolic implication

Non-communicable metabolic disorders (NMDs) are a major cause of mortality worldwide. This term describes a group of conditions that are not primarily caused by acute infections but instead have enduring implications for overall health. Consequently, these pathologies often necessitate ongoing treatment and support (World Health Organization, 2002). Examples of NMDs include diabetes mellitus (DM), obesity, cardiovascular disease, and cancer. These conditions can be prevented by reducing or eliminating common risk factors as a preventive therapeutic objective. The impact of KD implementation has been subject to investigation. Adopting preventive, therapeutic goals to reduce common risk factors to prevent these conditions is recommended. Additionally, the potential impact of implementing the KD requires further study. (Zhang, 2021).

3.1.1 Diabetes Mellitus

The global incidence of diagnosed DM in adults has risen, with undiagnosed cases and individuals at risk of developing the disease (Abuyassin, 2016) also needing to be acknowledged. Type 2 DM is a widely studied disease characterized by chronic hyperglycemia and elevated HbA1c concentrations. As dietary carbohydrates primarily increase these levels, it is logical to assume that reducing carbohydrate intake could be a valuable tool for managing the

disease (American Diabetes Association, 2008; Hallberg, 2018), with potential benefits for glycaemic control, HbA1c levels and body weight (Michalczyk, 2020; Ahmed, 2020). In diabetics, a 24-week study indicated that a very low-carbohydrate diet led to a greater reduction in blood glucose levels than a low-calorie diet (Rafiullah, 2021). Furthermore, a 12-month study found that people with type 2 DM experienced greater weight loss with a high-fat diet than with a high-carbohydrate diet. Similarly, Nanri's (2015) five-year prospective study found an association between low-carbohydrate diets and a lower risk of DM in women, as well as a significant decrease in postprandial glucose concentrations and HbA1c, which was also reported in studies by Dashti (2007), Gannon (2010), Rizza (2010), Hussain (2012), and Nuttall (2008). Consequently, these diets hold promise in aiding patient weight loss and reversing metabolic syndrome manifestations in individuals with type 2 DM (Hallberg, 2018).

In addition, the observed improvement in clinical trials could potentially result in reduced or eliminated insulin requirements. This can be attributed to the strong correlation between insulin resistance and the main ketosis pathways. Glucose transporter type 4, a protein regulated by insulin, has been found to have a direct correlation with proteins involved in DC induced pathways such as 3-hydroxyacyl-coenzyme A dehydrogenase and acyl-coenzyme A oxidase 1 (Farrés, 2010). Furthermore, research conducted on mice suffering from type 2 DM exhibited that KD reduced the expression of type 2 glucose transporter mRNA in the liver, implying a decrease in insulin levels (Zhang, 2018).

On the other hand, both positive and negative outcomes have been noted in individuals with type 1 DM. While KD may enhance glycemic control, they can also potentially cause dyslipidemia, which is a particular worry for those with diabetes who already have an elevated risk of cardiovascular events. Likewise, metabolic irregularities and sustained ketosis are associated with this pathology in individuals with type 1 DM, which may heighten the likelihood of complications (Kanikarla-Marie, 2016; McClean, 2019; Leow, 2018).

The advantages of the KD have predominantly been linked to type 2 diabetes studies. Its efficacy relates to decreased blood glucose levels, HbA1c, and significant weight loss. However, the benefits of KD appear to decrease over time (Brouns, 2018). Short-term studies have reported only a few adverse effects (Ellenbroek,

2014; Westman, 2008; Colica, 2017). However, it should be noted that the use of this diet is not recommended for individuals with type 1 diabetes mellitus, as it may increase the risk of dyslipidemia, even though it may improve glycemic control.

3.1.2 Obesity

In recent years, researchers have noted the advantages of KD in treating patients with obesity. It has been previously stated that in patients with DM, KD can result in weight loss (Foster, 2003); (Westman, 2008); (Dashti, 2004); (Dashti, 2006). A meta-analysis of randomized controlled trials indicated that, compared to low-fat diets, KD was more effective in enhancing metabolic parameters linked to blood glucose, weight, and lipids in obese individuals, chiefly those with pre-existing diabetes (Choi, 2020). In the short term, the KD has significantly reduced body mass index (BMI), body weight, body fat percentage, waist circumference, hip circumference, blood pressure, and insulin resistance significantly. Furthermore, it has substantially decreased serum levels of inflammatory markers like C-reactive protein, proinflammatory cytokines, leptin, and adiponectin (Michalczyk, 2020; Castaldo, 2016; Kong, 2020; Walton, 2019; Monda, 2020). Therefore, the KD would impact hormonal levels, as evidenced in a 12-week dietary intervention study with sedentary obese adults. The study detected a noteworthy decrease in insulin and leptin levels and an increase in adiponectin (Mohorko, 2019).

On the other hand, in the long run, a KD notably lowered weight, body mass index (BMI), glucose levels (Dashti, 2007), and overall serum cholesterol (TC) in obese patients with high cholesterol, mitigating the risks of various chronic illnesses linked to obesity (Dashti, 2004). Similarly, a study conducted over two years compared the efficacy of a low-calorie diet with a very low-calorie KD in treating obesity. The findings indicated that KD led to higher weight loss percentages despite side effects such as fatigue, headache, constipation, and nausea, which did not cause patients to withdraw from the trial (Moreno, 2016). Thus, evidence highlights KD's potential in enhancing biochemical, hormonal, and anthropometric markers in obese patients.

3.1.3 Cardiovascular diseases

Cardiovascular diseases (CVD) encompass various conditions adversely affecting cardiac and vascular function (Virani, 2020). The heart is a constantly functioning pump, demanding a lot of energy. Fatty acids serve as the primary fuel for mitochondrial ATP production in the adult heart, while glucose is also a significant energy substrate, enabling adaptive changes in utilization during development and in response to nutritional conditions (Dorn, 2015). Drawing from the evidence that the malfunctioning heart enhances the utilization of KB as a protective mechanism against metabolic stress, a down-regulation of heart failure (HF) was observed in the absence of β HB oxidation, compared to controls, indicating the potential efficacy of ketone supplementation for treating HF (McMurray, 2019). CVD has been linked to chronic HF (CHF), indicating that providing ketones exogenously could enhance cardiovascular function and prevent CHF development (Nielsen, 2019; Horton, 2019). Although no recent studies have directly addressed new paradigms, KD has been associated indirectly with atherogenic risk due to observed lipid and lipoprotein profile modifications.

3.1.4 Lipoprotein metabolism

KD is enriched in lipid content, and there is a natural concern regarding the resulting elevated serum lipid levels. On the one hand, Ozdemir et al. point out that prescribing to patients with at least 12 months of KD could significantly elevate TC and low-density lipoprotein (LDL-C) and TG without affecting the high-density lipoprotein (HDL-C) level. In addition, another investigation (Zamani, 2016) found that a 6-month KD could markedly increase median triglycerides, TC, LDL-C and HDL-C. Another study revealed that a KD rich in fat significantly elevated lipoproteins containing apolipoprotein B (apoB) and decreased HDL-C, the anti-atherogenic par excellence, inferring that the diet impairs endothelial function and facilitates inflammation and the formation of atherosclerotic lesions. (Kwiterovich, 2003) Regarding LDL-C with a very low carbohydrate diet, in a 6-month study, 29% of the participants had an average increase of 18mg/dL of this lipoprotein (Westman, 2002). In a similar study of the same duration, 30% of participants had increased LDL-C, which is related to an atherogenic effect (Yancy, 2004). However, recent

studies have provided evidence that reducing dietary carbohydrates can reduce serum concentrations of TC, TG and increase HDL-C, data that are considered beneficial to health (Tragni, 2021); (Alarim, 2020). In relation to the LDL-C particles, it is known that KD can increase the size and volume (Volek, 2021), which is thought to reduce the risk of cardiovascular disease, since smaller and denser LDL particles have greater atherogenic activity. Furthermore, depending on the model, it has been observed that KD affects the levels of HDL-C, LDL-C and TG in rodents (Ellenbroek, 2014); (Bielohuby, 2013); (Douris, 2015), while in humans it does the opposite (Tay, 2018). All this leaves conflicting results depending on the study model and the fact that this could be due to the different composition of the diets, considering that animal studies generally use diets that are higher not only in total fat, but also in saturated fat (Kosinski, 2017).

3.1.5 Gut microbiota

It is interesting to describe how the gut microbiota and diet interact and how this interaction relates to overall health to determine whether changes in dietary habits, such as a low-calorie diet, have a positive or negative effect on overall diversity. The microbiota consists of more than eight thousand different species of bacteria, viruses, and fungi living in a complex ecosystem in the human gastrointestinal tract (Wallace, 2018). Its composition plays a fundamental role in human health, which is mainly determined by factors such as diet (David, 2014). According to one study, the average heritability of gut microbiota taxa is only 1.9%, while more than 20% of the variability is associated with diet and lifestyle (Rothschild, 2018). This composition is important because an alteration can lead to intestinal dysbiosis, which has been linked to a wide range of chronic metabolic disorders (Turnbaugh, 2009); (Le Chatelier, 2013); (Qin, 2012); (Karlsson, 2013) such as obesity (Tremaroli, 2015) and weight loss after bariatric surgery (Ridaura, 2013), in addition to findings in mice suggesting specific bacteria that could cause insulin resistance (Pedersen, 2016). This highlights the importance of the state of the microbiota in influencing overall health. Based on the analysis of popular diets, low carbohydrate diets have a higher risk of being nutritionally inadequate due to the lack of fiber, vitamins, minerals, and iron (Adam-Perrot, 2006); (Kennedy, 2001). Thus, positive changes in the gut microbiota and general health have been observed depending on the food group, e.g.

energy-restricted diets or diets rich in fiber and vegetables (Claesson, 2012), (Lynch, 2016). In contrast, KD alters the intestinal microbiota, causing changes in the intestinal microbiota due to the production of KB, as in the case of β HB, which selectively inhibits the growth of Bifidobacterium, a protective barrier bacteria against inflammation (Turroni, 2008); (Ang, 2020). Furthermore, compared to high-fat diets, KD reduces the levels of proinflammatory intestinal Th17 cells, which supports the role of KD in reducing mucosal protective mechanisms, which could generate uncertainty about its implementation (Ang, 2020); (Aguilar-Jimenez, 2011).

3.2 Adverse effects of implementation

Important factors to consider are directly related to the implementation of KD in adults. On the one hand, KD is often low in thiamine, folate, vitamin A, vitamin E, vitamin B6, calcium, magnesium, iron, and potassium (Freedman, 2001). Without multivitamin supplementation, people on low-carbohydrate diets risk significant nutritional deficiencies (Bilsborough, 2003). And very low carbohydrate diets may also lack fiber and phytochemicals (Liu, 2013); (Patterson, 2020); (Slavin, 2012). Thus, extreme carbohydrate restriction can have a profound effect on diet quality.

Dietary adherence remains a major challenge in KD. Inefficacy, side effects, food restriction, and unpleasant taste can reduce patient motivation and lead to discontinuation and subsequent treatment failure (Howrie, 1998); (Zarnowska, 2020). The ability to control hunger is also a key component of success, and low carbohydrate diets are more effective in controlling hunger (McClernon, 2007); (Martin, 2011); (Castro, 2018). In addition, there is a measurable biomarker, β HB, when a person is in ketosis, the body begins to produce ketones, and β HB levels increase, indicating adherence to the diet (Mohorko, 2019).

Various adverse effects have been reported, depending on the type of restriction. Short-term effects such as fatigue, irritability, headache, nausea, hypoglycemia, diarrhea, and refusal to eat are common in the first few weeks of the diet, as are reactions to the metabolic changes induced by the diet, which are generally predictable and preventable. One of the most common is mild to moderate dehydration due to reduced fluid intake, acidosis, reduced renal tubular reabsorption, and increased urinary

excretion. There are also adverse effects that can last for the duration of the diet, often including gastrointestinal disturbances such as constipation, abdominal pain, vomiting, and gastroesophageal reflux disease.

On the other hand, most studies have not been long-term due to the difficulty of adhering to the diet, as food choices are limited and not sustainable over time. In addition, KD has been described to reduce bone mineral density, nephrolithiasis, cardiomyopathy, and anemia (Zarnowska, 2020); (Furth, 2000); (Crosby, 2021); (Włodarek, 2019).

4. CONCLUSIONS

KB is involved in several metabolic pathways. The protective effects of KB and the implementation of KD may lead to improved health status.

Regarding chronic metabolic disorders, KD was positively associated with type 2 DM by reducing blood glucose levels, HbA1c, and greater weight loss. However, it was not recommended in type 1 DM, where it improved blood glucose levels but favored the development of dyslipidemia. In addition, KD reduced BMI, body weight, anthropometric measures, and inflammatory markers, demonstrating its benefits in improving obesity-related factors.

Moreover, KD has been shown to reduce serum concentrations of TC, TG, and LDL-C and increase HDL-C, which could be related to an anti-atherogenic pattern, although studies have been reported that show the opposite, increasing these parameters. Another factor to consider is the effect of dietary composition and how it affects the microbiota, where KD has been negatively associated because KB inhibits the growth of bifidobacterium, bacteria that protect against inflammation.

Although KD has promising therapeutic potential, its clinical implementation remains uncertain. Therefore, further studies are necessary to deliver high-quality clinical evidence regarding its efficacy and safety. It is crucial to modify treatment plans to minimize adverse effects and enhance tolerability while comprehensively understanding the mechanisms involved, guiding personalized application for individuals with pre-existing diseases.

5. DECLARATIONS

5.1. Study Limitations

This research is limited to the references consulted during the study.

5.2. Acknowledgements

The work team thanks the scholarship recipient Franco Manuel Pérez Roperro for the support provided.

5.3. Funding source

The authors funded this research.

5.4. Competing Interests

The authors declare no conflict of interest.

5.5. Open Access

This article is licensed under a Creative Commons Attribution 4.0 (CC BY 4.0) International License, which permits use, sharing, adaptation, distribution, and reproduction in any medium or format, as long as you give appropriate credit to the original author(s) and the source, provide a link to the Creative Commons license, and indicate if changes were made. The images or other third-party material in this article are included in the article's Creative Commons license unless indicated otherwise in a credit line to the material. Suppose material is not included in the article's Creative Commons license, and your intended use is not permitted by statutory regulation or exceeds the permitted use. In that case, you will need to obtain permission directly from the copyright holder. To view a copy of this license, visit <http://creativecommons.org/licenses/by/4.0/>.

7. REFERENCES:

1. Abuyassin, B.; Laher, I. (2016). Diabetes epidemic sweeping the Arab world. *World*

- journal of diabetes*, 7(8), 165–174. <https://doi.org/10.4239/wjd.v7.i8.165>
2. Achanta, L. B.; Rae, C. D. (2017). β -Hydroxybutyrate in the Brain: One Molecule, Multiple Mechanisms. *Neurochemical research*, 42(1), 35–49. <https://doi.org/10.1007/s11064-016-2099-2>
 3. Adam-Perrot, A.; Clifton, P.; Brouns, F. (2006). Low-carbohydrate diets: nutritional and physiological aspects. *Obesity reviews: an official journal of the International Association for the Study of Obesity*, 7(1), 49–58. <https://doi.org/10.1111/j.1467-789X.2006.00222.x>
 4. Aguilar-jimenez, W.; Zapata, W.; Rugeles, M. T. (2011). Participación de las células Th17 en la patogenia de la infección por el virus de la inmunodeficiencia humana de tipo 1. *Infect.* 15 (4), 259-267. <https://doi.org/10.22354/issn.2422-3794>
 5. Ang, Q. Y.; Alexander, M.; Newman, J. C.; et al. (2020). Ketogenic diets alter the gut microbiome resulting in decreased intestinal Th17 cells. *Cell*, 181(6), 1263–1275.e16. <https://doi.org/10.1016/j.cell.2020.04.027>
 6. Ahmed, S.R.; Bellamkonda, S.; Zilbermint, M.; et al. (2020). Effects of the low carbohydrate, high-fat diet on glycemic control and body weight in patients with type 2 diabetes: Experience from a community-based cohort. *BMJ Open Diabetes Res. Care*, 8(1), e000980. <https://doi.org/10.1136/bmjdr-2019-000980>
 7. Alarim, R.; Alasmre, F. A.; Alotaibi, H. A.; et al. (2020). Effects of the ketogenic diet on glycemic control in diabetic patients: meta-analysis of clinical trials. *Cureus*, 12(10), e10796. <https://doi.org/10.7759/cureus.10796>
 8. American Diabetes Association; Bantle, J.P.; Wylie-Rosett, J.; et al. (2008). Nutrition recommendations and interventions for diabetes: a position statement of the American Diabetes Association. *Diabetes Care*, 31 Suppl 1, S61–S78. <https://doi.org/10.2337/dc08-S061>
 9. Bielohuby, M.; Sisley, S.; Sandoval, D.; et al. (2013). Impaired Glucose Tolerance in Rats Fed Low-Carbohydrate, High-Fat Diets. *American Journal of physiology. Endocrinology and metabolism*, 305(9), E1059–E1070. <https://doi.org/10.1152/ajpendo.00208.2013>
 10. Bilsborough, S. A.; Crowe, T. C.; (2003). Low-carbohydrate diets: what are the potential short- and long-term health implications? *Asia Pacific journal of clinical nutrition*, 12(4), 396–404.
 11. Bueno, N. B.; de Melo, I. S.; de Oliveira, S. L.; et al. (2013). Very-low carbohydrate ketogenic diet v. low-fat diet for long-term weight loss: a meta-analysis of randomised controlled trials. *The British Journal of Nutrition*, 110(7), 1178–1187. <https://doi.org/10.1017/S0007114513000548>
 12. Brouns, F. (2018). Overweight and diabetes prevention: is a low-carbohydrate-high-fat diet recommendable? *European Journal of Nutrition*, 57(4), 1301–1312. <https://doi.org/10.1007/s00394-018-1636-y>
 13. Castaldo, G.; Palmieri, V.; Galdo, G.; et al. (2016). Aggressive nutritional strategy in morbid obesity in clinical practice: safety, feasibility, and effects on metabolic and haemodynamic risk factors. *Obesity research & clinical practice*, 10(2), 169–177. <https://doi.org/10.1016/j.orcp.2015.05.00>
 14. Castro, A.I.; Gomez-Arbelaez, D.; Crujeiras, A.B.; et al. (2018). Effect of A Very Low-Calorie Ketogenic Diet on Food and Alcohol Cravings, Physical and Sexual Activity, Sleep Disturbances, and Quality of Life in Obese Patients. *Nutrients*; 10(10), 1348. <https://doi.org/10.3390/nu10101348>
 15. Choi, Y.J.; Jeon, S.M.; Shin, S. (2020). Impact of a ketogenic diet on metabolic parameters in patients with obesity or overweight and with or without type 2 diabetes: a meta-analysis of randomized controlled trials. *Nutrients*; 12(7), 2005. <https://doi.org/10.3390/nu12072005>
 16. Claesson, M.J.; Jeffery, I.B.; Conde, S.; et al. (2012). Gut microbiota composition correlates with diet and health in the elderly. *Nature*, 488(7410), 178–184. <https://doi.org/10.1038/nature11319>
 17. Colica, C.; Merra, G.; Gasbarrini, A.; et al. (2017). Efficacy and safety of very-low-calorie ketogenic diet: a double-blind randomized crossover study. *European review for medical and pharmacological sciences*, 21(9), 2274–2289.
 18. Coppola, G.; Veggiotti, P.; Cusmai, R.; et

- al. (2002). The ketogenic diet in children, adolescents and young adults with refractory epilepsy: an Italian multicentric experience. *Epilepsy research*, 48(3), 221–227. [https://doi.org/10.1016/s0920-1211\(01\)00315-1](https://doi.org/10.1016/s0920-1211(01)00315-1)
19. Crosby, L.; Davis, B.; Joshi, S.; et al. (2021). Ketogenic diets and chronic disease: weighing the benefits against the risks. *Frontiers in nutrition*, 8, 702802. <https://doi.org/10.3389/fnut.2021.702802>
 20. Dashti, H.M.; Mathew, T.C.; Hussein, T.; et al. (2004). Long-term effects of a ketogenic diet in obese patients. *Experimental and clinical cardiology*, 9(3), 200–205.
 21. Dashti, H.M.; Al-Zaid, N.S.; Mathew, T.C.; et al. (2006). Long term effects of ketogenic diet in obese subjects with high cholesterol level. *Molecular and cellular biochemistry*, 286(1-2), 1–9. <https://doi.org/10.1007/s11010-005-9001-x>
 22. Dashti, H.M.; Mathew, T.C.; Khadada, M.; et al. (2007). Beneficial effects of ketogenic diet in obese diabetic subjects. *Molecular and cellular biochemistry*, 302(1-2), 249–256. <https://doi.org/10.1007/s11010-007-9448-z>
 23. David, L.; Maurice, C.; Carmody, R.; et al. (2014). Diet rapidly and reproducibly alters the human gut microbiome. *Nature*, 505, 559–563. <https://doi.org/10.1038/nature12820>
 24. Diemel, G. A. (2019) Brain glucose metabolism: integration of energetics with function. *Physiological reviews*, 99(1), 949–1045. <https://doi.org/10.1152/physrev.00062.2017>
 25. Douris, N.; Melman, T.; Pecherer, J.M.; et al. (2015). Adaptive Changes in Amino Acid Metabolism Permit Normal Longevity in Mice Consuming a Low-Carbohydrate Ketogenic Diet. *Biochimica et biophysica acta*, 1852 (10 Pt A), 2056–2065. <https://doi.org/10.1016/j.bbadis.2015.07.009>
 26. Dorn, G.W.; Vega, R.B.; Kelly, D.P. (2015). Mitochondrial biogenesis and dynamics in the developing and diseased heart. *Genes & development*, 29(19), 1981–1991. <https://doi.org/10.1101/gad.269894.115>
 27. Ellenbroek, J.H.; Van Dijck, L.; Töns, H.A.; et al. (2014). Long-term ketogenic diet causes glucose intolerance and reduced β - and α -cell mass but no weight loss in mice. *American Journal of physiology*. *Endocrinology and metabolism*, 306(5), E552–E558. <https://doi.org/10.1152/ajpendo.00453.2013>
 28. Farrés, J.; Pujol, A.; Coma, M.; et al. (2010). Revealing the molecular relationship between type 2 diabetes and the metabolic changes induced by a very-low-carbohydrate low-fat ketogenic diet. *Nutrition & metabolism*, 7, 88. <https://doi.org/10.1186/1743-7075-7-88>
 29. Foster, G.D.; Wyatt, H.R.; Hill, J.O.; et al. (2003). A randomized trial of a low-carbohydrate diet for obesity. *The New England journal of medicine*, 348(21), 2082–2090. <https://doi.org/10.1056/NEJMoa022207>
 30. Freeman, J.M.; Kossoff, E.H. (2010). Ketosis and the ketogenic diet, 2010: advances in treating epilepsy and other disorders. *Advances in pediatrics*, 57(1), 315–329. <https://doi.org/10.1016/j.yapd.2010.08.003>
 31. Freedman, M.R.; King, J.; Kennedy, E. (2001). Popular diets: a scientific review. *Obesity research*, 9(1), 1S–40S. <https://doi.org/10.1038/oby.2001.113>
 32. Furth, S. L.; Casey, J. C.; Pyzik, P. L.; et al. (2000). Risk factors for urolithiasis in children on the ketogenic diet. *Pediatric nephrology* (Berlin, Germany), 15(1-2), 125–128. <https://doi.org/10.1007/s004670000443>
 33. Gannon, M. C.; Hoover, H.; Nuttall, F. Q. (2010). Further decrease in glycated hemoglobin following ingestion of a LoBAG30 diet for 10 weeks compared to 5 weeks in people with untreated type 2 diabetes. *Nutrition & metabolism*, 7, 64. <https://doi.org/10.1186/1743-7075-7-64>
 34. Gangitano, E.; Tozzi, R.; Gandini, O.; et al. (2021). Ketogenic diet as a preventive and supportive care for COVID-19 patients. *Nutrients*, 13(3), 1004. <https://doi.org/10.3390/nu13031004>
 35. Hallberg, S.J.; McKenzie, A.L.; Williams, P.T.; et al. (2018). Effectiveness and Safety of a Novel Care Model for the Management of Type 2 Diabetes at 1 Year: An Open-Label, Non-Randomized, Controlled Study. *Diabetes therapy : research, treatment and education of diabetes and related disorders*, 9(2), 583–612. <https://doi.org/10.1007/s13300-018-0373-9>
 36. Hassan, A. M.; Keene, D. L.; Whiting, S. E.; et al. (1999). Ketogenic diet in the

- treatment of refractory epilepsy in childhood. *Pediatric neurology*, 21(2), 548–552. [https://doi.org/10.1016/s0887-8994\(99\)00045-4](https://doi.org/10.1016/s0887-8994(99)00045-4)
37. Horton, J. L.; Davidson, M. T.; Kurishima, C.; et al. (2019). The failing heart utilizes 3-hydroxybutyrate as a metabolic stress defense. *JCI insight*, 4(4), e124079. <https://doi.org/10.1172/jci.insight.124079>
 38. Howrie, D.L.; Kraisinger, M.; McGhee, H.W.; et al. (1998). The ketogenic diet: the need for a multidisciplinary approach. *Annals of pharmacotherapy*, 32(3), 384–385. <https://doi.org/10.1345/aph.17201>
 39. Hussain, T. A.; Mathew, T. C.; Dashti, A. A.; et al. (2012). Effect of low-calorie versus low-carbohydrate ketogenic diet in type 2 diabetes. *Nutrition (Burbank, Los Angeles County, Calif.)*, 28(10), 1016–1021. <https://doi.org/10.1016/j.nut.2012.01.016>
 40. Huttenlocher, P.R.; Wilbourn, A.J.; Signore, J.M. (1971). Mediumchain triglycerides as a therapy for intractable childhood epilepsy. *Neurology*, 21(11):1097–1103. <https://doi.org/10.1212/wnl.21.11.1097>
 41. Kang, H. C.; Lee, H. S.; You, S. J.; et al. (2007). Use of a modified Atkins diet in intractable childhood epilepsy. *Epilepsia*, 48(1), 182–186. <https://doi.org/10.1111/j.1528-1167.2006.00910.x>
 42. Kanikarla-Marie, P.; Jain, S. K. (2016). Hyperketonemia and ketosis increase the risk of complications in type 1 diabetes. *Free radical biology & medicine*, 95, 268–277. <https://doi.org/10.1016/j.freeradbiomed.2016.03.020>
 43. Karlsson, F.H.; Tremaroli, V.; Nookaew, I.; et al. (2013). Gut metagenome in European women with normal, impaired and diabetic glucose control. *Nature*, 498(7452), 99–103. <https://doi.org/10.1038/nature12198>
 44. Kennedy, E.T.; Bowman, S.; Spence, J.T.; et al. (2001). Popular Diets. *Journal of the American Dietetic Association*, 101(4), 411–420. [https://doi.org/10.1016/S0002-8223\(01\)00108-0](https://doi.org/10.1016/S0002-8223(01)00108-0)
 45. Kong, Z.; Sun, S.; Shi, Q.; et al. (2020). Short-Term Ketogenic Diet Improves Abdominal Obesity in Overweight/Obese Chinese Young Females. *Frontiers in physiology*, 11, 856. <https://doi.org/10.3389/fphys.2020.00856>
 46. Kong, C.; Yan, X.; Liu, Y.; et al. (2021). Ketogenic diet alleviates colitis by reduction of colonic group 3 innate lymphoid cells through altering gut microbiome. *Signal transduction and targeted therapy*, 6(1), 154. <https://doi.org/10.1038/s41392-021-00549-9>
 47. Kosinski, C.; Jornayvaz, F.R. (2017). Effects of Ketogenic Diets on Cardiovascular Risk Factors: Evidence From Animal and Human Studies. *Nutrients*, 9(5):517. <https://doi.org/10.3390/nu9050517>
 48. Kossoff, E. H.; Krauss, G. L.; McGrogan, J. R.; et al. (2003). Efficacy of the Atkins diet as therapy for intractable epilepsy. *Neurology*, 61 (12), 1789–1791. <https://doi.org/10.1212/01.wnl.0000098889.35155.72>
 49. Kossoff, E. H.; McGrogan, J. R.; Bluml, R. M.; et al. (2006). A modified Atkins diet is effective for the treatment of intractable pediatric epilepsy. *Epilepsia*, 47(2), 421–424. <https://doi.org/10.1111/j.1528-1167.2006.00438.x>
 50. Kossoff, E. H.; Turner, Z.; Bluml, R. M.; et al. (2007). A randomized, crossover comparison of daily carbohydrate limits using the modified Atkins diet. *Epilepsy & behavior: E&B*, 10(3), 432–436. <https://doi.org/10.1016/j.yebeh.2007.01.012>
 51. Kossoff, E.H.; Zupec-Kania, B.A.; Auvin, S.; et al. (2018). Optimal clinical management of children receiving dietary therapies for epilepsy: Updated recommendations of the International Ketogenic Diet Study Group. *Epilepsia Open*, 3(2):175-192. <https://doi.org/10.1002/epi4.12225>
 52. Kwiterovich, P.O.; Jr.; Vining, E.P.; Pyzik, P.; et al. (2003). Effect of a High-Fat Ketogenic Diet on Plasma Levels of Lipids, Lipoproteins, and Apolipoproteins in Children. *Jama*, 290(7):912–920. <https://doi.org/10.1001/jama.290.7.912>
 53. Le Chatelier, E.; Nielsen, T.; Qin, J.; et al. (2013). Richness of human gut microbiome correlates with metabolic markers. *Nature*, 500(7464), 541–546. <https://doi.org/10.1038/nature12506>
 54. Leow, Z.Z.X.; Guelfi, K.J.; Davis, E.A.; et al. (2018). The glycaemic benefits of a very-low-carbohydrate ketogenic diet in adults with type 1 diabetes mellitus may be opposed by increased hypoglycaemia risk

- and dyslipidaemia. *Diabetic medicine : a journal of the British Diabetic Association*, 10.1111/dme.13663. Advance online publication. <https://doi.org/10.1111/dme.13663>
55. Liu, R. H. (2013). Health-promoting components of fruits and vegetables in the diet. *Advances in nutrition (Bethesda, Md.)*, 4(3), 384S–92S. <https://doi.org/10.3945/an.112.003517>
 56. Liu, Y. M.; Wang, H. S. (2013). Medium-chain triglyceride ketogenic diet, an effective treatment for drug-resistant epilepsy, and a comparison with other ketogenic diets. *Biomedical Journal*, 36(1), 9–15. <https://doi.org/10.4103/2319-4170.107154>
 57. Lynch, S.V.; Pedersen, O. (2016). The Human Intestinal Microbiome in Health and Disease. *The New England journal of medicine*, 375(24), 2369–2379. <https://doi.org/10.1056/NEJMra1600266>
 58. Martin, C.K.; Rosenbaum, D.; Han, H.; et al. (2011). Change in Food Cravings, Food Preferences, and Appetite During a Low-Carbohydrate and Low-Fat Diet. *Obesity*; 19(10), 1963–1970. <https://doi.org/10.1038/oby.2011.62>
 59. McClean, A.M.; Montorio, L; McLaughlin, D.; et. al. (2019). Can a ketogenic diet be safely used to improve glycaemic control in a child with type 1 diabetes? *Archives of disease in childhood*, 104(5), 501–504. <https://doi.org/10.1136/archdischild-2018-314973>
 60. McClernon, F.J.; Yancy, W.S.; Eberstein, J.A.; et al. (2007). The Effects of a Low-Carbohydrate Ketogenic Diet and a Low-Fat Diet on Mood, Hunger, and Other Self-Reported Symptoms. *Obesity*, 15(1), 182–187. <https://doi.org/10.1038/oby.2007.516>
 61. McCue, M. D. (2010). Starvation physiology: reviewing the different strategies animals use to survive a common challenge. *Comparative biochemistry and physiology. Part A, Molecular & integrative physiology*, 156(1), 1–18. <https://doi.org/10.1016/j.cbpa.2010.01.002>
 62. McDonald, T. J. W.; Cervenka, M. C. (2018). The expanding role of ketogenic diets in adult neurological disorders. *Brain sciences*, 8(8), 148. <https://doi.org/10.3390/brainsci8080148>
 63. McMurray, J. J. V.; Solomon, S. D.; Inzucchi, S. E.; et al. (2019). Dapagliflozin in patients with heart failure and reduced ejection fraction. *The New England journal of medicine*, 381(21), 1995–2008. <https://doi.org/10.1056/NEJMoa1911303>
 64. Michalczyk, M.M.; Klonek, G.; Maszczyk, A.; et al. (2020). The Effects of a Low Calorie Ketogenic Diet on Glycaemic Control Variables in Hyperinsulinemic Overweight/Obese Females. *Nutrients*, 12(6), 1854. <https://doi.org/10.3390/nu12061854>
 65. Mohorko, N.; Cerniĉ-Bizjak, M.; Poklar-Vatovec, T.; et al. (2019). Weight loss, improved physical performance, cognitive function, eating behavior, and metabolic profile in a 12-week ketogenic diet in obese adults. *Nutrition Research*, 62, 64–77. <https://doi.org/10.1016/j.nutres.2018.11.007>
 66. Monda, V.; Polito, R.; Lovino, A.; et al. (2020). Short-Term Physiological Effects of a Very Low-Calorie Ketogenic Diet: Effects on Adiponectin Levels and Inflammatory States. *International Journal of molecular sciences*, 21(9), 3228. <https://doi.org/10.3390/ijms21093228>
 67. Moreno, B.; Crujeiras, A.B.; Bellido, D.; et al. (2016). Obesity treatment by very low-calorie-ketogenic diet at two years: Reduction in visceral fat and on the burden of disease. *Endocrine*, 54(3), 681–690. <https://doi.org/10.1007/s12020-016-1050-2>
 68. Muscogiuri, G.; et al. (2019). The management of very low-calorie ketogenic diet in obesity outpatient clinic: a practical guide. *Journal of Translational Medicine*, 17(1):356 <https://doi.org/10.1186/s12967-019-2104-z>
 69. Nanri, A.; Mizoue, T.; Kurotani, K.; et al. (2015). Low-carbohydrate diet and type 2 diabetes risk in Japanese men and women: the Japan Public Health Center-Based Prospective Study. *PLoS one*, 10(2), e0118377.
 70. Neal, E. G.; Chaffe, H.; Schwartz, R. H.; et al. (2008). The ketogenic diet for the treatment of childhood epilepsy: a randomised controlled trial. *The Lancet. Neurology*, 7(6), 500–506. [https://doi.org/10.1016/S1474-4422\(08\)70092-9](https://doi.org/10.1016/S1474-4422(08)70092-9)
 71. Neal, E. G.; Chaffe, H.; Schwartz, R. H.; et al. (2009). A randomized trial of classical and medium-chain triglyceride ketogenic diets in the treatment of childhood epilepsy. *Epilepsia*, 50(5), 1109–1117.

- <https://doi.org/10.1111/j.1528-1167.2008.01870.x>
72. Newman, J.C.; Verdin, E. (2017). β -Hydroxybutyrate: a signaling metabolite. *Annual review of nutrition*, 37, 51–76. <https://doi.org/10.1146/annurev-nutr-071816-064916>
 73. Nielsen, R.; Møller, N.; Gormsen, L. C.; et al. (2019). Cardiovascular effects of treatment with the ketone body 3-hydroxybutyrate in chronic heart failure patients. *Circulation*, 139(18), 2129–2141. <https://doi.org/10.1161/CIRCULATIONAHA.118.036459>
 74. Nuttall, F. Q.; Schweim, K.; Hoover, H.; et al. (2008). Effect of the LoBAG30 diet on blood glucose control in people with type 2 diabetes. *The British Journal of nutrition*, 99(3), 511–519. <https://doi.org/10.1017/S0007114507819155>
 75. Owen, O. E. (2005). Ketone bodies as a fuel for the brain during starvation. *Biochem. Biochemistry and Molecular Biology Education*, 33(4):246 – 251. DOI:10.1002/bmb.2005.49403304246
 76. Özdemir, R.; Güzel, O.; Küçük, M.; et al. (2016). The Effect of the Ketogenic Diet on the Vascular Structure and Functions in Children With Intractable Epilepsy. *Pediatric neurology*, 56, 30–34. <https://doi.org/10.1016/j.pediatrneurol.2015.10.017>
 77. Qin, J.; Li, Y.; Cai, Z.; et al. (2012). A metagenome-wide association study of gut microbiota in type 2 diabetes. *Nature*, 490(7418), 55–60. <https://doi.org/10.1038/nature11450>
 78. Paoli, A.; Bianco, A.; Damiani, E.; et al. (2014). Ketogenic diet in neuromuscular and neurodegenerative diseases. *BioMed research international*, 2014, 474296. <https://doi.org/10.1155/2014/474296>
 79. Paoli, A.; Mancin, L.; Bianco, A. (2014). Ketogenic Diet for Obesity: Friend or Foe? *International Journal of environmental research and public health*, 11(2), 2092–2107. <https://doi.org/10.3390/ijerph110202092>
 80. Paoli, A.; Mancin, L.; Bianco, A.; et al. (2019). Ketogenic diet and microbiota: friends or enemies? *Genes*, 10(7), 534. <https://doi.org/10.3390/genes10070534>
 81. Pedersen, H.K.; Gudmundsdottir, V.; Nielsen, H.B.; et al. (2016). Human gut microbes impact host serum metabolome and insulin sensitivity. *Nature*, 535(7612), 376–381. <https://doi.org/10.1038/nature18646>
 82. Patterson, M.A.; Maiya, M.; Stewart, M.L. (2020). Resistant starch content in foods commonly consumed in the United States: a narrative review. *Journal of the Academy of Nutrition and Dietetics*, 120(2), 230–244. <https://doi.org/10.1016/j.jand.2019.10.019>
 83. Rafiullah, M.; Musambil, M.; David, S. K. (2021). Effect of a very low-carbohydrate ketogenic diet vs recommended diets in patients with type 2 diabetes: a meta-analysis. *Nutrition reviews*, 80(3), 488–502. <https://doi.org/10.1093/nutrit/nuab040>
 84. Ridaura, V.K.; Faith, J.J.; Rey, F.E.; et al. (2013). Gut microbiota from twins discordant for obesity modulate metabolism in mice. *Science*, 341(6150), 1241214. <https://doi.org/10.1126/science.1241214>
 85. Rizza, R. A. (2010). Pathogenesis of fasting and postprandial hyperglycemia in type 2 diabetes: implications for therapy. *Diabetes*, 59(11), 2697–2707. <https://doi.org/10.2337/db10-1032>
 86. Rothschild, D.; Weissbrod, O.; Barkan, E.; et al. (2018) Environment dominates over host genetics in shaping human gut microbiota. *Nature*, 555 (7695), 210–215. <https://doi.org/10.1038/nature25973>
 87. Rusek, M.; Pluta, R.; Ulamek-Kozioł, M.; Czuczwar, S. J. (2019). Ketogenic diet in Alzheimer's disease. *International Journal of molecular sciences*, 20(16), 3892. <https://doi.org/10.3390/ijms20163892>
 88. Seo, J.H.; Lee, Y.M.; Lee, J.S.; et al. (2007). Efficacy and tolerability of the ketogenic diet according to lipid:nonlipid ratios--comparison of 3:1 with 4:1 diet. *Epilepsia*, 48(4):801-805. <https://doi.org/10.1111/j.1528-1167.2007.01025.x>
 89. Schutz, Y. (2011). Protein turnover, ureagenesis and gluconeogenesis. *International Journal for vitamin and nutrition research. Internationale Zeitschrift für Vitamin- und Ernährungsforschung. Journal international de vitaminologie et de nutrition*, 81(2-3), 101–107. <https://doi.org/10.1024/0300-9831/a000064>
 90. Schwartz, R. H.; Eaton, J.; Bower, B. D.; et al. (1989). Ketogenic diets in the treatment of epilepsy: short-term clinical effects. *Developmental medicine and child*

- neurology*, 31(2), 145–151.
<https://doi.org/10.1111/j.1469-8749.1989.tb03972.x>
91. Slavin, J.L.; Lloyd, B. (2012). Health benefits of fruits and vegetables. *Advances in nutrition (Bethesda, Md.)*, 3(4), 506–516.
<https://doi.org/10.3945/an.112.002154>
 92. Stafstrom, C. E.; Rho, J. M. (2012). The ketogenic diet as a treatment paradigm for diverse neurological disorders. *Frontiers in pharmacology*, 3, 59.
<https://doi.org/10.3389/fphar.2012.00059>
 93. Tay, J.; Thompson, C.H.; Luscombe-Marsh, N.D.; et al. (2018). Effects of an Energy-Restricted Low-Carbohydrate, High Unsaturated Fat/Low Saturated Fat Diet Versus a High-Carbohydrate, Low-Fat Diet in Type 2 Diabetes: A 2-Year Randomized Clinical Trial. *Diabetes, obesity & metabolism*, 20(4), 858–871.
<https://doi.org/10.1111/dom.13164>
 94. Tragni, E.; Vigna, L.; Ruscica, M.; et al. (2021). Reduction of cardio-metabolic risk and body weight through a multiphasic very-low calorie ketogenic diet program in women with overweight/obesity: a study in a real-world setting. *Nutrients*, 13(6), 1804.
<https://doi.org/10.3390/nu13061804>
 95. Tremaroli, V.; Karlsson, F.; Werling, M.; et al. (2015). Roux-en-Y gastric bypass and vertical banded gastroplasty induce long-term changes on the human gut microbiome contributing to fat mass regulation. *Cell metabolism*, 22(2), 228–238.
<https://doi.org/10.1016/j.cmet.2015.07.009>
 96. Turnbaugh, P.J.; Hamady, M.; Yatsunencko, T.; et al. (2009). A core gut microbiome in obese and lean twins. *Nature*, 457(7228), 480–484.
<https://doi.org/10.1038/nature07540>
 97. Turrioni, F.; Ribbera, A.; Foroni, E.; et al. (2008). Human gut microbiota and bifidobacteria: from composition to functionality. *Antonie van Leeuwenhoek*, 94(1), 35–50.
<https://doi.org/10.1007/s10482-008-9232-4>
 98. Ulamek-Kozioł, M.; Czuczwar, S. J.; Januszewski, S.; et al. (2019). Ketogenic diet and epilepsy. *Nutrients*, 11(10), 2510.
<https://doi.org/10.3390/nu11102510>
 99. Vaisleib, I. I.; Buchhalter, J. R.; Zupanc, M. L. (2004). Ketogenic diet: outpatient initiation, without fluid, or caloric restrictions. *Pediatric neurology*, 31(3), 198–202.
<https://doi.org/10.1016/j.pediatrneurol.2004.03.007>
 100. Veldhorst, M. A.; Westerterp-Plantenga, M. S.; Westerterp, K. R. (2009). Gluconeogenesis and energy expenditure after a high-protein, carbohydrate-free diet. *The American Journal of clinical nutrition*, 90(3), 519–526.
<https://doi.org/10.3945/ajcn.2009.27834>
 101. Vining, E. P. (1999). Clinical efficacy of the ketogenic diet. *Epilepsy research*, 37(3), 181–190.
[https://doi.org/10.1016/s0920-1211\(99\)00070-4](https://doi.org/10.1016/s0920-1211(99)00070-4)
 102. Virani, S.S.; Alonso, A.; Benjamin, E.J.; et al. (2020). Heart disease and Stroke Statistics-2020 Update: A Report from the American Heart Association. *Circulation*, 141(9): e139–e596.
<https://doi.org/10.1161/CIR.0000000000000757>
 103. Volek, J. S.; Sharman, M. J.; Forsythe, C. E. (2005). Modification of lipoproteins by very low-carbohydrate diets. *The Journal of nutrition*, 135(6), 1339–1342.
<https://doi.org/10.1093/jn/135.6.1339>
 104. Walton, C.M.; Perry, K.; Hart, R.H.; et al. (2019). Improvement in Glycemic and Lipid Profiles in Type 2 Diabetics with a 90-Day Ketogenic Diet. *Journal of diabetes research*, 2019, 8681959.
<https://doi.org/10.1155/2019/8681959>
 105. Wallace, C. (2018). Dietary advice based on the bacteria in your gut. *Wall Street Journal*. [(accessed on 12 May 2021)]; Available online: <https://www.wsj.com/articles/dietary-advice-based-on-the-bacteria-in-your-gut-1519614301>
 106. Weber, D.D.; Aminzadeh-Gohari, S.; Tulipan, J.; et al. (2019). Ketogenic Diet in the Treatment of Cancer - Where do We Stand? *Molecular metabolism*, 33, 102–121.
<https://doi.org/10.1016/j.molmet.2019.06.026>
 107. Westman, E.C.; Yancy, W. S.; Edman, J. S.; et al. (2002). Effect of 6-month adherence to a very low carbohydrate diet program. *The American Journal of medicine*, 113(1), 30–36.
[https://doi.org/10.1016/s0002-9343\(02\)01129-4](https://doi.org/10.1016/s0002-9343(02)01129-4)
 108. Westman, E.C.; Feinman, R.D.; Mavropoulos, J.C.; et al. (2007). Low-

- carbohydrate nutrition and metabolism. *The American Journal of clinical nutrition*, 86(2), 276–284. <https://doi.org/10.1093/ajcn/86.2.276>
109. Westman, E. C.; Tondt, J.; Maguire, E.; et al. (2018). Implementing a low-carbohydrate, ketogenic diet to manage type 2 diabetes mellitus. *Expert review of endocrinology & metabolism*, 13(5), 263–272. <https://doi.org/10.1080/17446651.2018.1523713>
110. Westman, E.C.; Yancy, W.S.; Mavropoulos, J.C.; et al. (2008). The effect of a low-carbohydrate, ketogenic diet versus a low-glycemic index diet on glycemic control in type 2 diabetes mellitus. *Nutrition & metabolism*, 5, 36. <https://doi.org/10.1186/1743-7075-5-36>
111. Wheless, J. W. (2008). History of the ketogenic diet. *Epilepsia*, 49(8), 3–5. <https://doi.org/10.1111/j.1528-1167.2008.01821.x>
112. Wilder, R. M. (1921). The effect on ketonemia on the course of epilepsy. *Mayo Clin. Bull*, 2, 307–308.
113. Włodarek, D. (2019). Role of Ketogenic Diets in Neurodegenerative Diseases (Alzheimer's Disease and Parkinson's Disease). *Nutrients*, 11(1), 169. <https://doi.org/10.3390/nu11010169>
114. Woodyatt, R. T. (1921). Objects and method of diet adjustment in diabetes. *Archives of Internal Medicine*, 28, 125–141.
115. Guilbert, J. J. (2003). The world health report 2002 - reducing risks, promoting healthy life. *Education for health (Abingdon, England)*, 16(2), 230. <https://doi.org/10.1080/1357628031000116808>
116. Yancy, W. S.; Jr, Olsen, M. K.; Guyton, J. R.; Bakst, R. P.; et al. (2004). A low-carbohydrate, ketogenic diet versus a low-fat diet to treat obesity and hyperlipidemia: a randomized, controlled trial. *Annals of internal medicine*, 140(10), 769–777. <https://doi.org/10.7326/0003-4819-140-10-200405180-00006>
117. Yuen, A. W.; Sander, J. W. (2014). Rationale for using intermittent calorie restriction as a dietary treatment for drug resistant epilepsy. *Epilepsy & behavior*, 33, 110–114. <https://doi.org/10.1016/j.yebeh.2014.02.026>
118. Zamani, G.R.; Mohammadi, M.; Ashrafi, M.R.; et al. (2016). The Effects of Classic Ketogenic Diet on Serum Lipid Profile in Children With Refractory Seizures. *Acta neurologica Belgica*, 116(4), 529–534. <https://doi.org/10.1007/s13760-016-0601-x>
119. Zarnowska, I. M. (2020). Therapeutic use of the ketogenic diet in refractory epilepsy: what we know and what still needs to be learned. *Nutrients*, 12(9), 2616. <https://doi.org/10.3390/nu12092616>
120. Zhang, Q.; Zhang, Q.; Xu, L.; Xia, J.; et al. (2018). Treatment of Diabetic Mice with a Combination of Ketogenic Diet and Aerobic Exercise via Modulations of PPARs Gene Programs. *PPAR research*, 2018, 4827643. <https://doi.org/10.1155/2018/4827643>
121. Zhang, W.; Guo, X.; Chen, L.; et al. (2021). Ketogenic Diets and Cardio-Metabolic Diseases. *Frontiers in endocrinology*, 12, 753039. <https://doi.org/10.3389/fendo.2021.753039>

COMPARATIVE STUDY OF DPD REAGENTS FOR CHLORINE MEASUREMENT IN DRINKING WATER AND DEVELOPMENT OF A JAVASCRIPT INTERPOLATION TOOL

TREIN, Felipe de Almeida^{1*}; DE BONI, Luis Alcides Brandini²;

¹ Escola Estadual Técnica São João Batista, Departamento Técnico em Química. Brazil.

² Dr. D. Scientific Consulting, Chemistry Department. Brazil.

* Corresponding author
e-mail: treinfelipea@gmail.com

Received 28 June 2023; received in revised form 30 November 2023; accepted 14 December 2023

ABSTRACT

Background: Determining chlorine in water ensures safety. Among other methods, the DPD colorimetric method is used. The DPD Method relies on colorimetric reactions to measure free and total chlorine concentration in water samples with pink compound formation. **Aims:** To perform a comparative chlorine analysis using DPD, assessing reagents from 3 makers and 2 Hach instruments to identify disparities and propose adjustments for more accurate measurements. **Methods:** Hach High-Range and Low-Range Free chlorine determination procedures were followed. DR300 and POCKET Colorimeter II spectrophotometers were used. Tests were conducted for each DPD manufacturer in low/high ranges and in two HACH devices to determine the chlorine concentrations. Hach was used as the reference; LaMotte and PoliControl compared against it. Statistical analyses were compiled using MS Excel. **Results:** The tests findings were gathered in Tables 1-5. JavaScript and HTML scripts were created to convert LaMotte and PoliControl outcomes into values equivalent to those of HACH through linear interpolation. **Discussion:** Various DPD reagents and equipment provided slightly different readings, prompting empirical evaluation of these differences. Adjusting the results to Hach's results was selected as both the reagent and spectrophotometer were from the same brand. Differences in spectrophotometer readings were more pronounced in high-range tests nearing the upper limit of the test. **Conclusions:** Equipment variations caused minor result differences; DPD reagents are not interchangeable without correlation. The Open-source code developed aided in reducing reading disparities.

Keywords: *DPD chlorine determination, comparative analyses, linear interpolation, water quality, water safety.*

1. INTRODUCTION:

Determining chlorine in water is crucial for ensuring water safety and quality. Various methods are employed for this purpose, including the DPD method, which relies on colorimetric reactions, iodometric titration for precise measurement, nephelometric method detecting turbidity due to chlorine reactions, chlorine ion-selective electrode for direct ion measurement, mercurimetric titration providing accurate quantification, and argentometric method utilizing silver nitrate reactions. These methods play a vital role in monitoring disinfection byproducts, ensuring compliance with regulatory standards, and safeguarding public health by accurately

assessing chlorine levels in water sources, thereby contributing significantly to maintaining safe drinking water for communities worldwide.

DPD method (N,N-diethyl-p- phenylenedia_mine): From the manufacturer Hach website (<https://www.hach.com/p-dpd-free-chlorine-reagent-powder-pillows-10-ml-pk100/2105569>), the sources "Chlorine, Free and Total, High Range" (2022), and "Chlorine, Free and Total, Low Range" (2022) were retrieved. The DPD method is widely used for measuring free residual chlorine in water. It relies on the reaction between free chlorine and the DPD reagent, forming a pink-colored compound proportional to the chlorine concentration. The color intensity is measured either spectrophotometrically or using colorimetric

kits to quantify the chlorine level. The primary reagents involved are the DPD reagent and the sample containing free chlorine. (Moberg, L., and Karlberg, B., 2000; WILDE, E.1991)

The DPD (reagent) was added to the water sample and was oxidized by chlorine in the sample to two oxidation products, Würster dye and imine. Würster dye was relatively stable and would form a magenta color at neutral pH. At the same time, imine was relatively unstable and colorless, which would be formed at higher oxidant levels, i.e., higher chlorine concentration. The intensity of the magenta color was then measured photometrically, representing chlorine concentration in the samples. The DPD-chlorine reactions are illustrated in Figure 1. (Astuti, M. P., Xie, R., & Aziz, N. S. (2017).

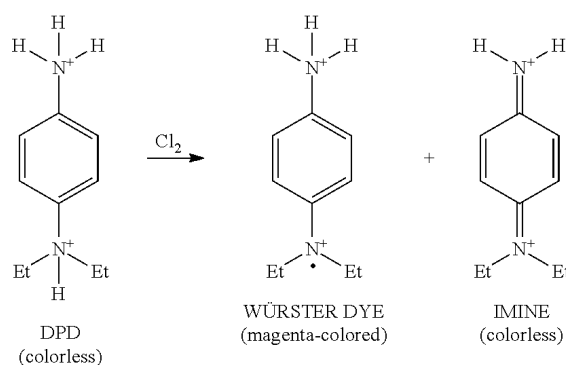


Figure 1. Image source: US20150050195A1.

Iodometric titration: According to ISO 7393-3:1990, and the method 4500-Cl B. iodometric method I. Iodometric titration is employed for determining chlorine levels by titrating a sample containing chlorine with a standardized iodine solution. Chlorine oxidizes iodide ions to form iodine, which is then titrated with a thiosulfate solution to calculate the chlorine concentration. Reagents include the sample with chlorine, iodine solution, sodium thiosulfate solution, starch indicator (to detect the endpoint), and sometimes potassium iodide as a catalyst.

Nephelometric method: The nephelometric method measures turbidity resulting from the reaction between residual chlorine and a specific reagent, causing solid particle formation. The turbidity produced correlates with the chlorine concentration (Lamb, Carleton, and Meldrum, 1920; Coll, 1957). The primary reagents used in this method are the sample, the specific reagent causing particle formation, and sometimes buffer solutions to maintain pH.

Chlorine ion-selective electrode: From

ASTM D512-04, test method C, the chlorine ion-selective electrode directly measures chloride ions in a solution. It operates based on the selective response of the electrode to chloride ions, generating an electrical potential proportional to their concentration. This potential is measured and used to determine the chloride ion concentration. The main reagents involved in this method are the sample solution containing chloride ions and the chlorine ion-selective electrode. Unlike titration-based methods, this technique does not consume reagents but depends on the functioning of the electrode to measure ion concentrations.

Mercurimetric titration: ASTM D512-04, Test method A, informs that the Mercurimetric titration quantifies chloride ions in a solution by titrating it with a standard mercuric nitrate solution. The formation of a white precipitate of mercury(II) chloride indicates the endpoint. Reagents include the sample with chloride ions, a standardized mercuric nitrate solution, and occasionally an indicator to signal the endpoint.

Argentometric method: ASTM D512-04, test method B, informs that this method relies on the reaction between chloride ions and a standardized solution of silver nitrate (AgNO₃), forming a white precipitate of silver chloride (AgCl) that marks the endpoint of the titration. The sample containing chloride ions is titrated with a standardized solution of silver nitrate. Potassium chromate (K₂CrO₄) or potassium dichromate (K₂Cr₂O₇) is commonly used as an indicator to detect the endpoint, which is signaled by the formation of a reddish-brown color due to the reaction between the indicator and the excess silver ions after all chloride ions have reacted. Reagents include a standardized silver nitrate (AgNO₃) solution as the titrant, potassium chromate or potassium dichromate as an indicator to detect the endpoint, and the sample solution containing chloride ions to be quantified.

This research aims to conduct a comparative analysis of chlorine determination using the DPD method. This study involves evaluating the analytical results obtained from reagents of three different manufacturers and the use of two different analytical instruments from Hach. By carefully examining the results derived from these variations in reagents and instruments, this study aims to identify potential disparities or discrepancies in chlorine level measurements. Additionally, if necessary, it seeks to propose adjustments to reduce the identified variations, aiming to enhance the accuracy and consistency

of chlorine measurements obtained with the DPD method.

2. MATERIALS AND METHODS:

2.1. Materials

- DPD Total Chlorine Reagent Powder Pillow (Hach);
- DPD Total Chlorine Reagent Powder Pillow (PoliControl);
- Chlorine DPD (6903A) (LaMotte);
- DR300 Pocket Colorimeter, Chlorine (Equipment);
- POCKET Colorimeter II Colorimeter for Chlorine analysis (Equipment);
- Chlorinated Water samples;
- Computer;
- Stopwatch;

2.2. Methods

2.2.1 DPD Chemical Methods

Hach procedures for the determination of chlorine were followed from "Chlorine, Free and Total, High Range" (2022), and "Chlorine, Free and Total, Low Range" (2022).

Two categories of samples were gathered for thorough analysis. The low-range free chlorine concentration of the samples was obtained from a chlorinated water sample prepared in the laboratory, which measured approximately 0.68 mg/L of chlorine, while the high-range free chlorine concentration of the samples was obtained from a sample prepared in the laboratory and its concentration measured around 5.80 mg/L of chlorine.

A blank sample was prepared for each device, and for each sample range by rinsing a sample cell and its cap three times with the respective sample. Each cell was placed into its respective reading device and the ZERO button (blue in both equipment) was pressed, and the display showed "0.00".

Subsequently, the cell was filled with the sample up to the 10-milliliter mark. This meticulous procedure was consistently followed for both pieces of equipment utilized, namely the DR300 Pocket Colorimeter and POCKET Colorimeter II Colorimeter for Chlorine analysis, as presented in Figure 2.



Figure 2. DR300 Pocket Colorimeter (left) and POCKET Colorimeter II Colorimeter for Chlorine analysis.

Following this, a series of tests were conducted for each DPD manufacturer (Hach, PoliControl, LaMotte), as in Figure 3. Five tests were made for each DPD manufacturer in the low range (L.R.) in each equipment, and five tests were made for each DPD manufacturer in the high range (H.R.) in each equipment, as summarized in Figure 4.

For each test, a water sample was acquired and placed in the cell, and a single DPD pillow (or equivalent) was employed for measurement. The chlorine content registered in the equipment corresponded proportionally to the chlorine content present in the sample.

The HACH DPD manufacturer was considered the reference because HACH was the manufacturer of the reading devices. The other products from LaMotte and PoliControl were compared against it.



Figure 3. 1- LaMotte DPD, 2- Hach DPD, and 3- PoliControl DPD.

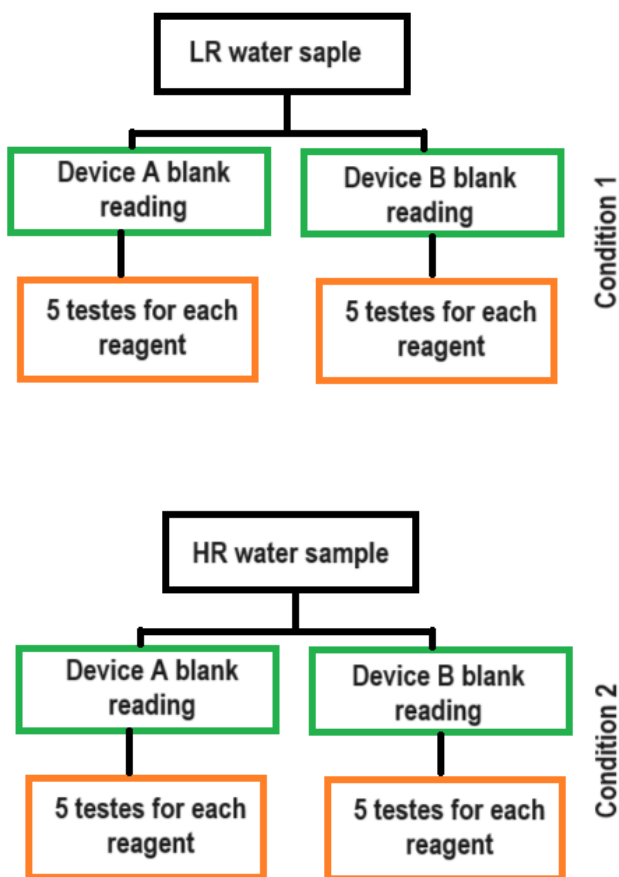


Figure 4. Test model.

2.2.2 Statistical methods

The test analysis data were collected and compiled into Tables 1 to 4 for subsequent MS-Excel statistical analyses. Later, the statistical analyses were used to write a linear interpolation script to present the analytical results of the DPD reagents from PoliControl and LaMotte in an equivalent form of the Hach DPD reagent. Table 5 represents the differences among the different models of spectrophotometers.

The equations used to calculate the Average and standard deviation came from MS-Excel functions: MED(XX:X) and DESVPAD.A(XX:X) (the names of the functions are in Portuguese).

The Percentage Difference was calculated using Equation 1. It was written in M.S. Excel as “=ABS((B1 - A1) / A1) * 100”. The ABS function in Excel stands for "Absolute Value.", and It was used to return the absolute (positive) value of the result.

$$\text{Percentage Difference} = \left| \frac{\text{New Value} - \text{Old Value}}{\text{Old Value}} \right| \times 100$$

(Eq. 1)

3. RESULTS AND DISCUSSION

3.1. Results

3.1.1. Analytical Results

Tables 1 to 4 summarize the statistical results from the tests done using the different DPD reagents.

Table 5 note the slight variations from the use of different spectrophotometers.

Table 5. Variation of the readings in the different equipment.

High range reading	Hach	Policontrol	LaMotte
pocket colorimeter II Average	0,67	0,67	0,52
DR300 Average	0,67	0,66	0,52
Equipment difference (%)	0	1,49	0
High range reading	Hach	Policontrol	LaMotte
pocket colorimeter II Average	5,8	6	4,7
DR300 Average	6,2	6,4	5
Equipment difference (%)	6,90	6,67	6,38

3.1.2.1. HTML / Javascript code for linear interpolating the results from the Policontrol reagent using the Hach reagent as “reference.”

```
<!DOCTYPE html>
<!--
This code is licensed under CC BY 4.0
(https://creativecommons.org/licenses/by/4.0/)
You are free to share and adapt the
code, but you must provide appropriate
credit to the original author.
DOI:
10.48141/SBJCHEM.v31.n36.2023_TREIN_pgs_
33_45.pdf
-->
<html lang="en">
<head>
<meta charset="utf8_general_ci">
<title>Linear Interpolation</title>
```

```

<style>
  body {
    font-family: Arial, sans-serif;
    display: flex;
    justify-content: center;
    align-items: center;
    height: 100vh;
    margin: 0;
  }
  h1 {
    text-align: center;
  }
  label,
  input,
  button {
    display: block;
    margin: 10px auto;
    text-align: center;
  }
  input,
  button {
    padding: 8px;
    border-radius: 5px;
    border: 1px solid #ccc;
    width: 200px;
  }
  button {
    cursor: pointer;
  }

  background-color: #007bff;
  color: white;
  transition: background-color 0.3s
ease;
}
button:hover {
  background-color: #0056b3;
}
p {
  text-align: center;
  margin-top: 20px;
}
#resultado {
  font-weight: bold;
}
</style>
</head>
<body>
  <div style="text-align: center;">
    <h1>Linear Interpolation</h1>
    <label for="valorB">

      Please insert the value of the
reagent "Policontrol":<br>
    </label>
    <input type="number"
id="valorB"><br><br>
    <button
onclick="calculateResult()">
      Calculate
    </button>
  </div>

  <p>
    The adjusted result of the value, to be
equivalent to the Hach product, is:
    <span id="resultado"></span>
  </p>

```

```

</p>
</div>
<script>
  function calculateResult() {
    // Reference values
    const x = [0.67, 5.80];
    const secondLineValues = [0.67, 6.0];
    // Get the value entered by the user for
    B
    const valueB =
parseFloat(document.getElementById('valorB').value);

    // Perform linear interpolation
    const result =
linearInterpolation(secondLineValues, x,
valueB);

    // Display the result on the page
    document.getElementById('resultado').tex
tContent = result.toFixed(2);
  }

  function linearInterpolation(x, y,
value) {
    const [x0, x1] = x;
    const [y0, y1] = y;

    // Linear interpolation formula
    const result = y0 + ((value - x0) * (y1
- y0)) / (x1 - x0);

    return result;
  }
</script>
</body>
</html>
</html>

```

Linear Interpolation

Please insert value of the reagent "Policontrol":

Calculate

The adjusted result of the value, to be equivalente of the Hach product is: **0.67**

Figure 5. The expected interface of the code from item 3.1.2.1. HTML / Javascript code for the linear interpolation of the results from the Policontrol.

To run the code, please visit <https://acaria.org/codes/code5.htm>.

3.1.2.2. HTML / Javascript code for linear interpolating the results from the LaMotte reagent using the Hach reagent as "reference."

```
<!DOCTYPE html>
<!--
This code is licensed under CC BY 4.0
(https://creativecommons.org/licenses/by/4.0/)
You are free to share and adapt the
code, but you must provide appropriate
credit to the original author.
DOI:
10.48141/SBJCHEM.v31.n36.2023_TREIN_pgs_
33_45.pdf
-->
<html lang="en">
  <head>
    <meta charset="utf8_general_ci">
    <title>Linear Interpolation</title>
    <style>
      body {
        font-family: Arial, sans-serif;
        display: flex;
        justify-content: center;
        align-items: center;
        height: 100vh;
        margin: 0;
      }
      h1 {
        text-align: center;
      }
      label,
      input,
      button {
        display: block;
        margin: 10px auto;
        text-align: center;
      }
      input,
      button {
        padding: 8px;
        border-radius: 5px;
        border: 1px solid #ccc;
        width: 200px;
      }
      button {
        cursor: pointer;

        background-color: #007bff;
        color: white;
        transition: background-color 0.3s
ease;
      }
      button:hover {
        background-color: #0056b3;
      }
      p {
        text-align: center;
        margin-top: 20px;
      }
      #resultado {
        font-weight: bold;
```

```
    }
  </style>
</head>
<body>
  <div style="text-align: center;">
    <h1>Linear Interpolation</h1>
    <label for="valorB">

      Please insert the value of the
reagent "LaMotte":<br>

    </label>
    <input type="number"
id="valorB"><br><br>
    <button
onclick="calculateResult()">
      Calculate
    </button>
  <p>
The adjusted result of the value, to be
equivalent to the Hach product, is:
<span id="resultado"></span>
  </p>
</div>
<script>
  function calculateResult() {
    // Reference values
    const x = [0.67, 5.8]; // Values from
Hach
    const secondLineValues = [0.52, 4.7]; //
Values from LaMotte

    // Get the value entered by the user for
B
    const valueB =
parseFloat(document.getElementById('valo
rB').value);

    // Perform linear interpolation
    const result =
linearInterpolation(secondLineValues, x,
valueB);

    // Display the result on the page
    document.getElementById('resultado').tex
tContent = result.toFixed(2);
  }

  function linearInterpolation(x, y,
value) {
    const [x0, x1] = x;
    const [y0, y1] = y;

    // Linear interpolation formula
    const result = y0 + ((value - x0) * (y1
- y0)) / (x1 - x0);

    return result;
  }
</script>
</body>
</html>
```

Linear Interpolation

Please insert value of the reagent "LaMotte":

Calculate

The adjusted result of the value, to be equivalent of the Hach product is: 0.67

Figure 6. The expected interface of the code from item 3.1.2.2. HTML / Javascript code for the linear interpolation of the results from the LaMotte.

To run the code, please visit <https://acaria.org/codes/code6.htm>.

3.2. Discussions

3.2.1. Different results for the same sample

Unsurprisingly, the DPD reagents from different suppliers or the different types of equipment provided slightly different readings. However, it was relevant to infer values, or magnitudes, to the differences empirically observed.

As it is commonly known, one of the best methods to determine the chlorine concentration is the Argentometric method (ASTM D512-04, Test method B). However, the method has its challenges and limitations that make it unattractive when it is necessary to perform the analyses of hundreds of samples daily. So, it is worth pointing out that the goal of the research was not to find the best method to determine the chlorine concentration in water samples but to observe if there were variations in the same method with different manufacturers of the DPD reagent and types of equipment.

Additionally, it is relevant to observe that if the experimental conditions were different, other results would be found, such as if the spectrophotometer were from a different brand; the results that were considered the most accurate could be others. Therefore, the authors are not saying that the quality of reagent "A" or "B" is better or worse than reagent "C", but that in any serious company, the acquisition department can not buy the DPD reagents as if they were interchangeable.

3.2.2. Adjusting the different results to be expressed in terms of the Hach result.

The authors chose to express the

analytical results of the study in terms of the Hach DPD reagent because it was available for the study both the reagent and the spectrophotometer from the same brand.

To do this representation a simple linear interpolation was performed, and the mathematical aspect was represented in a friendly format using HTML and JavaScript code.

3.2.3. Different results in different spectrophotometers from the same brand

The differences among the two spectrophotometer models in the low-range sample reading were less representative than in the high-range. This increased variation in the high-range tests was also expected since was approaching the upper limit of the test method.

3.2.4. Practical implications of the different results

Real-world applications may face some challenges, such as in the low-range readings; depending on the test conditions, the test results with low values may induce a water treatment plant operator to unnecessarily increase the addition of chlorine, increasing the cost of operation. A simple solution to this possible issue would be the production of a linear correlation chart between the Argentometric method and the conditions of the DPD test method being used in this hypothetical situation.

3.2.5. Practical implications of the different results

Table 6. Representation of the 95% confidence intervals of different DPD reagents and equipment.

Confidence intervals LR pocket colorimeter II					
Hach		Policontrol		LaMotte	
From	To	From	To	From	To
0,66	0,70	0,66	0,68	0,51	0,53
Confidence intervals LR DR300					
0,66	0,70	0,65	0,67	0,51	0,52
Confidence intervals HR pocket colorimeter II					
5,71	5,89	5,87	6,09	4,65	4,79
Confidence intervals HR DR300					
6,11	6,33	6,31	6,45	4,95	5,09

Table 6 outlines the 95% confidence intervals of sample readings for different DPD reagents and equipment combinations. With a 95% confidence level, the true mean of the population readings is estimated to be within these

intervals.

4. CONCLUSIONS:

Reading the same chlorinated water samples using different equipment resulted in slight variations in test outcomes. DPD reagents from various manufacturers are not entirely interchangeable and must not be utilized without proper correlation against a reference standard. The open-source codes developed for linear interpolation of obtained data yielded satisfactory values and reduced the disparity in the results.

5. DECLARATIONS

5.1. Study Limitations

The study is limited to the sample size, materials (DPD from different manufacturers), and experimental conditions.

5.2. Acknowledgements

Chat GPT and Google Bard generated part of this manuscript's text and codes.

5.3. Funding source

The authors funded this research.

5.4. Competing Interests

The authors have no financial, personal, or professional connections that might bias or influence the research, analysis, or conclusions presented in this work. Therefore we declare no conflict of interest associated with this publication.

5.5. Open Access

This article is licensed under a Creative Commons Attribution 4.0 (CC BY 4.0) International License, which permits use, sharing, adaptation, distribution, and reproduction in any medium or format, as long as you give appropriate credit to the original author(s) and the source, provide a link to the Creative Commons license, and indicate if changes were made. The images or other third-party material in this article are included in the article's Creative Commons license unless indicated otherwise in a credit line to the material. Suppose material is not included in the article's Creative Commons license, and your intended use

is not permitted by statutory regulation or exceeds the permitted use. In that case, you will need to obtain permission directly from the copyright holder. To view a copy of this license, visit <http://creativecommons.org/licenses/by/4.0/>.

7. REFERENCES:

1. Moberg, L., & Karlberg, B. (2000, February). An improved N,N'-diethyl-p-phenylenediamine (DPD) method for the determination of free chlorine based on multiple wavelength detection. *Analytica Chimica Acta*. Elsevier B.V. Retrieved from [http://dx.doi.org/10.1016/S0003-2670\(99\)00780-1](http://dx.doi.org/10.1016/S0003-2670(99)00780-1)
2. WILDE, E. (1991, October). Comparison of three methods for measuring residual chlorine. *Water Research*. Elsevier B.V. Retrieved from [http://dx.doi.org/10.1016/0043-1354\(91\)90071-W](http://dx.doi.org/10.1016/0043-1354(91)90071-W)
3. Chlorine, Free and Total, Low Range. USEPA DPD Method 1 Method 8021 (Free) 8167 (Total) 0.02 to 2.00 mg/L Cl 2 (L.R.) Powder Pillows or AccuVac ® Ampuls. (n.d.). Retrieved December 9, 2023, from https://cdn.bfldr.com/7FYZVWYB/at/bjxnnj q6pzjbmpns2cvxbf/DOC3165301450_5ed.pdf
4. Chlorine, Free and Total, High Range. (2022) USEPA DPD Method 1 Method DPD 0.1 to 8.0 mg/L Cl 2 Powder Pillows. (n.d.). Retrieved December 9, 2023, from https://cdn.bfldr.com/7FYZVWYB/at/xtn3q r6g6gzrvfgr3c7kg43/DOC3165301449_7ed.pdf
5. NEMI Method Summary - 4500-Cl B. (n.d.). [Www.nemi.gov](http://www.nemi.gov). Retrieved December 9, 2023, from https://www.nemi.gov/methods/method_summary/7429/
6. International Organization for Standardization. (1990). ISO 7393-3:1990, Water quality - Determination of free chlorine and total chlorine - Part 3: Iodometric titration method for the determination of total chlorine (pp. 1-5).
7. Lamb, A. B., Carleton, P. W., & Meldrum, W. B. (1920, February). THE

- DETERMINATION OF CHLORINE WITH THE NEPHELOMETER. Journal of the American Chemical Society. American Chemical Society (ACS). Retrieved from <http://dx.doi.org/10.1021/ja01447a008>
8. Coll, Hans, "Spectrophotometric Determination of Chloride Ion." (1957). LSU Historical Dissertations and Theses. 197. Retrieved from https://repository.lsu.edu/gradschool_dissertations/197
 9. ASTM International. (2004). ASTM D512-04, Standard Test Methods for Chloride Ion in Water (Withdrawn 2015). ASTM International.
 10. Astuti, M. P., Xie, R., & Aziz, N. S. (2017). Laboratory and pilot plant scale study on water dechlorination by medium pressure ultraviolet (U.V.) radiation. (I. Iskandar, S. Ismadji, T. E. Agustina, I. Yani, L. N. Komariah, & S. Hasyim, Eds.) MATEC Web of Conferences. EDP Sciences. Retrieved from <http://dx.doi.org/10.1051/mateconf/201710102003>
 11. Ismail, I. A., Hertel, M., & Swanson, T. L. (2015). Chlorine analytical test element and a stabilized n, n-diethyl-p-phenylenediamine solution (U.S. Patent No. US20150050195A1). Hach Co. <https://patents.google.com/patent/US20150050195A1/en>

Table 1. Low-Range test results in the pocket colorimeter II.

Low range reading	Hach	Instantaneous reading	
		Policontrol	LaMotte
Test 1	0,69	0,65	0,51
Test 2	0,67	0,66	0,53
Test 3	0,72	0,68	0,51
Test 4	0,67	0,67	0,52
Test 5	0,67	0,67	0,52
Statistics	-	-	-
Mean	0,684	0,666	0,518
Standard error	0,009798	0,00509902	0,0037417
Median	0,67	0,67	0,52
Mode	0,67	0,67	0,51
Standard deviation	0,0219089	0,011401754	0,0083666
Sample variance	0,00048	0,00013	7E-05
Kurtosis	1,7447917	-0,177514793	-0,6122449
Skewness coefficient	1,5309606	-0,404796009	0,5122408
Range	0,05	0,03	0,02
Minimum	0,67	0,65	0,51
Maximum	0,72	0,68	0,53
Sum	3,42	3,33	2,59
Count	5	5	5
Confidence level (95.0%)	0,0272035	0,014157148	0,0103885
% of the difference of the mean from the HACH		2,63%	24,27%

Table 2. Low-Range test results in the DR300 Pocket Colorimeter.

Low range reading	Hach	Instantaneous reading	
		Policontrol	LaMotte
Test 1	0,68	0,64	0,52
Test 2	0,71	0,66	0,52
Test 3	0,67	0,67	0,51
Test 4	0,67	0,67	0,52
Test 5	0,67	0,66	0,5
Statistics	-	-	-
Mean	0,68	0,66	0,514
Standard error	0,007746	0,005477226	0,004
Median	0,67	0,66	0,52
Mode	0,67	0,66	0,52
Standard deviation	0,0173205	0,012247449	0,0089443
Sample variance	0,0003	0,00015	8E-05
Kurtosis	3,6666667	2	0,3125
Skewness coefficient	1,9245009	-1,360827635	-1,2577882
Range	0,04	0,03	0,02
Minimum	0,67	0,64	0,5
Maximum	0,71	0,67	0,52
Sum	3,4	3,3	2,57
Count	5	5	5
Confidence level (95.0%)	0,0215063	0,015207216	0,0111058
% of the difference of the mean from the HACH		2,94%	24,41%

Table 3. The high-range test results from the pocket colorimeter II.

High range reading	Hach	Instantaneous reading	
		Policontrol	LaMotte
Test 1	5,7	6	4,8
Test 2	5,8	5,9	4,7
Test 3	5,7	6,1	4,7
Test 4	5,9	5,8	4,8
Test 5	5,9	6,1	4,6
Statistics	-	-	-
Mean	5,8	5,98	4,72
Standard error	0,0447214	0,058309519	0,0374166
Median	5,8	6	4,7
Mode	5,7	6,1	4,8
Standard deviation	0,1	0,130384048	0,083666
Sample variance	0,01	0,017	0,007
Kurtosis	-3	-1,487889273	-0,6122449
Skewness coefficient	2,22E-14	-0,541387051	-0,5122408
Range	0,2	0,3	0,2
Minimum	5,7	5,8	4,6
Maximum	5,9	6,1	4,8
Sum	29	29,9	23,6
Count	5	5	5
Confidence level (95.0%)	0,1241664	0,161893178	0,1038851
% of the difference of the mean from the HACH		3,10%	18,62%

Table 4. High-range test results in the DR300 Pocket Colorimeter.

High range reading	Instantaneous reading		
	Hach	Policontrol	LaMotte
Test 1	6,1	6,4	5,1
Test 2	6,2	6,3	4,9
Test 3	6,1	6,4	5
Test 4	6,4	6,3	5,1
Test 5	6,3	6,5	5
Statistics	-	-	-
Mean	6,22	6,38	5,02
Standard error	0,0583095	0,037416574	0,0374166
Median	6,2	6,4	5
Mode	6,1	6,4	5,1
Standard deviation	0,130384	0,083666003	0,083666
Sample variance	0,017	0,007	0,007
Kurtosis	-1,4878893	-0,612244898	-0,6122449
Skewness coefficient	0,5413871	0,512240833	-0,5122408
Range	0,3	0,2	0,2
Minimum	6,1	6,3	4,9
Maximum	6,4	6,5	5,1
Sum	31,1	31,9	25,1
Count	5	5	5
Confidence level (95.0%)	0,1618932	0,103885063	0,1038851
% of the difference of the mean from the HACH		2,57%	19,29%

STATISTICAL VALIDATION OF TRIPLE COLOCALIZATION ANALYSIS

BUONFIGLI Julio^{1*}; QUINTERO Cristian^{2,3}; SÁNCHEZ Diego¹; LEIVA Natalia^{4,5}; DAMIANI Maria Teresa¹

¹Universidad Nacional de Cuyo, Facultad de Medicina, Laboratorio de Fagocitosis y Transporte intracelular, IMBECU-CONICET, Mendoza, Argentina.

²Laboratorio de Biología Molecular y Celular. Universidad Juan Agustín Maza, Mendoza, Argentina.

³Facultad de Ciencias Médicas, Universidad de Mendoza, Mendoza, Argentina.

⁴CONICET, Facultad de Ciencias Médicas, Universidad Nacional de Cuyo, M5500 Mendoza, Argentina.

⁵Facultad de Ciencias Exactas y Naturales, Universidad Nacional de Cuyo, M5500 Mendoza, Argentina.

* Corresponding author

e-mail: juliobuonfigli@yahoo.com.ar

Received 30 July 2023; received in revised form 07 December 2023; accepted 15 December 2023

ABSTRACT

Background: in the last decades, colocalization analysis of fluorescently tagged biomolecules has proven to be a powerful approach to studying functional relationships between these biomolecules. However, in many cases, to give this analysis a biological meaning, colocalization coefficients must be tested statistically, comparing them with the colocalization expected by chance. **Aim:** It addressed the statistical significance of triple colocalization to distinguish real triple colocalization and classify different triple signal scenarios. **Methods:** we use biological and generated images of triple signal scenarios to contrast seven independent statistical facts with independent statistical tests. Three of these tests correspond to pairwise relationships (double scrambling tests), and the others correspond to triple relationships: single scrambling tests (red, green, and blue scrambling) and the triple scrambling test. The analysis and methodology proposed can be reproduced using the application developed in our laboratory. **Results:** In the study approach, we found true triple relationships ignored by using traditional methods of computing the statistical significance, while we could reinterpret cases of not significant triple colocalization wrongly considered as significant by traditional methods. **Discussion:** single scrambling tests can reveal significant triple colocalization for low levels of triple co-occurrence, even when all pairwise relationships were exclusion relationships. Moreover, on the other hand, single scrambling tests can reveal the absence of a significant triple colocalization for high levels of triple co-occurrence, even when all pairwise relationships were significant colocalization. **Conclusion:** all scrambling tests are useful to classify a specific scenario of a triple relationship. Dynamics like mitosis can be distinguished into their phases by triple signal relationships using these 7 independent statistical tests.

Keywords: Scrambling, overlapping, significance, correlation, triple.

1. INTRODUCTION:

Colocalization in fluorescence images is one of the most commonly used approaches to study functional interactions between biomolecules. Using fluorescence microscopy techniques, the spatial distribution of two biomolecules is recorded on independent images. Then, the spatial overlapping of the signal of both fluorophores is quantified as a colocalization coefficient (Bolte & Cordelieres, 2006; Dunn, Kamocka, & McDonald, 2011; Oheim & Li, 2007; Zinchuk & Zinchuk, 2008). Unfortunately, colocalization coefficients use fluorescent light signals as inputs, and fluorescence intensity is a non-reproducible parameter. Fluorescence intensity is sensitive to many variables related to the setting of the microscope, fluorophores, and experimental conditions, including variables that are not fully manageable by users, such as the efficiency of the optical coupling, cleanness of optics, environmental perturbations (vibrations and electromagnetic fields), output power and output instability of laser in confocal microscopy, to name a few (Pawley, 2000). Small changes in such variables can make colocalization coefficients yield very different results. Thus, colocalization coefficients cannot be linked to biophysical variables. Statistical analysis gives a probabilistic approach, improving the biological interpretation of colocalization analysis (French, Mills, Swarup, Bennett, & Pridmore, 2008; Lachmanovich *et al.*, 2003; McDonald & Dunn, 2013). This analysis determines if there exists 'significant colocalization' (SC), which indicates biomolecules tend to be close to each other, 'not significant colocalization' (NS), which means that biomolecules only meet each other by chance, or 'significant exclusion' (SE) which means that biomolecules avoid each other. Then, depending on the resolution of images, this tendency to be close (SC) can be associated with biophysical variables ranging from physicochemical similarities and co-compartmentalization to direct interactions (Jeremy Adler & Parmryd, 2010; French *et al.*, 2008; Lagache, Sauvonnet, Danglot, & Olivo-Marin, 2015; Malkusch *et al.*, 2012)

Costes et al. developed one of the most used approaches to address statistical significance for two-channel colocalization analysis (*Costes et al.*, 2004). They proposed to compare actual colocalization coefficients with

the one obtained when pixels (or blocks of pixels) of one or both channels are randomly rearranged, an approach known as 'scrambling'. This coefficient, measured using scrambled images, serves as a virtual control that simulates random colocalization. The scrambling procedure is repeated as many times as necessary to validate the existence or absence of a significant difference with the actual coefficient. Other approaches can be cited (Fay, Taneja, Shenoy, Lifshitz, & Singer, 1997; Li *et al.*, 2004; Lifshitz, 1998; McDonald & Dunn, 2013; Ramírez, García, Rojas, Couve, & Härtel, 2010; Van Steensel *et al.*, 1995), but all of them are strictly focused on pairwise colocalization analysis, and although, some of these approaches can be adapted for three channels, this matter is loosely addressed in the existent bibliography. Triple colocalization cannot be inferred from the analysis of pairwise relationships. A triple grouping behaves differently from pairwise groupings (Fletcher, Scriven, Schulson, & Moore, 2010). Thus, considering any three channels analysis with red (R), green (G) and blue (B) signals, a triple colocalization (RGB) may exist in the absence of significant pairwise colocalization (RG; RB; GB), and conversely, even when all pairwise colocalizations (RG; RB; GB) were significant, this does not necessarily imply the existence of a significant triple colocalization (RGB). Some authors have addressed the issue of triple colocalization (Fletcher *et al.*, 2010; Goucher, Wincovitch, Garfield, Carbone, & Malik, 2005; Wörz *et al.*, 2010) but Fletcher *et al.* are the only authors who have performed a statistical significance on triple colocalization analysis (Fletcher *et al.*, 2010). They proposed a statistical test of triple colocalization in which random triple colocalization is simulated by scrambling all channels to simulate random colocalization. Although this test yields valuable information for colocalization analysis, it fails when it is isolated to judge a triple colocalization.

This work explores the scope of triple colocalization analysis from a statistical perspective. We use biological and generated images to show the importance of triple colocalization analysis as an independent subject not inferrable from pairwise relationships. In this respect, we follow a methodology based on co-occurrence analysis using MOC (Manders overlap coefficient). We contrast seven independent statistical facts with seven different statistical tests. Three of these tests correspond to pairwise relationships (double scrambling tests), and the others

correspond to triple relationships: single scrambling tests (red, green, and blue scrambling) and the triple scrambling test. The study shows how all these tests are useful to understand pairwise and triple colocalization. The proposed analysis and methodology can be reproduced using the application at <https://gitlab.com/juliobuonfigli/tcss>

2. MATERIALS AND METHODS

2.1. Materials

Both the generation of simulated colocalization images and manipulation (crops and rotations) of the microscopy image were performed using ImageJ 1.52p. All colocalization and statistical analysis were performed by an ImageJ application available at <https://gitlab.com/juliobuonfigli/tcss>. The script mentioned above also details of how to use it. Histograms of Figure 1 were made using the stats program SPSS Statistics 24.0.0.

2.1.1 List of software used in script writing:

- Notepad;
- ImageJ;

2.2. Methods

Biological and generated images were used to recreate different triple colocalization scenarios and test our approach.

2.2.1 Biological and generated images

It was generate 2 and 3 channels binary images with 20 (Figure 1Ai and 1Bi), 35 (Figure 1Ci), and 10 (Figure 1Ciii) round objects of 15 (Figure 1Ai, 1Bi, and 1Ci) and 30 (Figure 1Ciii) pixels diameter on each channel, in a total area of 200x200 pixels. To generate random triple overlapping, the center of all blue objects (Figure 1Bi) and all overlapped pairs of objects (Figure 1Ciii) were randomly positioned using the random function of the ImageJ. After 100 randomizations for each case, the merge with the median MOC_{RGB} was selected in both cases. Scrambling examples (Figure 1Aii, 1Aiv, 1Avi, 1Bii, 1Bv, 1Bvii, and 1Bix) were generated by rendering a series of rearranged actual images of 15 pixels block (Figure 3B) and merging with

actual or other scrambled images.

A single image with seven selected samples of the mitosis phases was downloaded from <https://wellcomecollection.org/works/r8ppshar>. The original image (Figure 3A) shows all mitosis phases (interphase, prophase, prometaphase, metaphase, early anaphase, anaphase, and telophase) in which kinetochores are labeled in red, tubulin in green, and DNA in blue, in a 3000x2250 pixels JPG image. Each phase was cropped and rotated to be analyzed separately. No treatments or filters were applied to the full-size image and crops.

2.2.2 Coefficients

For pairwise relationships, the Manders overlap coefficient (MOC) is given by:

$$MOC_{RG} = \frac{\sum(R_i * G_i)}{(\sum R_i^2 * \sum G_i^2)^{1/2}} \quad (\text{Eq. 1})$$

Where R_i is the intensity of the i^{th} pixel in the red channel, and G_i is the intensity of the i^{th} pixel in the green channel. This coefficient ranges from 0 to 1 and measures the proportion of colocalized signals over the total amount of both signals (MANDERS, VERBEEK, & ATEN, 1993). To measure triple overlapping, we add a third series to the equation:

$$MOC_{RGB} = \frac{\sum(R_i * G_i * B_i)}{(\sum R_i^3 * \sum G_i^3 * \sum B_i^3)^{1/3}} \quad (\text{Eq. 2})$$

where B_i is the intensity of the i^{th} pixel in the blue channel. MOC_{RGB} ranges from 0 to 1 and measures the proportion of colocalized signals over the total amount of signals. Manders colocalization coefficient (MCC) (MANDERS *et al.*, 1993) is given by:

$$MCC_{RG} = \frac{\sum(R_{iG})}{(\sum R_i)} \quad (\text{Eq. 3})$$

$$MCC_{R-GB} = \frac{\sum(R_{iGB})}{(\sum R_i)} \quad (\text{Eq. 4})$$

Where R_{iG} is the intensity of the i^{th} pixel in the red channel that colocalizes with a green pixel above the intensity threshold, and R_{iGB} is the intensity of the i^{th} pixel in the red channel that

colocalizes with a green and blue pixel above their respective intensity thresholds. MCC_{RG} measures the proportion of red signal that colocalizes with green signal, and MCC_{R-GB} measures the proportion of red signal that colocalizes with green and blue signals. With three channels, there are 9 MCC coefficients with subscripts: RG, GR, RB, BR, GB, and BG for pairwise relationships, and R-GB, G-RB and B-RG for triple colocalization.

2.2.3 Running the plugin

The script runs as a plugin of the opensource program ImageJ, available at <https://imagej.net/ij/>. The script is available at <https://gitlab.com/julioBuonfigli/tcss>. To run the script:

1) Install the plugin by saving this file in the ImageJ\plugins\Macros folder and restart ImageJ

Then click in plugins->macros->install and search this file in the ImageJ\plugins\Macros folder.

2) Open the three channels to use and generate the mask if necessary

The mask is a binary image of the same dimensions as the channels, with intensities of 255 inside and 0 outside the ROI

3) Run the macro by clicking plugins->macros->TCSS or pressing the 'c' key

4) Load the channels and the mask

5) Select an approach to set thresholds as:

- The average intensity value inside the ROI plus x standard deviations settled by the user from -2 to 2

- A percentage of pixels higher than zero inside the ROI (from 0 to 100)

- An intensity value from 0 to 255

6) Set the intensity threshold values for each channel according to the approach selected

7) Select the scrambling approach:

- Coordinates: randomly changes the origin of coordinates of actual channels (Lifshitz approach)

- Pixels: randomly relocates all pixels (Costes approach)

- Blocks of pixels: randomly relocates

blocks of pixels (Costes approach)

If 'Blocks of pixels' is selected the, the block size must be set as an area of pixels

Block of pixels approach will not run with a mask-loaded

8) Set the hypothesis test:

- T-test approach

- Non-parametric approach: the ratio of the amount of random coefficients higher than the actual value and the totality of random coefficients measured

9) Set the number of generated images: the number of times actual channels will scramble to generate the random overlapping distribution. set it to zero to calculate just coefficients

10) Set the significance level (0.01 or 0.05): the cut-off point of p-values to consider the test SC, SE or NS

11) Set the random seed: a positive integer that points to the beginning of the series of pseudorandom numbers. Please set it to zero for a random beginning

RESULTS:

A table shows the coefficient (MOC or MCC) for each relationship;

The average of random coefficients (random); the significance result (significance); and the p-value.

The least related channel (LRC) is indicated with an arrow ('<') in the first column of triple colocalization relationships

Graphical results are summarized in a stack that displays examples of scrambled channels and the merge of the thresholded channels

2.2.4 Data processing

Statistical significances of analysis performed in Fig. 1 were made by repeating the scrambling procedure (Figure 3B) 1000 times and then performing a one-tailed hypothesis test with an error tolerance of 5%. The block size was settled according to the diameter of the objects. For microscopy images, due to the difficulty of object segmentation and thus setting the proper block size and avoiding altering the autocorrelation of each channel (Bolte & Cordelieres, 2006), we followed the Lifshitz

approach (Lifshitz, 1998). Scrambled images were generated by randomly changing the coordinates of the origin of actual channels (Figure 3C). To find p-values, a non-parametric approach was used: the ratio of the number of random coefficients higher than the actual MOC value and the totality of random coefficients measured. To avoid altering autocorrelation by the scrambling process (Lifshitz approach), squared regions of interest (ROIs) were used. ROIs were set as the biggest square that can be fitted inside cell edges (Figure 2B). Experiments of Fig. 1 were done using both randomization approaches and yielded the same significant results. For microscopy images, signal thresholds were set at the average intensity value of the signal inside the ROI.

2.2.5 Source code (tcss / TCSS.txt)

```

/*
*Triple Colocalization Statistical
Significance (TCSS)
*Author: Julio Federico Buonfigli
*e-mail: juliobuonfigli@yahoo.com.ar
Version 6.01
This code is licensed under CC BY 4.0
(https://creativecommons.org/licenses/
by /4.0/).
You are free to share and adapt the
code, but you must provide appropriate
credit to the original author.
DOI:
10.48141/SBJCHEM.v31.n36.2023_BUONFIGLI
I_pg_s_45_62.pdf
*/
macro "TCSS [c]" {

  BATCH=false;
  if(BATCH) arg1=getArgument();
  MCC=false;
  //MCC=true;

  //FUNCTIONS

  function TheLeast(vec, c0, c1, c2)
  //Finds the least related channel
  using p-values
  {
    v=vec; m=c0;
    if(c1<m) m=c1;
    if(c2<m) m=c2;
    if(m==c0)
      v[2]=vec[2]+"<";
    if(m==c1)
      v[1]=vec[1]+"<";
    if(m==c2)
      v[0]=vec[0]+"<";
    return v;
  }

```

```

//'A Fairly Accurate Approximation to
the Area Under Normal Curve', AMIT
CHOUDHURY AND PARAMITA ROY, 2009
function Pvalue(x) //calculates p-
value
{
  if(x<0) {indi=1; x=(-1)*x; }
  else indi=0;

  if(x<=2.0885 && x>0){
    t=0.5 + (1/sqrt(2*PI))*exp(-pow(x,
2)/2)*((654729075*x + 45945900*pow(x,
3)
    + 6486480*pow(x, 5) +
154440*pow(x, 7) + 4785*pow(x,
9))/(654729075
    - 172297125*pow(x, 2) +
20270250*pow(x, 4) - 1351350*pow(x, 6)
+ 51975
    *pow(x, 8) - 945*pow(x, 10)));}

  if(x<1.8735 && x>0) y=t;

  if(x>=1.8735 && x<=2.0885)
  y = t - 0.00007237 + 0.0000768*x -
0.00002041*pow(x, 2);

  if(x>2.0885 && x<=5.75){
    t=1 - (1/(2*sqrt(2*PI)))*exp(-
pow(x, 2)/2)*((5790*x + 5280*pow(x, 3)
+ 1176*
    pow(x, 5) + 88*pow(x, 7) +
2*pow(x, 9))/(945 + 4725*pow(x, 2) +
3150*
    pow(x, 4) + 630*pow(x, 6) +
45*pow(x, 8) + pow(x, 10)));}

  if(x>2.0885 && x<2.43)
  y = t - 0.00004861 + 0.00004021*x
- 0.00000833*pow(x, 2);

  if(x>2.43 && x<=5.75) y=t;
  if(x>5.75) y=1;

  if(indi==0) z=1-y;
  else
  {
    if(x==0) z=0.5;
    else z=y;
  }
  return(z)
}

function Renderize(vec, masc, img)
//Transforms a vector to an image
{
  selectWindow(img);
  w=getWidth; h=getHeight;
  j=0; i=0;
  for(y=0; y<h; y++)
  {
    for(x=0; x<w; x++)

```

```

        {
            u[e]=false;
            if(masc[i]==255)
            {
                i++;
                setPixel(x, y,
            }
        }
        return rd;
    }

function CoordRand(vec, ones) //shifts
the beginning of a vector
{
    j=round((ones-1)*random);
    v=newArray(ones);
    for(i=0; i<ones; i++)
    {
        v[i]=vec[j];
        j++;
        if(j>ones-1) j=0;
    }
    return v;
}

function BlockRand(vec, w, h, r)
//generates the block scrambling of a
vector
{
    X=w/r; Y=h/r;
    pos=newArray(X*Y);
    i=0;
    for(y=0; y<Y; y++)
    {
        for(x=0; x<X; x++)
        {
            pos[i]=w*y*r+x*r;
            i++;
        }
    }
    ran=newArray(X*Y);
    ran=PixelRand(pos);
    v=newArray(w*h);
    for(i=0; i<ran.length; i++)
    {
        j=ran[i]; k=pos[i];
        for(y=0; y<r; y++)
        {
            for(x=0; x<r; x++)
            {
                v[k]=vec[j];
                j++; k++;
            }
        }
        j=j+w-r;
        k=k+w-r;
    }
    return v;
}

function Threshold(vec, um, ones)
//Thresholds an array
{
    ar=newArray(ones);
    for(i=0; i<ones; i++)
    {
        if(vec[i]>=um)
            ar[i]=vec[i];
    }
}

function Pthreshold(canal, unos, prop)
//Calculates the threshold to keep a
specific percentage of signal inside
the ROI
{
    umbral=256;
    vec=newArray(umbral);
    for(j=0; j<umbral; j++)
        vec[j]=0;
    for(i=0; i<unos; i++)
        vec[canal[i]]=vec[canal[i]]+1;
    cuenta=0;
    do {
        umbral--;
        cuenta=cuenta+vec[umbral];
    } while(cuenta <
unos*(prop/100))
    return umbral;
}

function Vectorize(image, w, h)
//Vectorize an image
{
    selectWindow(image);
    vec=newArray(w*h);
    i=0;
    for (y=0; y<h; y++)
    {
        for (x=0; x<w; x++)
        {
            vec[i] = getPixel(x,y);
            i++;
        }
    }
    return vec;
}

function PixelRand(vector) //Shuffles
an array
{
    ones=vector.length;
    u=newArray(ones+1);
    for(i=0; i<ones; i++)
        u[i]=true;
    rd=newArray(ones);
    i=0;
    while(i<ones)
    {
        e=round(random*ones);
        if(u[e]==true)
        {
            rd[i]=vector[e];
            u[e]=false;
            i++;
        }
    }
}

function CoordRand(vec, ones) //shifts
the beginning of a vector
{
    j=round((ones-1)*random);
    v=newArray(ones);
    for(i=0; i<ones; i++)
    {
        v[i]=vec[j];
        j++;
        if(j>ones-1) j=0;
    }
    return v;
}

function BlockRand(vec, w, h, r)
//generates the block scrambling of a
vector
{
    X=w/r; Y=h/r;
    pos=newArray(X*Y);
    i=0;
    for(y=0; y<Y; y++)
    {
        for(x=0; x<X; x++)
        {
            pos[i]=w*y*r+x*r;
            i++;
        }
    }
    ran=newArray(X*Y);
    ran=PixelRand(pos);
    v=newArray(w*h);
    for(i=0; i<ran.length; i++)
    {
        j=ran[i]; k=pos[i];
        for(y=0; y<r; y++)
        {
            for(x=0; x<r; x++)
            {
                v[k]=vec[j];
                j++; k++;
            }
        }
        j=j+w-r;
        k=k+w-r;
    }
    return v;
}

function Threshold(vec, um, ones)
//Thresholds an array
{
    ar=newArray(ones);
    for(i=0; i<ones; i++)
    {
        if(vec[i]>=um)
            ar[i]=vec[i];
    }
}

```

```

        else
            ar[i]=0;
    }
    return ar;
}

function Sig(rat, lev) //Evaluates the
significance
{
    if(rat<lev)
        sig="SC";
    else
    {
        if(rat>1-lev)
            sig="SE";
        else
            sig="NS";
    }
    return sig;
}

function Tcoloc(c1, c2, c3, mcc)
//calculates MOC or MCC coefficient
for three channels
{
    l=c1.length;
    coef=0; denC1=0; denC2=0; denC3=0;
num=0;
    if(mcc)
    {
        for(i=0; i<l; i++)
        {
            if(c2[i]>0 && c3[i]>0)
num=num+c1[i];
            denC1=denC1+c1[i];
        }
        coef=num/denC1;
    }
    else
    {
        for(i=0; i<l; i++)
        {
            denC1=denC1+c1[i]*c1[i]*c1[i];
            denC2=denC2+c2[i]*c2[i]*c2[i];
            denC3=denC3+c3[i]*c3[i]*c3[i];
            num=num+c1[i]*c2[i]*c3[i];
        }

        coef=num/cbrt(denC1*denC2*denC3);
    }
    return coef;
}

function Dcoloc(c1, c2, mcc)
//calculates MOC or MCC coefficient
for two channels
{
    l=c1.length;
    coef=0; denC1=0; denC2=0; num=0;
    if(mcc)
    {
        for(i=0; i<l; i++)
        {
            if(c2[i]>0) num=num+c1[i];
            denC1=denC1+c1[i];
        }
        coef=num/denC1;
    }
    else
    {
        for(i=0; i<l; i++)
        {
            denC1=denC1+c1[i]*c1[i];
            denC2=denC2+c2[i]*c2[i];
            num=num+c1[i]*c2[i];
        }
        coef=num/sqrt(denC1*denC2);
    }
    return coef;
}

function Msd(v) //calculates the mean
and standard deviation of an array
{
    l=v.length;
    pd=newArray(2);
    pd[0]=0;
    for(i=0; i<l; i++)
        pd[0]=pd[0]+v[i];
    pd[0]=pd[0]/l;
    pd[1]=0;
    for(j=0; j<l; j++)
        pd[1]=pd[1]+(v[j]-
pd[0])*(v[j]-pd[0]);
    pd[1]=sqrt(pd[1]/(l-1));
    return pd;
}

function Cut(vec, mas, an, al, ones)
{
    j=0;
    ar=newArray(ones);
    for(i=0; i<an*al; i++)
    {
        if(mas[i]==255) {
            ar[j]=vec[i];
            j++;
        }
    }
    return ar;
}

function Count(m) //counts non-zero
pixels
{
    cont=0;
    for(i=0; i<m.length; i++) {
        if(m[i]>0)
            cont++; }
    return cont;
}

function cbrt(w) //calculates the
cubic root
{

```

```

x=w; y=1; e=0.0001;
while(x-y>e)
{
x=(2*x+y)/3;
y=w/(x*x);
}
return x;
}

//DIALOG WINDOW
img=getList("image.titles");
if(img.length==0) exit("At least 2
images opened");
img2=newArray(nImages+1);
img2[0]="none";
for(i=1; i<nImages+1; i++)
img2[i]=img[i-1];

TNUM=newArray(3);
if(BATCH==false)
{
Dialog.create("TCSS");
Dialog.addChoice("Red", img);
Dialog.addChoice("Green", img);
Dialog.addChoice("Blue", img2);
Dialog.addChoice("Mask", img2);
Dialog.addChoice("Thresholding
approach", newArray("Mean+sd (-2/2)",
"Porcentual (0/100)", "Numeric
(0/255)"));
Dialog.addNumber("Red threshold",
0);
Dialog.addNumber("Green threshold",
0);
Dialog.addNumber("Blue threshold",
0);
Dialog.addChoice("Scrambling
approach", newArray("Coordinates",
"Blocks of Pixels", "Pixels"));
Dialog.addNumber("Block area
(pixels)", 225);
Dialog.addChoice("Hypothesis test",
newArray("Non-parametric", "T-test"));
Dialog.addNumber("Number of
generated images", 30);
Dialog.addChoice("Significance
level", newArray(0.05, 0.01));
Dialog.addNumber("Random seed
(positive integer)", 1);

Dialog.show();
RED=Dialog.getChoice();
GREEN=Dialog.getChoice();
BLUE=Dialog.getChoice();
PMASK=Dialog.getChoice();
STCRITERION=Dialog.getChoice();
TNUM[0]=Dialog.getNumber();
TNUM[1]=Dialog.getNumber();
TNUM[2]=Dialog.getNumber();
RANDCRITERION=Dialog.getChoice();
BAREA=Dialog.getNumber();
HTAPPROACH=Dialog.getChoice();
GIMAGES=Dialog.getNumber();
SLEVEL=Dialog.getChoice();

SEED=Dialog.getNumber();
}
else
{
//BATCH SETTINGS
RED=img[2];
GREEN=img[1];
BLUE=img[0];
PMASK="none";//img[3];
STCRITERION="Mean+sd (-5/5)";
TNUM[0]=0;
TNUM[1]=0;
TNUM[2]=0;
RANDCRITERION="Blocks of Pixels";
BAREA=400;
HTAPPROACH="Simple sampling";
GIMAGES=1000;
SLEVEL=0.05;
SEED=1;
RIBOOLEAN=true;
}

//GENERAL SETTINGS
if(RANDCRITERION=="Blocks of Pixels"
&& PMASK!="none")
exit("No masking allowed if
'Blocks of Pixels' randomization
approach is selected");

BAREA=round(sqrt(BAREA));

if(SEED==0) random("seed",
round(random*100000));
else random("seed", SEED);

selectWindow(RED); run("Select None");
run("8-bit");
selectWindow(GREEN); run("Select
None"); run("8-bit");
if(BLUE!="none") {selectWindow(BLUE);
run("Select None"); run("8-bit");}
W = getWidth;
H = getHeight;

if(RANDCRITERION=="Blocks of Pixels")
{ //adjusts the size of the images
according to an integer number of
blocks
W=W-1; H=H-1;
do{W++;}while(W%BAREA!=0)
do{H++;}while(H%BAREA!=0)
selectWindow(RED); run("Size...",
"width=W height=H depth=1
interpolation=Bilinear");
selectWindow(GREEN);
run("Size...", "width=W height=H
depth=1 interpolation=Bilinear");
if(BLUE!="none")
{selectWindow(BLUE); run("Size...",
"width=W height=H depth=1
interpolation=Bilinear");}}

//MASKING

```

```

R1=newArray(W*H); R1=Vectorize(RED, W,
H);
G1=newArray(W*H); G1=Vectorize(GREEN,
W, H);
if(BLUE!="none") {B1=newArray(W*H);
B1=Vectorize(BLUE, W, H);}
M=newArray(W*H); for(i=0; i<W*H; i++)
M[i]=255;
MAREA=W*H;
if(PMASK!="none") {
selectWindow(PMASK); run("Select
None");
M=Vectorize(PMASK, W, H);
MAREA=Count(M);
R=Cut(R1, M, W, H, MAREA);
G=Cut(G1, M, W, H, MAREA);
if(BLUE!="none") B=Cut(B1, M, W,
H, MAREA); }
else { R=R1; G=G1; if(BLUE!="none")
B=B1; }

//SIGNAL THRESHOLD
if(STCRITERION=="Mean+sd (-2/2)") {
msd=Msd(R);
TNUM[0]=msd[0]+TNUM[0]*msd[1];
msd=Msd(G);
TNUM[1]=msd[0]+TNUM[1]*msd[1];
if(BLUE!="none") {msd=Msd(B);
TNUM[2]=msd[0]+TNUM[2]*msd[1]; }
if(STCRITERION=="Porcentual (0/100)")
{
TNUM[0]=Pthreshold(R, MAREA,
TNUM[0]);
TNUM[1]=Pthreshold(G, MAREA,
TNUM[1]);
if(BLUE!="none")
TNUM[2]=Pthreshold(B, MAREA, TNUM[2]);
}
//print(TNUM[0]+" "+TNUM[1]+"
"+TNUM[2]);
R=Threshold(R, TNUM[0], MAREA);
G=Threshold(G, TNUM[1], MAREA);
if(BLUE!="none") B=Threshold(B,
TNUM[2], MAREA);

//COEFFICIENTS
RG=Dcoloc(R, G, MCC);
if(BLUE!="none") { RB=Dcoloc(R, B,
MCC); GB=Dcoloc(G, B, MCC);
RGB=Tcoloc(R, G, B, MCC); RGBR=RGB;
if(MCC==true) { RGBG=Tcoloc(G, R, B,
MCC); RGBB=Tcoloc(B, G, R, MCC); }
else { RGBG=RGB; RGBB=RGB; }}

//RANDOM IMAGES AND RANDOM OVERLAPPING
rg=newArray(GIMAGES);
if(BLUE!="none") {
rb=newArray(GIMAGES);
gb=newArray(GIMAGES);
rgb=newArray(GIMAGES);
rgbr=newArray(GIMAGES);
rgbg=newArray(GIMAGES);
rgbb=newArray(GIMAGES);}

for(s=0; s<GIMAGES; s++)
{
showStatus(s);
if(RANDCRITERION=="Blocks of
Pixels") {
rR=BlockRand(R, W, H, BAREA);
rG=BlockRand(G, W, H, BAREA);
if(BLUE!="none") rB=BlockRand(B, W, H,
BAREA); }
if(RANDCRITERION=="Pixels") {
rR=PixelRand(R);
rG=PixelRand(G); if(BLUE!="none")
rB=PixelRand(B); }
if(RANDCRITERION=="Coordinates") {
rR=CoordRand(R, MAREA);
rG=CoordRand(G, MAREA);
if(BLUE!="none") rB=CoordRand(B,
MAREA); }
rg[s]=Dcoloc(rR, rG, MCC);
if(BLUE!="none") {
rb[s]=Dcoloc(rR, rB, MCC);
gb[s]=Dcoloc(rG, rB, MCC);
rgb[s]=Tcoloc(rR, rG, rB, MCC);
rgbr[s]=Tcoloc(rG, R, B, MCC);
rgbg[s]=Tcoloc(rG, R, B, MCC);
rgbb[s]=Tcoloc(rB, R, G, MCC); }
//if(s==0) print("RG double
scrambling, RG red scrambling, RG
green scrambling, RGB triple
scrambling, RGB red scrambling, RGB
green scrambling, RGB blue
scrambling");
//print(d2s(rg[s], 6)+"",
"+d2s(Dcoloc(rR, G, MCC), 6)+"",
"+d2s(Dcoloc(R, rG, MCC), 6)+"",
"+d2s(rgb[s], 6)+"", "+d2s(rgbr[s],
6)+"", "+d2s(rgbg[s], 6)+"",
"+d2s(rgbb[s], 6));
}

//SIGNIFICANCE
pRG=Msd(rg);
if(BLUE!="none") { pRB=Msd(rb);
pGB=Msd(gb);
pRGBR=Msd(rgbr); pRGBG=Msd(rgbg);
pRGBB=Msd(rgbb); pRGB=Msd(rgb); }

if(GIMAGES>1)
{
if(HTAPPOROACH=="T-test")
{
cRG=Pvalue((RG-
pRG[0])/pRG[1]);
if(BLUE!="none") {
cRB=Pvalue((RB-pRB[0])/pRB[1]);
cGB=Pvalue((GB-pGB[0])/pGB[1]);
cRGBR=Pvalue((RGBR-
pRGBR[0])/pRGBR[1]);
cRGBG=Pvalue((RGBG-
pRGBG[0])/pRGBG[1]);
cRGBB=Pvalue((RGBB-
pRGBB[0])/pRGBB[1]); cRGB=Pvalue((RGB-
pRGB[0])/pRGB[1]); }
}
}

```

```

else
{
    cRG=0; if(BLUE!="none") {
cRB=0; cGB=0; cRGR=0; cRGBG=0;
cRGRB=0; cRGB=0; }
    for(i=0; i<GIMAGES; i++)
    {
        if(rg[i]>RG) cRG++;
        if(BLUE!="none") {
if(rb[i]>RB) cRB++;
        if(gb[i]>GB) cGB++;
        if(rgbr[i]>RGR) cRGR++;
        if(rgbg[i]>RGBG) cRGBG++;
        if(rgbb[i]>RGRB) cRGRB++;
        if(rgb[i]>RGB) cRGB++; }
        cRG=cRG/GIMAGES;
        if(BLUE!="none") {
cRB=cRB/GIMAGES; cGB=cGB/GIMAGES;
        cRGR=cRGR/GIMAGES;
cRGBG=cRGBG/GIMAGES;
cRGRB=cRGRB/GIMAGES;
cRGB=cRGB/GIMAGES; }
        }
        sRG=Sig(cRG, SLEVEL);
        if(BLUE!="none") { sRB=Sig(cRB,
SLEVEL); sGB=Sig(cGB, SLEVEL);
sRGR=Sig(cRGR, SLEVEL);
sRGBG=Sig(cRGBG, SLEVEL);
sRGRB=Sig(cRGRB, SLEVEL);
sRGB=Sig(cRGB, SLEVEL); }
        cRG=d2s(cRG, 7);
        if(BLUE!="none") { cRB=d2s(cRB,
7); cGB=d2s(cGB, 7); cRGR=d2s(cRGR,
7); cRGBG=d2s(cRGBG, 7);
cRGRB=d2s(cRGRB, 7); cRGB=d2s(cRGB,
7); }
    }
else
{
    pRG[0]=" *****"; if(BLUE!="none")
{ pRB[0]=" *****"; pGB[0]=" *****";
pRGB[0]=" *****"; pRGR[0]=" *****";
pRGBG[0]=" *****"; pRGRB[0]=" *****";
}
    sRG=" *****"; if(BLUE!="none") {
sRB=" *****"; sGB=" *****"; sRGB="
*****"; sRGR=" *****"; sRGBG="
*****"; sRGRB=" *****"; }
    cRG=" *****"; if(BLUE!="none") {
cRB=" *****"; cGB=" *****"; cRGB="
*****"; cRGR=" *****"; cRGBG="
*****"; cRGRB=" *****"; }
}

//RESULTS TABLE
if(BATCH==false) {
LEAST=newArray(" Red", " Green", "
Blue");
if(GIMAGES>1 && BLUE!="none")
LEAST=TheLeast(LEAST, cRG, cRB, cGB);
titulo1 = "Results";
titulo2 = "["+titulo1+"]";
f = titulo2;

if (isOpen(titulo1))
    print(f, "\\Clear");
else
run("Table...", "name="+titulo1+
width=250 height=600");
print(f, "\\Headings:for\\t Overlap\\t
random\\t Significance\\t p-value");
print(f, "Double colocalization");
print(f, " RG"+"\\t "+RG+"\\t
"+pRG[0]+"\\t "+sRG+"\\t "+cRG);
//poner el coso decimal arriba en el
resultado
if(BLUE!="none") {
print(f, " RB"+"\\t "+RB+"\\t
"+pRB[0]+"\\t "+sRB+"\\t "+cRB);
print(f, " GB"+"\\t "+GB+"\\t
"+pGB[0]+"\\t "+sGB+"\\t "+cGB);
print(f, "Triple colocalization");
print(f, LEAST[0]+"\\t "+RGR+"\\t
"+pRGR[0]+"\\t "+sRGR+"\\t "+cRGR);
print(f, LEAST[1]+"\\t "+RGBG+"\\t
"+pRGBG[0]+"\\t "+sRGBG+"\\t "+cRGBG);
print(f, LEAST[2]+"\\t "+RGRB+"\\t
"+pRGRB[0]+"\\t "+sRGRB+"\\t "+cRGRB);
print(f, " Triple"+"\\t "+RGB+"\\t
"+pRGB[0]+"\\t "+sRGB+"\\t "+cRGB); }
else {
LEAST=newArray("R", "G", "B");
if(BLUE!="none") LEAST=TheLeast(LEAST,
cRG, cRB, cGB);
print(arg1);
print(RG+", "+sRG+", "+cRG);
    if(BLUE!="none")
{print(RB+", "+sRB+", "+cRB);
print(GB+", "+sGB+", "+cGB);
print(RGR+", "+sRGR+", "+cRGR+", "+LEA
ST[0]);
print(RGBG+", "+sRGBG+", "+cRGBG+", "+LEA
ST[1]);
print(RGRB+", "+sRGRB+", "+cRGRB+", "+LEA
ST[2]);
print(RGB+", "+sRGB+", "+cRGB); }
print(""); }

//GRAPHICS RESULTS

if(GIMAGES>0) {
    newImage("stack-RandRed", "8-bit
black", W, H, 1);
    Renderize(rR, M, "stack-RandRed");
run("Red");
    newImage("stack-RandGreen", "8-bit
black", W, H, 1);
    Renderize(rG, M, "stack-
RandGreen"); run("Green");
    if(BLUE!="none") {
        newImage("stack-RandBlue", "8-bit
black", W, H, 1);
        Renderize(rB, M, "stack-
RandBlue"); run("Blue"); } //end if
newImage("Red", "8-bit black", W, H,
1); Renderize(R, M, "Red");

```

```

newImage("Green", "8-bit black", W, H,
1); Renderize(G, M, "Green");
if(BLUE!="none") { newImage("Blue",
"8-bit black", W, H, 1); Renderize(B,
M, "Blue");}
if(BLUE!="none") { run("Merge
Channels...", "c1=Red c2=Green c3=Blue
create"); run("RGB Color"); }
else run("Merge Channels...", "c1=Red
c2=Green create"); run("RGB Color");
selectWindow("Composite"); close();
selectWindow("Composite (RGB)");
rename("stack-Composite");
run("Images to Stack", "name=Stack
title=stack use");
} //END MACRO

```

3. RESULTS AND DISCUSSION

3.1. Results

The orientation of pixel based colocalization analysis is defined foremost by the election of the colocalization coefficient. Pixel based analysis can be classify in two main categories: co-occurrence and correlation (Aaron, Taylor, & Chew, 2018). The first one describes the degree of spatial overlap between signals and use mainly Manders colocalization coefficient (MCC) and Manders overlap coefficient (MOC) (MANDERS *et al.*, 1993). Correlation analysis describes the degree of intensity correlation between the overlapped portion of signals, measured using Pearson and Sperman coefficients (J. Adler, Pagakis, & Parmryd, 2008; Manders, Stap, Brakenhoff, Van Driel, & Aten, 1992). In this work we focus on co-occurrence analysis and use MOC coefficient because of its sensibility and simplicity (each relationship is measured in a single coefficient). Additionally, MOC coefficient can be straightforwardly extended to measure triple overlapping (Eq. 2).

3.1.1 Identifying the channel that least colocalizes with the other two is the key to evaluate triple colocalization

The most used statistical test is the Costes scrambling approach. Figure 1Ai shows a two-channel merge of high overlapping (yellow tones). The merge of the left panel comprises 15 round objects of the red channel (R) and 15 objects of the green channel (G) deliberately centered in coordinates close to the center of objects of R. The scrambling approach consists of randomly rearranging the position of blocks of

pixels of both channels and then measuring the overlapping of these channels (Figure 1Aii). This procedure is repeated as many times as necessary to compose a distribution of random overlapping and contrasts the actual overlapping value with the distribution. Significant colocalization (SC) is assumed if the area under the Gaussian distribution is lesser than 5% of the total area to the right of the actual overlapping value; significant exclusion (SE) for an area greater than 95%; and not significant colocalization (NS) otherwise (Figure 1Aiii, v, and vii). A key point to consider in two channel analysis is that the same result is obtained by scrambling R, G or both channels (Figure 1Aii, iv and vi), as shown on the overlapping distributions for each case, all sharing the same mean and kurtosis (Figure 1Aiii, v and vii). Contrastingly, on triple colocalization analysis, the scrambling of each channel generates different overlapping distributions. In Figure 1Bi a third blue channel (B) with 15 objects was added to the merge shown in Figure 1Ai. Objects of B were randomly distributed generating a weak overlapping with isolated R objects (magenta pixels), with isolated G objects (cyan pixels) and with the overlapped R and G signals (white pixels). Pairwise relationships with B, RB and GB are NS (Figure 1Biv). The result of triple colocalization statistical significance depends on which channel is scrambled to compose the random overlapping distribution. Red scrambling generates a triple overlapping distribution far to the left of actual overlapping value ($MOC_{RGB}=0.1887$), thus this test yield SC (Figure 1Bii and iii). Equivalent distributions are generated by green scrambling and triple scrambling, both resulting in SC (Figure 1Bv, vi, ix and x). Blue scrambling is the only test in which the strong existing colocalization between R and G is conserved. This shifts the distribution to the right, including the actual overlapping value inside the area of NS results (Figure 1Bvii and viii). Regarding in this scenario, randomly arranged blue objects generated triple overlapping triple colocalization should be taken as NS, and blue scrambling is the only test that yields this result. B is the channel that least colocalizes with the other two in pairwise relationships or the least related channel (LRC), formally established as the channel that is not involved in the pairwise relationship with the smallest p-value (Figure 1Biv).

3.1.2 Triple colocalization cannot be inferred by double scrambling tests or the triple scrambling

test

In Figure 1Ci, all objects exclude each other, except for a single event of perfect triple overlapping (white object in the center). Albeit low ($MOC_{RGB}=0.0286$), this triple overlapping cannot be taken as casual, as it would be interpreted if only taken into consideration double scrambling and triple scrambling tests (SE-SE-SE and NS, respectively) (Figure 1Cii). In this scenario, there are no yellow, magenta nor cyan pixels, all pixels involved in a pairwise overlapping are also involved in a triple one (Figure 1Ci). This colocalization is difficult to occur by chance, as single scrambling tests show all SC (Figure 1Cii). Conversely, Figure 1Ciii shows an image with randomly positioned overlapped pairs of objects. Yellow objects are actually R and G overlapped objects, magenta objects are R and B objects, and cyan objects are G and B objects. Casual overlapping of pairs of a different kind generates casual triple overlapping. Single scrambling tests (all NS) reveal the casual nature of this triple overlapping, contrasting to the triple scrambling test (SC) (Figure 1Civ). These examples show how the triple scrambling test fails to judge triple colocalization by overestimation (Figure 1Civ and Fig. 1Biv) or underestimation (Figure 1Cii). In these examples, single scrambling tests are consistent with the real nature of images. For a triple overlapping deliberately generated (Figure 1Ci), the test yields SC even regarding the small MOC_{RGB} (0.0286) and opposite results of pairwise relationships (SE-SE-SE) (Figure 1Cii). On the other hand, when triple overlapping was generated by a random procedure (Figure 1Ciii), the test yields NS, even when MOC_{RGB} yields a higher value (0.1573) and pairwise relationships are all SC (Figure 1Civ). It's useful to mention that it is worthless to search the LRC in these examples, since pairwise relationships are almost symmetrical (similar p-values in double scrambling tests).

3.1.3 All scrambling tests contribute to interpret and classify different triple colocalization scenarios

To show the importance of a multitest approach, we made a colocalization analysis for all phases of the cell division. The complete cycle was taken from a single image downloaded from the library <https://wellcomecollection.org/works/r8ppshar>. Figure 2 shows the phases

of the mitosis in raw merges (Figure 2A), binarized merges with regions of interest delimited (Figure 2B), and analytical results (Figure 2C), in which R represents kinetochores, G tubulin, and B DNA. As in the previous sections, in this biological model, the LRC test shows more consistent results with the nature of images and biological facts than the triple scrambling test. The LRC test (Figure 2C, highlighted in bold type) and triple scrambling test yielded different results in the interphase, early anaphase, and telophase (Figure 2C). In the interphase, tubulin (G) is restricted to the cytosol, and kinetochores (R) and DNA (B) are located in the nucleus. Although limitations on the resolution of images mainly generate a certain degree of triple overlapping, this is an exclusion scenario since the biomolecules are located in different compartments. The LRC test judges this relationship as SE, while the triple scrambling test yields NS. In early anaphase, kinetochores (R) and tubulin (G), which are mostly located at the poles of the cell, colocalize significantly. Chromosomes (B), whose ends are still centered, are overlapped with the other two channels in a degree comparable to random levels. This phase resembles the scenario of Figure 1B, with the same significance in all tests (Figure 1B and Figure 2C early anaphase). As in Figure 1B, in the early anaphase, the LRC (B) overlaps with the other two channels at a degree close to the mean of the random distribution of this channel. The LRC test (NS) allows to distinguish the triple relationship of the early anaphase to the one of the anaphases, in which chromosomes concluded their migration to the cell poles, and all single and triple tests yield SC. The LRC test also detects the disruption of the mitotic spindle in the telophase and the reorganization of the cytoskeleton towards the interphase. Although the LRC test allows better discrimination of the triple relationships of the mitosis phases, all statistical tests are useful for classifying all phases analytically. Prophase and telophase share the same results for double scrambling tests, and the LRC test. However, triple scrambling is NS in prophase and SC in telophase, evidencing that the general trend of triple overlapping is stronger than in prophase. Additionally, red scrambling is NS in prophase and SC in telophase, evidencing (in telophase) a significant trend of red signal to look for overlapped blue and green signals. Each scrambling test unveils a particular statistical fact, and from the synthesis of all of them, it is possible to classify all phases of mitosis analytically.

For reasons of convenience to show the results, the MOC coefficient was used for this work. Nevertheless, to overcome the controversy generated around this tool (Jeremy Adler & Parmryd, 2010, 2019), we performed all analyses for MCC coefficients too, obtaining equivalent results for all significances of all figures (Figure 3C)

3.2. Discussions

This work highlighted three important issues about triple colocalization analysis: **first**, the LRC test is a better test to judge significant triple colocalization than the triple scrambling test, which is the test performed by Fletcher (Fletcher *et al.*, 2010). The LRC test evidences the exclusion existing in the interphase where interactors reside in different compartments. The LRC test also evidences the random nature of the configuration simulated in Figure 1B and reproduced in the early anaphase and the telophase. **Second**, triple colocalization cannot be inferred from pairwise relationships. This point is mainly evidenced by Figure 1C in which a triple SC can be found in a scenario where all pairwise relationships are SE; and adversely, a NS triple colocalization is yielded when all pairwise relationships are SC. **Third**, all scrambling tests are important to classify different scenarios. All phases of mitosis are distinguished by the result of at least one scrambling test, and each scrambling test is useful to contrast a specific statistical fact.

Although we restrict the study to 2D co-occurrence analysis, the concepts discussed in this work can be extrapolated to other branches of colocalization analysis, such as correlation approaches, object-based approaches, and coordinate-based analysis (Jaskolski, Mülle, & Manzoni, 2005; Malkusch *et al.*, 2012), as well as other data features as 3D or super-resolution images.

4. CONCLUSIONS:

Identifying the channel that least colocalizes with the other two is the key to evaluating triple colocalization in cases of strong asymmetries of double relationships. In other scenarios, single scrambling tests can reveal significant triple colocalization for low levels of

triple co-occurrence, even when all pairwise relationships were excluded. And, on the other hand, single scrambling tests can reveal the absence of a significant triple colocalization for high levels of triple co-occurrence, even when all pairwise relationships were significant colocalization. Furthermore, all scrambling test are useful for classifying a specific scenario of a triple relationship.

5. DECLARATIONS

5.1. Study Limitations

Besides the sample size, no other limitations were known at the time of the study.

5.2. Acknowledgements

We thank Thomas Surrey (Cancer Research UK, London, England), Oscar Bello (Yale School of Medicine New Haven, USA), and Luis Mayorga (IHEMCONICET, Mendoza, Argentina) for critically reading this manuscript.

5.3. Funding source

This work was supported by Foncyt PICT 2116, PIP-CONICET and SeCTyP grants to M. T. D.

5.5. Open Access

This article is licensed under a Creative Commons Attribution 4.0 (CC BY 4.0) International License, which permits use, sharing, adaptation, distribution, and reproduction in any medium or format, as long as you give appropriate credit to the original author(s) and the source, provide a link to the Creative Commons license, and indicate if changes were made. The images or other third-party material in this article are included in the article's Creative Commons license unless indicated otherwise in a credit line to the material. Suppose material is not included in the article's Creative Commons license, and your intended use is not permitted by statutory regulation or exceeds the permitted use. In that case, you will need to obtain permission directly from the copyright holder. To view a copy of this license, visit <http://creativecommons.org/licenses/by/4.0/>.

6. REFERENCES:

1. Aaron, J. S., Taylor, A. B., & Chew, T. L. (2018). Image colocalization - Co-occurrence versus correlation. *Journal of Cell Science*, 131(3). <https://doi.org/10.1242/JCS.211847>
2. Adler, J., Pagakis, S. N., & Parmryd, I. (2008). Replicate-based noise corrected correlation for accurate measurements of colocalization. *Journal of Microscopy*, 230(1), 121–133. <https://doi.org/10.1111/j.1365-2818.2008.01967.x>
3. Adler, Jeremy, & Parmryd, I. (2010). Quantifying colocalization by correlation: The pearson correlation coefficient is superior to the Mander's overlap coefficient. *Cytometry Part A*, 77(8), 733–742. <https://doi.org/10.1002/cyto.a.20896>
4. Adler, Jeremy, & Parmryd, I. (2019). Quantifying colocalization: The MOC is a hybrid coefficient - An uninformative mix of co-occurrence and correlation. *Journal of Cell Science*, 132(1), 1–3. <https://doi.org/10.1242/JCS.222455>
5. Bolte, S., & Cordelieres, F. P. (2006). A guided tour into subcellular colocalization analysis in light microscopy. *Journal of Microscopy*, 224(December), 213–232.
6. Costes, S. V., Daelemans, D., Cho, E. H., Dobbin, Z., Pavlakis, G., & Lockett, S. (2004). Automatic and quantitative measurement of protein-protein colocalization in live cells. *Biophysical Journal*, 86(6), 3993–4003. <https://doi.org/10.1529/biophysj.103.038422>
7. Dunn, K. W., Kamocka, M. M., & McDonald, J. H. (2011). A practical guide to evaluating colocalization in biological microscopy. *American Journal of Physiology - Cell Physiology*, 300(4), 723–742. <https://doi.org/10.1152/ajpcell.00462.2010>
8. Fay, F. S., Taneja, K. L., Shenoy, S., Lifshitz, L., & Singer, R. H. (1997). Quantitative digital analysis of diffuse and concentrated nuclear distributions of nascent transcripts, SC35 and poly(A). *Experimental Cell Research*, 231(1), 27–37. <https://doi.org/10.1006/excr.1996.3460>
9. Fletcher, P. A., Scriven, D. R. L., Schulson, M. N., & Moore, E. D. W. (2010). Multi-image colocalization and its statistical significance. *Biophysical Journal*, 99(6), 1996–2005. <https://doi.org/10.1016/j.bpj.2010.07.006>
10. French, A. P., Mills, S., Swarup, R., Bennett, M. J., & Pridmore, T. P. (2008). Colocalization of fluorescent markers in confocal microscope images of plant cells. *Nature Protocols*, 3(4), 619–628. <https://doi.org/10.1038/nprot.2008.31>
11. Goucher, D. R., Wincovitch, S. M., Garfield, S. H., Carbone, K. M., & Malik, T. H. (2005). A quantitative determination of multi-protein interactions by the analysis of confocal images using a pixel-by-pixel assessment algorithm. *Bioinformatics*, 21(15), 3248–3254. <https://doi.org/10.1093/bioinformatics/bti531>
12. Jaskolski, F., Mulle, C., & Manzoni, O. J. (2005). An automated method to quantify and visualize colocalized fluorescent signals. *Journal of Neuroscience Methods*, 146(1), 42–49. <https://doi.org/10.1016/j.jneumeth.2005.01.012>
13. Lachmanovich, E., Shvartsman, D. E., Malka, Y., Botvin, C., Henis, Y. I., & Weiss, A. M. (2003). Colocalization analysis of complex formation among membrane proteins by computerized fluorescence microscopy: Application to immunofluorescence co-patching studies. *Journal of Microscopy*, 212(2), 122–131. <https://doi.org/10.1046/j.1365-2818.2003.01239.x>
14. Lagache, T., Sauvonnnet, N., Danglot, L., & Olivo-Marin, J. C. (2015). Statistical analysis of molecule colocalization in bioimaging. *Cytometry Part A*, 87(6), 568–579. <https://doi.org/10.1002/cyto.a.22629>
15. Li, Q., Lau, A., Morris, T. J., Guo, L., Fordyce, C. B., & Stanley, E. F. (2004). A Syntaxin 1, G α , and N-Type Calcium Channel Complex at a Presynaptic Nerve Terminal: Analysis by Quantitative Immunocolocalization. *Journal of Neuroscience*, 24(16), 4070–4081. <https://doi.org/10.1523/JNEUROSCI.0346-04.2004>
16. Lifshitz, L. M. (1998). Determining Data Independence on a Digitized Membrane in Three Dimensions. *Image (Rochester, N.Y.)*, 17(2), 299–303.
17. Malkusch, S., Endesfelder, U., Mondry, J., Gelléri, M., Verveer, P. J., & Heilemann, M. (2012). Coordinate-based colocalization analysis of single-molecule localization microscopy data. *Histochemistry and Cell Biology*, 137(1), 1–10.

- <https://doi.org/10.1007/s00418-011-0880-5>
18. Manders, E. M. M., Stap, J., Brakenhoff, G. J., Van Driel, R., & Aten, J. A. (1992). Dynamics of three-dimensional replication patterns during the S-phase, analysed by double labelling of DNA and confocal microscopy. *Journal of Cell Science*, 103(3), 857–862.
<https://doi.org/10.1242/jcs.103.3.857>
 19. MANDERS, E. M. M., VERBEEK, F. J., & ATEN, J. A. (1993). Measurement of colocalization of objects in dual-colour confocal images. *Journal of Microscopy*.
<https://doi.org/10.1111/j.1365-2818.1993.tb03313.x>
 20. McDonald, J. H., & Dunn, K. W. (2013). Statistical tests for measures of colocalization in biological microscopy. *Journal of Microscopy*, 252(3), 295–302.
<https://doi.org/10.1111/jmi.12093>
 21. Oheim, M., & Li, D. (2007). Quantitative Colocalisation Imaging: Concepts, Measurements, and Pitfalls, 117–155.
https://doi.org/10.1007/978-3-540-71331-9_5
 22. Pawley, J. (2000). The 39 steps: A cautionary tale of quantitative 3-D fluorescence microscopy. *BioTechniques*, 28(5), 884–888.
<https://doi.org/10.2144/00285bt01>
 23. Ramírez, O., García, A., Rojas, R., Couve, A., & Härtel, S. (2010). Confined displacement algorithm determines true and random colocalization in fluorescence microscopy. *Journal of Microscopy*, 239(3), 173–183. <https://doi.org/10.1111/j.1365-2818.2010.03369.x>
 24. Van Steensel, B., Brink, M., Van der Meulen, K., Van Binnendijk, E. P., Wansink, D. G., De Jong, L., ... Van Driel, R. (1995). Localization of the glucocorticoid receptor in discrete clusters in the cell nucleus. *Journal of Cell Science*, 108(9), 3003–3011.
<https://doi.org/10.1242/jcs.108.9.3003>
 25. Wörz, S., Sander, P., Pfannmöller, M., Rieker, R. J., Joos, S., Mechttersheimer, G., ... Rohr, K. (2010). 3D Geometry-based quantification of colocalizations in multichannel 3D microscopy images of human soft tissue tumors. *IEEE Transactions on Medical Imaging*, 29(8), 1474–1484.
<https://doi.org/10.1109/TMI.2010.2049857>
 26. Zinchuk, V., & Zinchuk, O. (2008). Quantitative colocalization analysis of confocal fluorescence microscopy images.

Current Protocols in Cell Biology, (SUPPL. 39), 1–16.
<https://doi.org/10.1002/0471143030.cb0419s39>

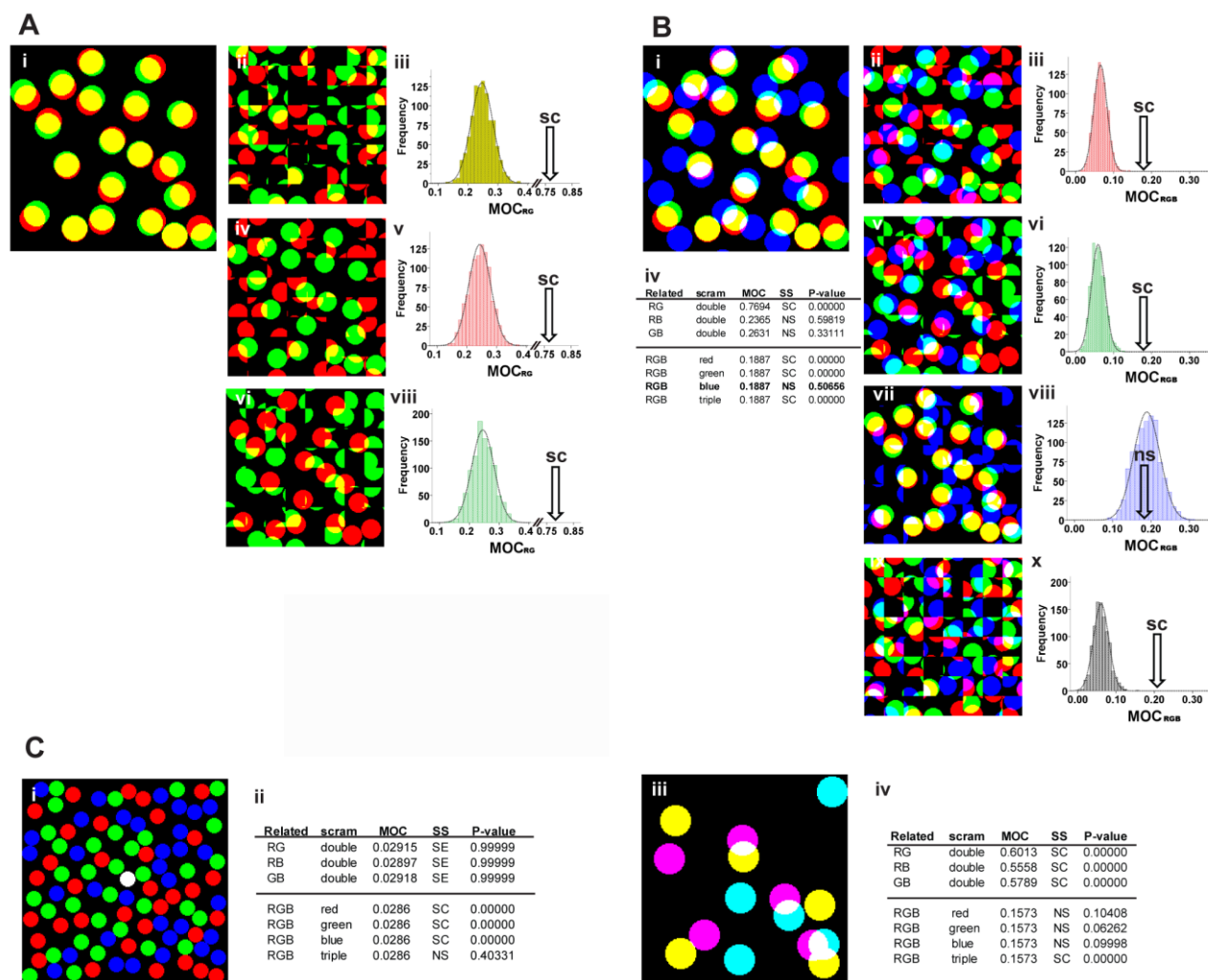


Figure 1: Different pairwise and triple colocalization scenarios. **A)** Left panel, two channels merge in a scenario of strong colocalization. Right panels, overlapping distribution of 1000 iterations of double, red, and green scrambling, actual overlapping value (arrow), and significance result. **B)** Left panels, three channels merge with the same red and green channels as in a) and a third blue channel with aleatory arranged objects; summary table showing the relationship analyzed, the channel/s scrambled, the MOC coefficient, the significance (SS) for an error of 0.05 and the p-value of significance calculated as the proportion of the area of the curve that is to the right of the actual overlapping value. The least related channel (LRC) (highlighted in bold type) is the channel that is not involved in the pairwise relationship with the smallest p-value. Middle panels include red, green, blue, and triple scrambling, respectively. Right panels, overlapping distribution of 1000 iterations of red, green, blue, and triple scrambling, actual overlapping value (arrow), and significance result. **C)** Left panels, the colocalization scenario of significant triple overlapping without significant pairwise colocalization and summary table. The right panel is the colocalization scenario of significant pairwise colocalization for the three relationships and not significant triple overlapping and summary table.

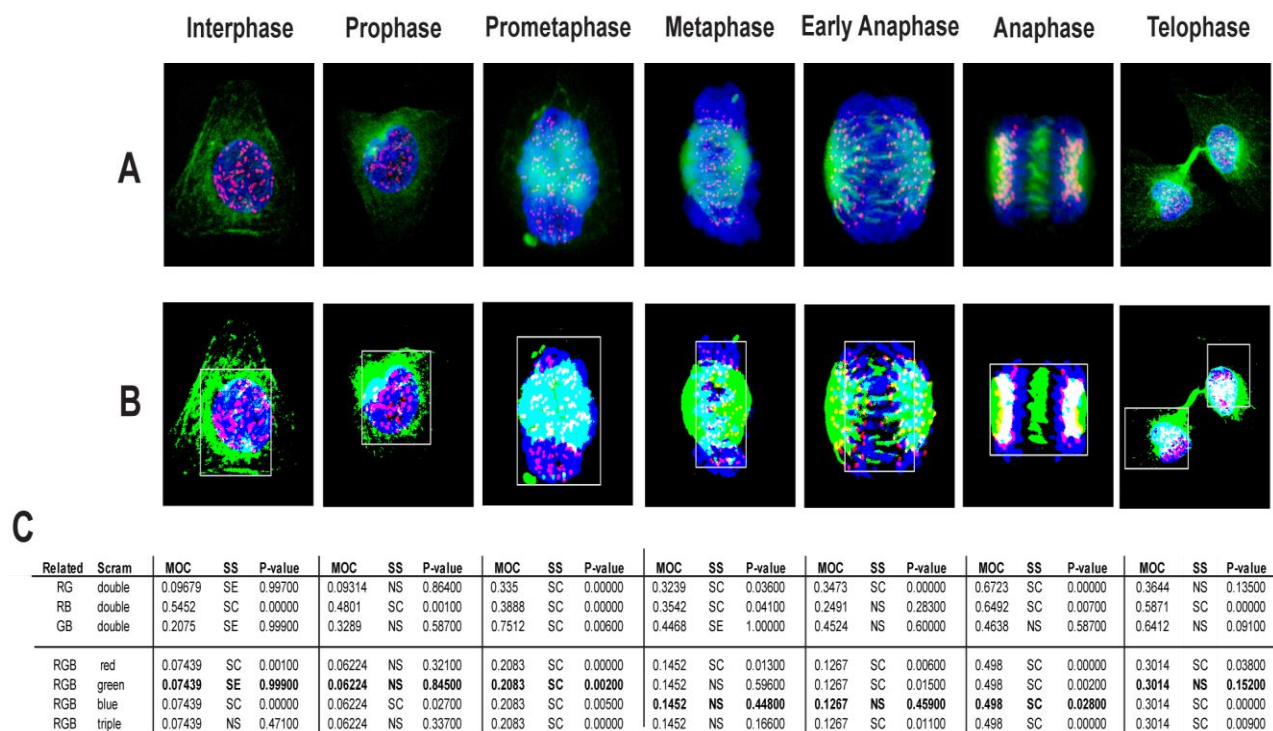


Figure 2: Colocalization analysis of the phases of the mitosis. **A)** three channels merge of HeLa cells of all phases of the mitosis. Kinetochores in red, tubulin in green and DNA in blue. **B)** merges binarized at the same intensity thresholds used to calculate colocalization coefficients. Gray squares show the ROIs used for the analysis. **C)** Colocalization analysis for each phase showing: the MOC coefficient, the significance (SS) for an error of 0.05 and the P-value of significance. The LRC (highlighted in bold type) is the channel which is not involved in the pairwise relationship with the smallest p-value. MOC values were calculated for signal thresholds equal to the average intensity value of signal inside the ROI.

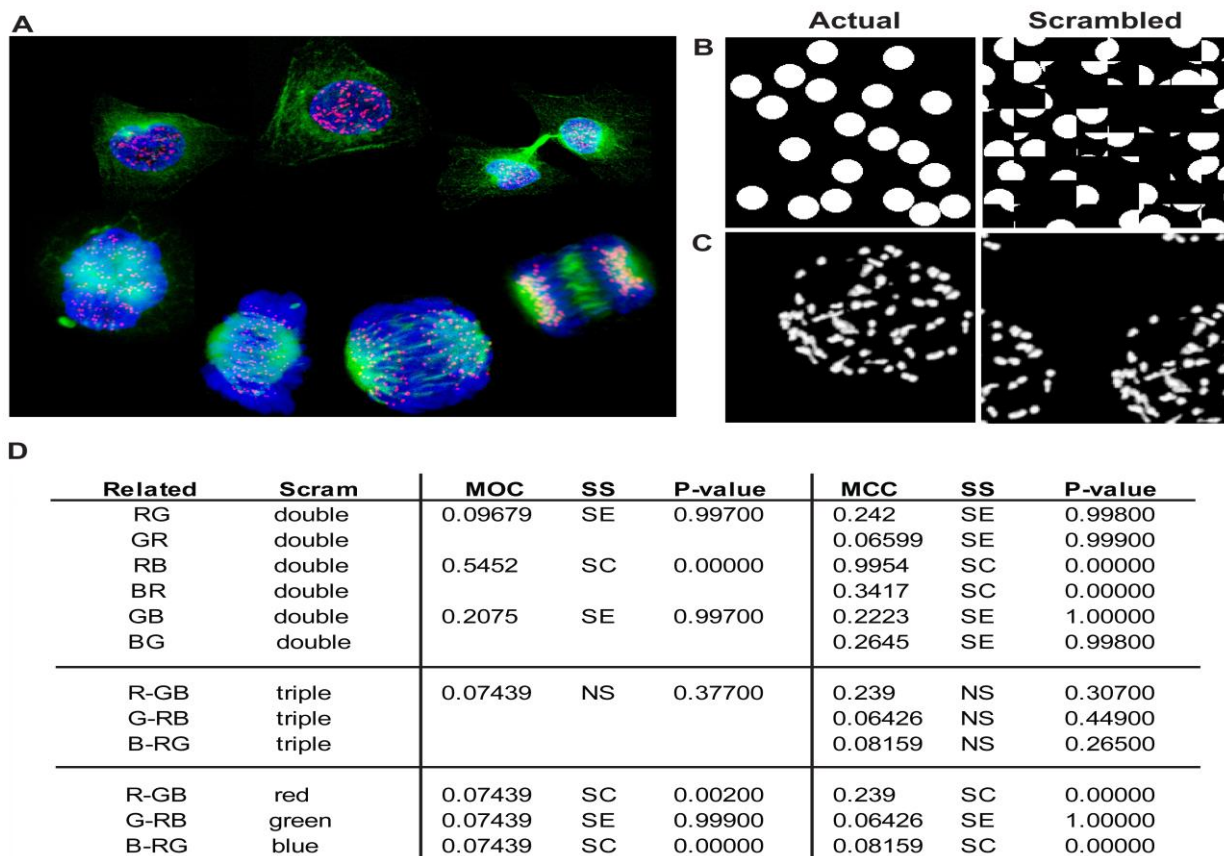


Figure 3: Original cell cycle image, scrambling examples, and MCC results. **A)** Original image of the cell cycle. **B)** Example of Costes scrambling approach. The original image is in the left panel, and the scrambled image is in the right panel. **C)** Example of Lifshitz scrambling approach. The original image is in the left, and the scrambled images in the right. **D)** comparison of the results obtained for MOC and MCC in the interphase. Significances of MOC and MCC were equivalent for the rest of the phases (data not shown).

DEAR READERS OF THE SOUTHERN JOURNAL OF SCIENCES

* Correspondence author
email: sjofsciences@sjofsciences.com

Accepted 27 December 2023

We are writing to inform you of an exciting change for our journal. As of 2024, the Southern Journal Of Sciences will be published by the Araucária Scientific Association (*Associação Científica Araucária - acararia.org*).

Southern Journal Of Sciences was initiated by Dr. Lavinel Ionescu from the Sarmisegetusa Research Group in 1993. Later, due to unforeseen circumstances, it was published with the support of the Tchê Química Group. After that it was transferred to Dr. D. Scientific Consulting. We are grateful to our previous publishers for their support over the years.

We are now excited to begin a new chapter in the journal's history with the Araucária Scientific Association. The Araucária Scientific Association is a new publisher of scientific journals in Brazil, and it is an association committed to sustainable development. We are confident that this partnership will help us to take Southern Journal Of Sciences to the next level.

As part of the Araucária Scientific Association, the Southern Journal Of Sciences will become part of a larger network of scientific journals, giving us access to a wider range of resources and expertise. This will allow us to continue publishing high-quality research, to a larger audience, and to have a greater impact on the fields of science.

We are thrilled to participate in the Araucária Scientific Association's vision for the future of scientific publishing. The Association is dedicated to open-access publication and ensuring that scientific knowledge is accessible to all. Our shared commitment aligns with theirs, and we believe that being part of the Association will enhance the accessibility of the Southern Journal Of Sciences for both researchers and the general public. Additionally, we take pride in contributing content to the Araucária Scientific Association newsletter, which is freely accessible at <https://www.acararia.org/archive.php>. This newsletter serves as a valuable resource for scientists and the general public, and we're delighted to contribute to its dissemination. We encourage you to subscribe to this newsletter to stay informed about the latest scientific news and advancements.

We are confident that this change is a step into the future for Southern Journal Of Sciences. We are committed to continuing to publish high-quality research in the chemistry field and making the journal accessible to everyone. We look forward to working with ACARIA to achieve these goals.

Thank you for your continued support.

Sincerely,

Walter José Peláez, Ph.D., Argentina, UNC. Editor-in-Chief of the Southern Journal Of Sciences.

Ketevan Kupatadze, Ph.D., Georgia, ISU. Assistant Editor of the Southern Journal Of Sciences.

Shaima R. Banoon, MsC., Iraq, University of Misan. Assistant Editor of the Southern Journal Of Sciences.

Cristián Andrés Quintero, Ph.D., Argentina, Universidad Juan Agustín Maza. Assistant Editor of the Southern Journal Of Sciences.

Aline Maria dos Santos, PhD., Assistant Editor, Brazil, IFRJ. Assistant Editor of the Southern Journal Of Sciences.

Cristiane de Souza Siqueira Pereira, PhD, Brazil, Universidade de Vassouras. Assistant Editor of the Southern Journal Of Sciences.

Luis Alcides B. D. Managing-Editor, Southern Journal Of Sciences.

SOUTHERN JOURNAL OF SCIENCES ANNUAL TRANSPARENCY REPORT

Walter José Pelaez¹; Luis Alcides Brandini De Boni²

¹ INFIQC, Departamento de Físicoquímica. Facultad de Ciencias Químicas, Universidad Nacional de Córdoba, Córdoba, Argentina.

² Southern Journal of Sciences, Brazil.

* Correspondence author
email: sjofsciences@sjofsciences.com

Accepted 27 December 2023

In 2022 The SOUTHERN JOURNAL OF SCIENCES introduced the practice of producing an annual transparency report to give authors and institutions access to useful information about the journal. It was chosen to present the main facts in the format of bullets to make the report succinct.

- **Current Editor-in-Cheife:** Dr. Walter José Pelaez.
- **Past Editors:** Dr. Lavinel G. Ionescu; Dr. Luis A. B. De Boni.
- **Currently Edited by:** Dr. D. Scientific Consulting (CNPJ # 34.958.677/0001-59) - (Luis Alcides Brandini De Boni). A Brazilian Micro Company. Until the end of 2023.
- **This journal is merging with the Aruacária Scientific Association.** From **2024** forward, this journal will be published by the Araucaria Associação Científica (CNPJ # 52.968.321/0001-88).
- **Number of countries represented in the journal council:** 12.
- **Number of conferences the journal was invited to publish the resulting material:** 1.
- **Number of conferences that the journal published the resulting material:** 1. (SOUTHERN BRAZILIAN JOURNAL OF CHEMISTRY - INTERNATIONAL VIRTUAL CONFERENCE. <https://www.21scon.org>)
- **Number of manuscripts received in 2023:** 22
- **Number of manuscripts published in 2023:** 11
- **Amount of manuscripts that will continue the publication process in 2023:** 1
- **Amount of improper submissions:** 4
- **Amount of rectified submissions:** 2
- **Innovative tools introduced in the journal**
 - *Abstract Maker tool:* <<https://www.sjofsciences.com/Abstract-maker.php>>
 - *Manuscript Sketch Tool:* <<https://www.sjofsciences.com/manuscript-sketch-maker.php>>
 - *Reference formatting tool*:* <https://www.sjofsciences.com/doi_to_apa.htm>. This tool reflects the page <https://citation.crosscite.org/>
 - *Use of avatars (sample):* <https://youtu.be/iIMVj6FLmMg>
- **Financial support received from other institutions (in USD):** \$ 0,00. A proudly independent journal.
- **Indexed in:** Index Copernicus, Latindex, and I2OR.

SECOND SOUTHERN SCIENCE CONFERENCE

Experiences that go beyond
science.

**Mendoza - Argentina is calling
you.**



SCAN ME

November 2024.





Dear colleagues,

We are pleased to invite you to participate in the II Southern Science Conference, organized by the University of Mendoza (Argentina) and the University of Vassouras (Brazil). The conference will take place from November 7th to 9th, 2024, at the "Centro de Convenciones y Eventos" of the University of Mendoza in the city of Mendoza, Argentina. The University of Vassouras (Brazil) will host the virtual conference. The conference website is <https://www.sscon.org/>.

As customary, the conference aims to serve as a platform for disseminating the latest advancements in various areas of Science, including Chemistry, Physics, Biology, Engineering, Medicine, and Pharmacy, among others. We will focus on areas such as Food Production, Energy Production, Environmental Sciences, Valuation of Endogenous Resources, Drug Production, Zero-Waste Production, and One Health. Thanks to the current sanitary situation, we will be able to meet again in person within a pleasant scientific environment conducive to sharing and discussing new ideas and discoveries, strengthening existing bonds, and establishing new contacts and collaborations, not only among Argentine and Brazilian scientists, professionals, and students but also with colleagues from other nationalities.

The Symposium will feature Plenary and Invited Lectures by prestigious foreign and national scientists. Furthermore, we look forward to the presentation of numerous works from the aforementioned areas in the form of Oral Communications and Poster Sessions, subject to evaluation and review by the ad-hoc Scientific Committee of each area. The list of speakers, along with instructions for abstract submission and poster preparation, will be provided in the upcoming circular scheduled for April 2024. Following are details regarding the event's host hotel and the composition of the scientific committees.



II SSSCON Organizing Committee

<https://www.sskon.org>

- Cristián Andrés Quintero, Ph.D., Argentina, Universidad de Mendoza/Universidad Juan Agustín Maza. Chair of the conference.
- Cristiane de Souza Siqueira Pereira, PhD. Brazil, Universidade de Vassouras. Chair of the conference.
- Walter José Peláez, PhD, Argentina, UNC | Editor-in-Chief of the Southern Journal of Sciences. Co-Chair of the conference
- Ketevan Kapatadze, Ph.D., Georgia, ISU | Editor-in-Chief of the Periódico Tchê Química.
- Shaima R. Banoon, MSc., Iraq, University of Misan | Editor-in-Chief of the Periódico Tchê Química.
- Olunmi Atolani, Ph.D., Nigeria, University of Ilorin. Facilitator.
- Eduardo Goldani, Ph.D., UK., Springer. Invited Editor.
- Luis Alcides Brandini De Boni, Ph.D., Brazil, A.S.A. General Secretary . Event Treasurer.

Open Access and Copyright Information

- All articles published by the Periódico Tchê Química and the Southern Journal of Sciences are made immediately available worldwide under an open access license Creative Commons Attribution License (CC BY 4.0). This means:
- Everyone has free and unlimited access to the full-text of all articles published in the Journals;
- Everyone is free to reuse the published material if proper accreditation/citation of the original publication is given;
- There will be **no** Article Processing Charge (APC) for accepted articles or materias.

Copyright Information

Authors who publish with this journal agree to the following terms:

The authors retain the copyrights and grant the journal right of first publication with the work simultaneously licensed under a Creative Commons Attribution License (CC BY 4.0) which permits use, sharing, adaptation, distribution, and reproduction in any medium or format, as long as you give appropriate credit to the original author(s) and the source, provide a link to the Creative Commons license, and indicate if changes were made. The images or other third-party material in this article are included in the article's Creative Commons license unless indicated otherwise in a credit line to the material. If material is not included in the article's Creative Commons license and your intended use is not permitted by statutory regulation or exceeds the permitted use, you will need to obtain permission directly from the copyright holder.

The authors can enter into separate, additional contractual arrangements for the non-exclusive distribution of the journal's published version of the work (e.g., post it to an institutional repository or publish it in a book), with an acknowledgment of its initial publication in this journal.

Authors are permitted and encouraged to post their work online (e.g., in institutional repositories or on their website) prior to and during the submission process, as it can lead to productive exchanges, as well as earlier and greater citation of published work (Effect of Open Access).

information@sscon.org